**THE EFFECT OF A HARD COATING ON THE DAMPING AND
FATIGUE LIFE OF TITANIUM**

THESIS

Frank T. Ivancic

AFIT/GAE/ENY/03-12

**DEPARTMENT OF THE AIR FORCE
AIR UNIVERSITY**

AIR FORCE INSTITUTE OF TECHNOLOGY

Wright-Patterson Air Force Base, Ohio

THE EFFECT OF A HARD COATING ON THE DAMPING AND FATIGUE LIFE OF
TITANIUM

THESIS

Presented to the Faculty

Department of Aeronautics and Astronautics

Graduate School of Engineering and Management

Air Force Institute of Technology

Air University

Air Education and Training Command

In Partial Fulfillment of the Requirements for the

Degree of Master of Science in Aeronautical Engineering

Frank T. Ivancic, BS, MS

March 2003

AFIT/GAE/ENY/03-12

THE EFFECT OF A HARD COATING ON THE DAMPING AND FATIGUE LIFE OF
TITANIUM

Frank T. Ivancic, BS, MS

Approved:

/signed/

Prof. Anthony N. Palazotto (Chairman)	date

/signed/

Maj Richard G. Cobb (Member)	date

/signed/

Dr. Peter J. Torvik (Member)	date

Acknowledgements

Table of Contents

List of Figures

List of Tables

AFIT/GAE/ENY/03-12

Abstract

This project compares the damping and fatigue life of bare titanium plates to those coated with magnesium aluminate spinel (mag spinel). Two different coating thicknesses were tested: .005" per side and .010" per side (total thicknesses of .010" and .020").

Dynamic ping tests were conducted on all specimens to determine their resonance frequencies. Laser vibrometry was used to determine the mode at each resonance frequency. Damping ratios were determined through the use of sine sweeps. A vibration mode was selected at which to fatigue the specimens, and the stress pattern was analyzed utilizing the Stress Pattern Analysis by Thermal Emissions (SPATE) process.   Once characterization was complete, fatigue testing was conducted on the thick plates utilizing the resonant dwell process. The specimens were vibrated by applying a harmonic excitation through the base. The strain level which would result in fatigue at 10^6 cycles, and the velocity necessary to achieve this strain were determined. The test specimens were excited at this velocity, and the number of cycles to failure was noted.   Results were compared for the uncoated, thin coated, and thick coated specimens.

This project demonstrated that the addition of magnesium aluminate spinel did increase the damping of the titanium plates. The thick coating did not provide noticeably better damping results than the thin coating at the amplitudes tested. Damping was found to be a function of mode shape, rather than frequency. The coating allowed the titanium plate to withstand a greater stress at the same life as the uncoated plate, or to endure a much greater number of cycles at the same applied force. The thick coating had a greater impact

on fatigue than the thin coating, but the thick coating was observed to flake off, while the

thin coating did not.

THE EFFECT OF A HARD COATING ON THE DAMPING AND FATIGUE LIFE OF

TITANIUM

I. Introduction

Fatigue

In structural design, engineers ensure the anticipated loads will not exceed the

ultimate stress of the material being used. However, materials can fail at stresses well

below the ultimate stress, through fatigue. Fatigue is the failure of material through

cyclic loading at stresses below the ultimate stress. This occurs by crack initiation and

growth. Fatigue is generally divided into two categories: low-cycle fatigue (LCF) and

high-cycle fatigue (HCF). Loads are higher under LCF, resulting in typical fatigue lives

of less than 10,000 cycles. Under HCF, loads are typically in the elastic range, and

fatigue lives are greater than 10,000 cycles (Grady, 1999). HCF failures occur quickly,

due to high frequency loading (Ritchie, 1999).

Fatigue in Aircraft Engines

Over the years, LCF failures in aircraft engines have been greatly reduced through

the use of fracture mechanics and a retirement-for-cause management philosophy,

leaving HCF as the primary cause of engine failures (Nicholas, 1996). As improvements

for increased performance and reduced weight have been implemented in engines,

operating temperatures and stresses have increased, making the HCF problem more acute

(Cowles, 1996). HCF is not limited to any single material or engine manufacturer, and affects all engine components (Nicholas, 1996).

As mentioned above, fatigue is caused by cyclic loading causing cracks to grow until the material fails. Microscopic cracks can be initiated by various phenomena, including fretting and foreign object damage (Ritchie, 1999). Sources of loads which can cause HCF include aerodynamic excitation caused by the gas flow through the engine; mechanical vibrations caused by rotor imbalance or by rubbing of components, such as blade tips against the casing; airfoil flutter caused by aeromechanical instability; and acoustics (Cowles, 1996). Fatigue in engine blades (fan, compressor, and turbine blades), the area of interest of this research, is the result of stresses generated by unsteady aerodynamic loading causing vibrations at or near resonance conditions (Shen, 2002).

While cracks typically grow at a slow rate under HCF, they can propagate to failure in a very short time. As an example, a crack in a 20 mm thick turbine component growing at a rate of 10^{-10} m/cycle will cause the component to fail in just 30 hours of operation, if the component is vibrating at 1,000 Hz (Ritchie, 1999). This may be as few as four missions for a transport aircraft, or two missions for a bomber. If the component is thinner, the crack growth rate is faster, or the frequency of vibration is higher, the time to failure can be much less than 30 hours.

HCF failures can be grouped into two broad categories: those where the forcing functions exceeded the anticipated design usage, and those where the material behavior did not meet that anticipated in the design. (Nicholas, 1996) Thus, at its root, HCF is a design problem. But HCF analysis is part of the standard design process for engine components (Cowles, 1996; Shen, 1999). The design process includes structural dynamic

analysis to determine the natural frequencies and modes throughout the anticipated

operating range, and a determination of the stress distribution for each excitation (Shen,

1999). The natural frequencies are compared to those expected to be generated in the

operating environment on a Campbell diagram (see Fig. 1); the design is iterated to avoid

strong resonance conditions. Intersections may be acceptable for higher order modes or

weak driving forces (Cowles, 1996). However, predicting the loading is not an exact

science, due to the large number of variables that go into the generation of these loads

(Shen, 1999). Thus, while HCF is considered in design, the process is not to the point

where HCF can be eliminated.
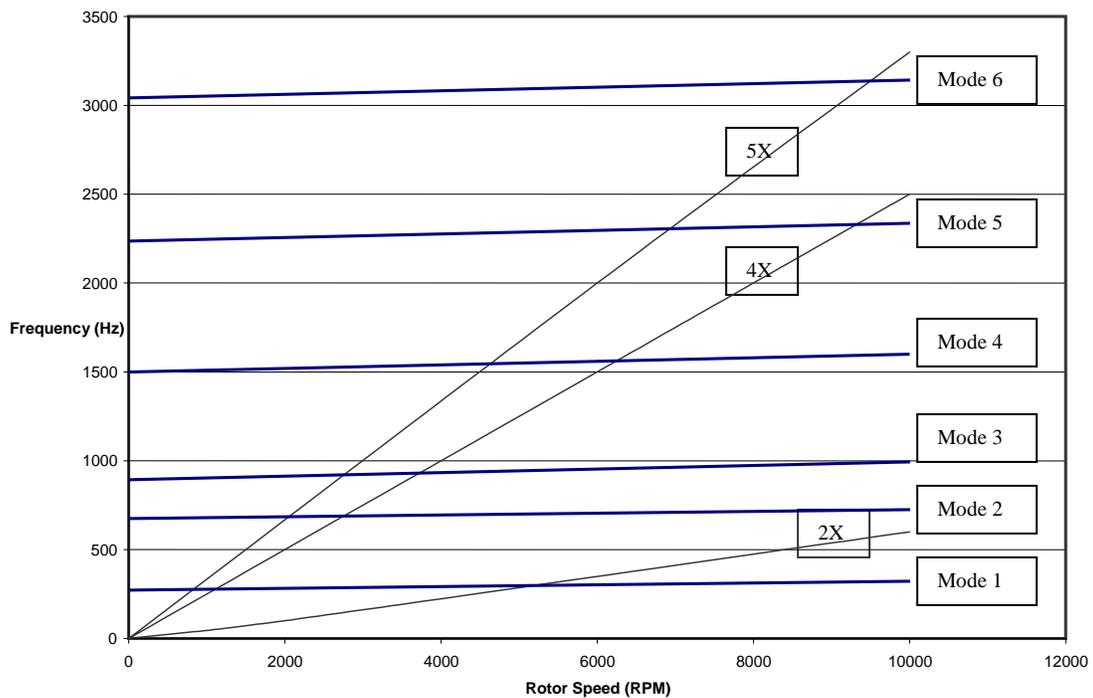
Figure 1. Example of a Campbell Diagram. Horizontal blue lines are modes, lines from the origin are multiples of engine RPM. Intersection points are design points to be avoided.

3

Throughout the 1980s and 1990s, HCF was the single largest cause of aircraft engine failure, resulting in lost aircraft, and the expenditure of many millions of maintenance man-hours and dollars (Cowles, 1996; Garrison, 2001). As a result, the High Cycle Fatigue Science and Technology Program was formed in 1994, with the goal of gaining a better understanding of HCF in order to eliminate it as a major cause of engine failures. Eight action teams were set up, including one focused on Passive Damping. Among the specific component objectives of the program is "Damp resonant stress by 60% in fans, 20% in compressors, and 25% in turbines" (Garrison, 2001).

Damping

Damping can be used to avoid premature fatigue by attenuating amplitudes of oscillations and suppressing undesirable resonances (Baz, 2001). By applying a damping material to the subject structure, mechanical energy can be dissipated by converting it to heat energy (Ungar, 2001).

There are two main approaches in damping design: passive and active damping. Passive damping techniques, such as the application of a damping coating, are simple and reliable. They are generally more effective for damping out high frequency vibrations, but are typically only effective for a small range of frequencies. Active damping employs sensors and actuators, and can be used for low frequency excitations. Hybrid methods combine the two approaches, to provide control over broader frequency ranges (Baz, 2001). Engine designers have had success in employing dry friction damping techniques to suppress low frequency vibrations (Shen, 2002). The propulsion

community has concentrated on passive damping in its search for a solution to the high cycle fatigue problem due to the simplicity of the approach and its effectiveness in attenuating high frequencies.

Traditionally, materials for damping additions have been viscoelastic polymeric plastics or elastomers. These materials are known as viscoelastic because they have the properties of both viscous (energy dissipating) and elastic (energy storing) materials. High-damping metal alloys, while having better damping properties than common metals, do not provide the same level of damping that viscoelastic materials do. However, viscoelastic materials are generally only effective for a small temperature range (Ungar, 2001). Metals, while they do not provide the same level of damping as viscoelastic materials, are effective over a greater temperature range. In aircraft engines, even a small amount of damping can have a pronounced effect, and effectiveness over an extended temperature range is crucial. Within the propulsion community, research over the past few years has shifted from viscoelastic damping materials to metallic or hard coatings.

Hard Coatings

The damping mechanism of hard coatings has been assumed to be internal friction between the applied coating and the surface to which it is applied. Recent laboratory test results from the University of Sheffield and Rolls Royce plc indicate this assumption is valid (Green, 2002). Shen (2002) observed that energy dissipated by a magnesium aluminate spinel coating did not behave in a manner consistent with hysteresis, suggesting that the energy dissipation may be from friction between the powder particles.

The two most common methods for applying hard coatings are air plasma spraying and physical vapor deposition. Air plasma spray offers advantages in cost, lower application temperatures, and fewer limitations on component size (Patsias, 2001). Plasma spraying provides a denser, stronger coating than most other spray processes. The high temperature of the plasma allows materials with high melting points to be applied as coatings that cannot be applied by other means. Disadvantages include high cost and the complexity of the process (England, 2002). The plasma spray process is described below.

Magnesium Aluminate Spinel

Magnesium aluminate spinel ($MgAl_2O_4$) is a powder coating commonly applied by plasma spray. Its properties make it useful for erosion resistance against gas streams at elevated temperature, an important characteristic for application in gas turbine engines (APS Materials, 2001). Torvik, et al. have reported mag spinel provides sufficient damping to be of interest to the propulsion community.

The Plasma Spray Process

Plasma spraying is the process of applying a coating to a substrate material by injecting a powder coating into a high temperature plasma gas and spraying it at high velocity onto the target substrate. The plasma gas (typically argon, nitrogen, hydrogen, or helium) converts the powder to a molten state. As the spray impacts the substrate, it cools very quickly, forming a bond with the surface (England, 2002). See Figure 2.
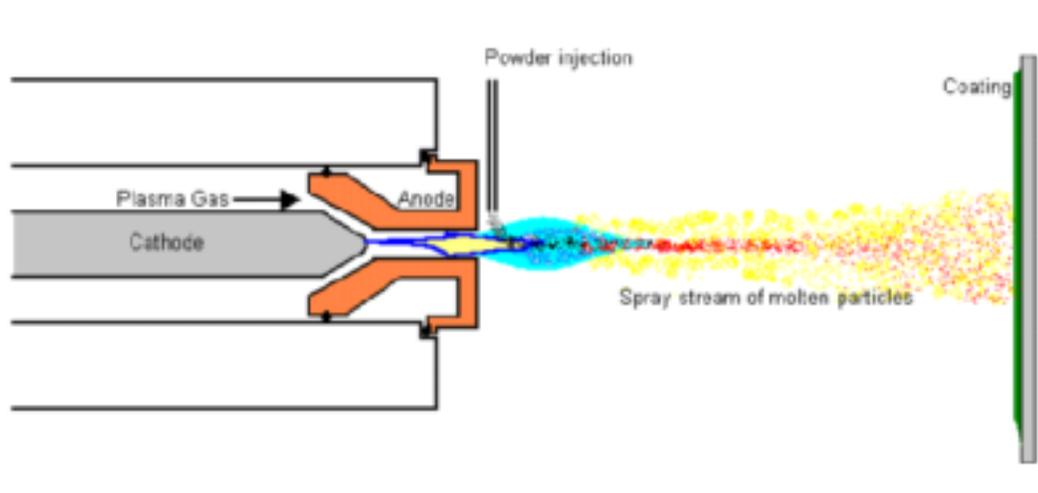
Figure 2. Schematic Diagram of the Plasma Spray Process (England, 2002)

When the spray chamber is occupied by the common atmosphere, the process is air plasma spraying, which is the most typical form of plasma spraying. Occasionally, the atmosphere can provide undesirable contaminants to the coating, and the chamber is filled with an inert gas at low pressure. This process is vacuum plasma spraying (England, 2002).

Objective

The objective of this investigation is to determine the effect of the application of a hard coating on the damping and fatigue life of titanium. Titanium (specifically, Ti-6Al-4V) was selected as the base metal for this investigation because of its common use in aircraft engine fan and compressor blades. The effects of coating thickness, frequency, and temperature will be observed, and results will be compared to those predicted by a finite element analysis model for selected conditions.

Related Work

Ritchie, et al. (1999) investigated crack growth in Ti-6Al-4V under HCF conditions, and found that varying the frequency did not affect the rate of crack propagation. They theorized frequency must influence crack initiation.

Torvik, et al. (2002) examined the damping effect of mag spinel on Hastalloy X, a nickel-based alloy commonly found in aircraft engines, and found that the coating provided sufficient damping to be effective in reducing vibration amplitudes in aircraft engines. They observed that the response functions were not symmetrical about the resonance frequency, and the resonance frequency decreases as the amplitude of the applied force is increased, indicating stiffness non-linearity, or softening. (This was also observed by Shen (2002), who likewise examined mag spinel applied to Hastalloy X.) The amount of energy dissipated by the coating was shown to be strain dependent. They further concluded that over the first four bending modes, the level of damping obtained was independent of frequency.

Smith (1994) studied the effect of applying coatings by plasma spray to Ti-6Al-4V orthopedic implants, and found a decrease in high-cycle fatigue performance. He found that increasing the bond strength between the coating and the implant did not extend the life of the implant, but rather caused fatigue in fewer cycles. He concluded that the metallurgical bonding created by the plasma spray process allows defects in the coating to propagate through to the substrate, bypassing the crack initiation stage, allowing failure to occur at lower stress levels.

Approach

This project compares the fatigue life of bare titanium plates to those coated with magnesium aluminate spinel (mag spinel). The test specimens were Ti-6Al-4V plates. The material and the aspect ratio of the plates were analogous to the low aspect ratio blades commonly found in the compressor sections of military fighter aircraft. The plates were tested in a cantilevered boundary condition. Investigations were conducted for two different size specimens: 5-1/4" x 4-1/4" x .050" (thin plate) and 6-1/2" x 4-1/2" x .125" (thick plate). The thin plate had 1.0" on the short side clamped, making the effective test area 4-1/4" x 4-1/4"; the thick plate had 2.0" on the short side clamped, making the effective area of the test specimen 4-1/2" x 4-1/2". The coatings were applied by plasma spray. Two different coating thicknesses were tested: .005" per side and .010" per side (total thicknesses of .010" and .020"). Damping tests were run at room temperature and 275 F, a typical operating temperature for the initial stages of engine compressors. Temperature testing was also conducted with the plate under a free-free-free-free boundary condition to eliminate inconsistencies caused by the clamp. Testing was conducted at the Turbine Engine Fatigue Facility, AFRL/PRTC, Wright-Patterson AFB OH.

The test specimens were characterized by frequency, mode shape, and stress pattern. Dynamic ping tests were conducted to determine resonance frequencies. Holography scans and laser vibrometry were used to determine the mode shape at each resonance frequency. Stress patterns were analyzed for two modes utilizing the Stress Pattern Analysis by Thermal Emissions (SPATE) process. Damping ratios were determined by conducting sine sweeps.

Once characterization was complete, fatigue testing was conducted utilizing the resonant dwell process, which excites the test specimen at a known velocity (which is related mathematically to displacement, strain, and stress) at a selected resonance condition until it fatigues. The specimens were vibrated by applying an initial acceleration condition at the base. The stress and amplitude (shaker head acceleration, in g's) to fail the baseline uncoated plate at 10^6 cycles were determined. The fatigue stresses for the coated plates were then determined for 10^6 cycles, and the amplitudes were compared to the baseline. Additionally, the acceleration needed to fail the baseline plate was applied to a coated plate, and the cycles to fail were noted.

The NASTRAN finite element analysis model and PATRAN postprocessor were used to determine the resonance frequencies and mode shapes for particular conditions.

II. Prediction Methods

Two methods were used to predict the natural frequencies and modes of the room temperature and bare metal titanium plates tested: mathematical modeling and computer modeling.

Mathematical Prediction of Natural Frequencies and Modes

When a structure is subjected to an initial condition or force which causes it to vibrate, the amplitude of the displacement of the structure will peak at specific frequencies, depending on the properties of the structure and its boundary conditions. These are its natural frequencies, and the shape of the displacement function at each frequency is the mode. Plate theory can be used to predict the natural frequencies and the modes at each frequency.

From Classical Plate Theory, utilizing the boundary conditions and the Rayleigh-Ritz method, equations can be derived to obtain the upper bound for the natural frequencies. Leissa cites Young for the derivation (Leissa, 1969). For a square plate in the clamped-free-free-free (cantilevered) condition, the natural frequencies are found from:

$$\omega_n = \frac{B_n \sqrt{(Et)}}{\sqrt{\rho a^4 \left(1 - v^2\right)}} \tag{1}$$

where

a = length of plate
t = plate thickness
ρ = material density

11

E = Young's modulus

ν = Poisson's ratio

B = modal constant. For the first five modes,

$B_1 = 1.01$

$B_2 = 2.47$

$B_3 = 6.20$

$B_4 = 7.94$

$B_5 = 9.01$

(Harris, 1988)

Using Equation 1 and the values for B, the first five natural frequencies can be

mathematically determined, in radians/sec. To convert to Hertz (cycles/sec):

$$f_n = \frac{\omega_n}{2\pi} \tag{2}$$

If no damping is present, the mode at each natural frequency is unique. However,

there is always some degree of damping, which results in a superposition of all modes at

each natural frequency, with varying degrees of intensity. If damping is negligible, the

intensity of the primary mode approaches unity, and all others approach zero. If the only

damping is as a result of the plate's inherent material properties and the test specimen is

simple, the modes obtained experimentally will closely approximate the undamped

natural modes (Soedel, 1993). In conducting this research, it has been assumed that only

the primary mode is significant at each natural frequency.

Using the same starting point as for the frequency equation, equations to solve for

modes are derived. Mode shapes are defined by the locations of node lines. For the

cantilevered square plate, Leissa displayed the nodal lines of the first five mode shapes

pictorially as:

Mode 1   Mode 2   Mode 3

Mode 4   Mode 5
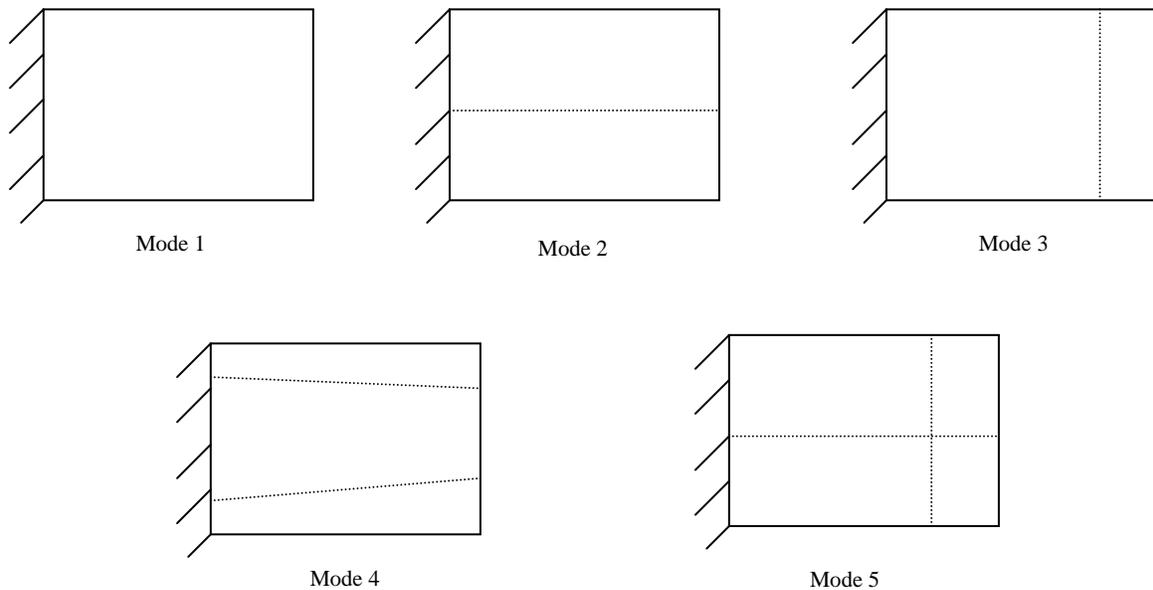
Figure 3. Nodal lines of the first five modes, cantilevered square plate (Leissa, 1969)

These mode shapes are first bend, first torsion, second bend, first chordwise bend, and

second torsion, respectively.

Finite Element Modeling

   Finite element modeling was conducted using NASTRAN version 2000.0.1 for

the uncoated plates. Both the 4-1/4" x 4-1/4" x .050" plate (thin plate) and the 4-1/2" x

4-1/2" x .125" plate (thick plate) were modeled. The thin plate model consisted of 289

grid points and 256 QUAD4 elements; the thick plate model utilized 441 grid points and

400 QUAD4 elements. All nodes along one side were constrained in all six degrees of

freedom, representing a cantilevered boundary condition. No other constraints were

13

assumed. Titanium material properties were obtained from MIL-HDBK-5H, Dec 1998.

SOL 103 statement in NASTRAN was used to determine the natural frequencies,

incorporating the Lanczos method to solve the eigenvalue problem. The consistent mass

parameter was incorporated, which yields an upper bound on the resonance frequencies.

The first twelve resonance frequencies were requested. Relative stress values were

requested as output to determine the location of the maximum stress in each mode.

III. Test Procedures

This chapter outlines procedures followed to obtain test data. Procedures used include dynamic ping testing, sine sweeps, laser holography, laser vibrometry, stress pattern analysis by thermal emissions (SPATE), and resonant dwell. The data collected is presented in Chapter IV, Results and Discussion.

Excitation Methods: Applied Load vs. Boundary Condition

Several different methods were used to excite the vibration modes in the test specimens. These methods comprise two different approaches: applying a load directly to the specimen, and exciting the specimen by applying an acceleration through a base excitation at the clamped end of the plate. Loads were applied directly to the plates by hammers (dynamic ping), air horns (sine sweep, laser vibrometry), and magnetic pulses (sine sweep). Piezo crystals were attached to vises to apply an acceleration for some sine sweep runs and while conducting laser holography; see Fig. 4. Piezos convert electrical energy to mechanical force. As a polarized electrical field is placed across a piezo, the piezo stretches longitudinally, and shrinks through the thickness. As the field is reversed, the movement of the piezo is reversed (Piezo Systems, 2002). This motion of the piezo imparts a force through the vise to which it is attached. The magnitude of the force applied by this movement is dependent on the voltage of the electricity being applied across the piezo. Shakers applied initial accelerations to the specimens undergoing SPATE and resonant dwell.

Each is an equally valid method of excitation. When conducting broadband sweeps to determine resonance frequencies, modes can be missed if loads are applied at nodal lines. As the shakers and piezo crystals apply loads through the boundaries rather than directly to the plate, modes are not missed. A drawback to the boundary condition methods is space consideration: shakers are not portable, and piezo crystals must be attached to a bulky vise.
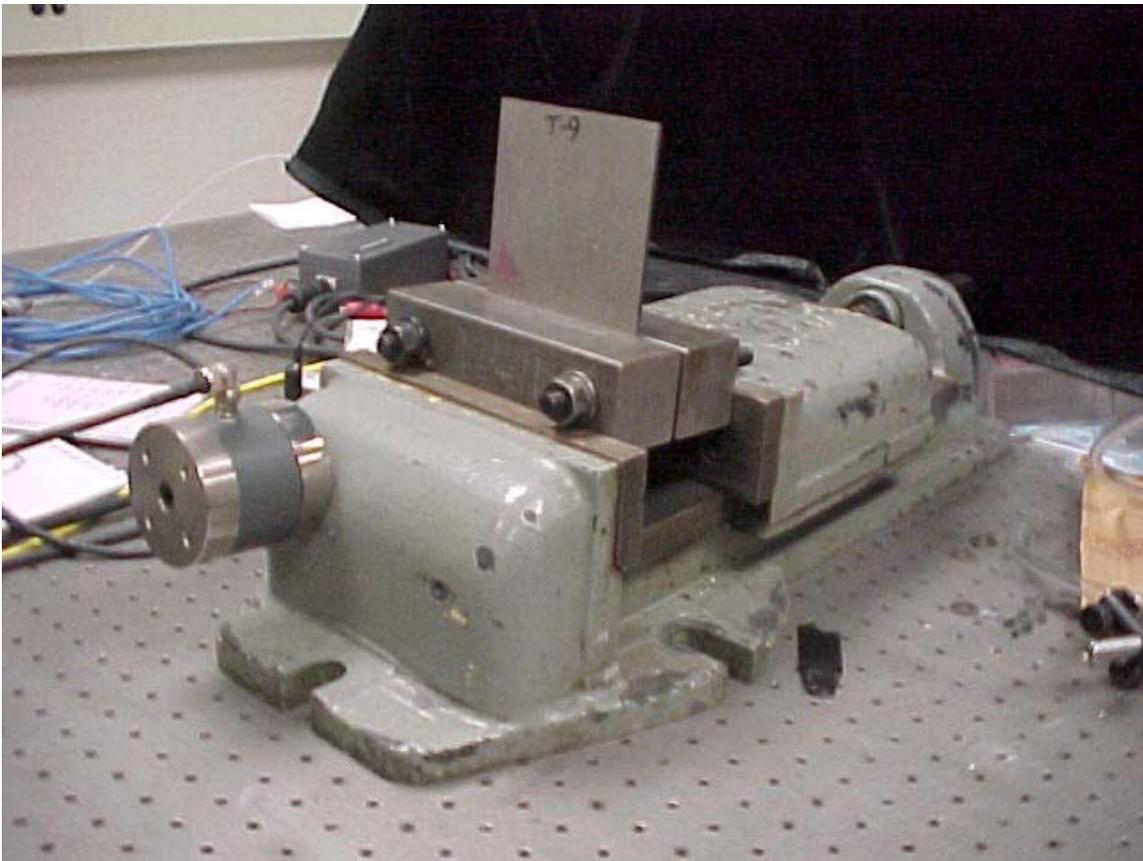
Figure 4. Piezo crystal attached to a vise, which is holding uncoated thick plate T-9. The piezo crystal excites the test specimen by applying an initial condition through the boundary.

Test Specimens

Test specimens were plates of titanium, Ti-6Al-4V. Two different sizes were used. The thin plates were 4-1/4" x 5-1/4" x .050", with a one-inch section to be held in the clamping device, for an effective cross-sectional test area of 4-1/4" x 4-1/4". Twelve plates of these dimensions were obtained for this testing from AFRL/ML. All were cut from the same sheet of titanium. The plates were numbered 116A-1 through 116A-12. Two additional plates of these dimensions were obtained at a different time; these plates were numbered B72 and B76. Upon receipt from AFRL/ML, each plate was measured and weighed. All length measurements were within 1/32"; thicknesses (measured with a NSK Precision Dial Caliper) were within .001". The specimens were weighed with a Pelouze PE5 mass balance. Plates 116A-3, -4, -5, and –6 weighed 80 grams, all others weighed 82 grams.

The thick plates were 4-1/2" x 6-1/2" x .125", with a two-inch section to be held in the clamping device, for an effective cross-sectional test area of 4-1/2" x 4-1/2". Fifteen specimens were acquired, all cut from the same sheet of titanium. The specimens were numbered T-1 through T-15. All lengths were consistent. Weights varied from 262 g (T-1, T-4, T-6, T-13) to 268 g (T-3, T-12). Each plate was weighed twice; six of the 15 plates had a difference of 2 g the second time. No reading was an odd number, indicating the precision of the instrument is probably ± 2 g. From this data, the density of the material was determined:

$$\rho = \frac{m}{V} \qquad (3)$$

$$\rho = \frac{265\,[grams]/454\,[grams/lbf]}{(6.5)(4.5)(0.125)} \qquad (4)$$

$$\rho = 0.159\,lbf/in^3 \qquad (5)$$

This agrees closely with MIL-HDBK-5H, which lists the density as 0.160 lbf/in^3.

      The magnesium aluminate spinel coatings were applied by Air Plasma Spray, Dayton, OH. Thin coatings (.005" each side) were applied to specimens 116A-5 through 116A-8, and T-1 through T-4. Thick coatings (.010" each side) were applied to specimens 116A-9 through 116A-12, and T-5 through T-8. Coatings were only applied to the test areas; the thin plates had a 4-1/4" x 1.0" area uncoated, and the thick plates had a 4-1/2" x 2.0" area uncoated. Plates 116A-1 through 116A-4, B72, B76, and T-9 through T-15 were left uncoated. Coated plate thicknesses were measured using a digital caliper. Measurements were taken at each of the four corners of each plate. For the thin plate, the target thickness was .060" for the thin coating (.050" plate + 2 x .005" coating = .060") and .070" for the thick coating. The thin coating was not uniform from plate to plate, or even throughout any single plate. Thickness varied from .061" to .066" for plate 116A-5; from .059" to .061" for 116A-6; from .061" to .065" for 116A-7; and .063" to .068" for 116A-8. The quality was better on the thick coatings. Variations were: 116A-9: .067" to .073"; 116A-10: .067" to .071"; 116A-11: .069" to .071"; 116A-12: .070" to .072". The quality of the coating application on the thick plates was very good; variation in thicknesses was minimal. See Fig. 5. Tables 1 and 2 identify the thin and thick plates, respectively, that were used in each of the procedures.
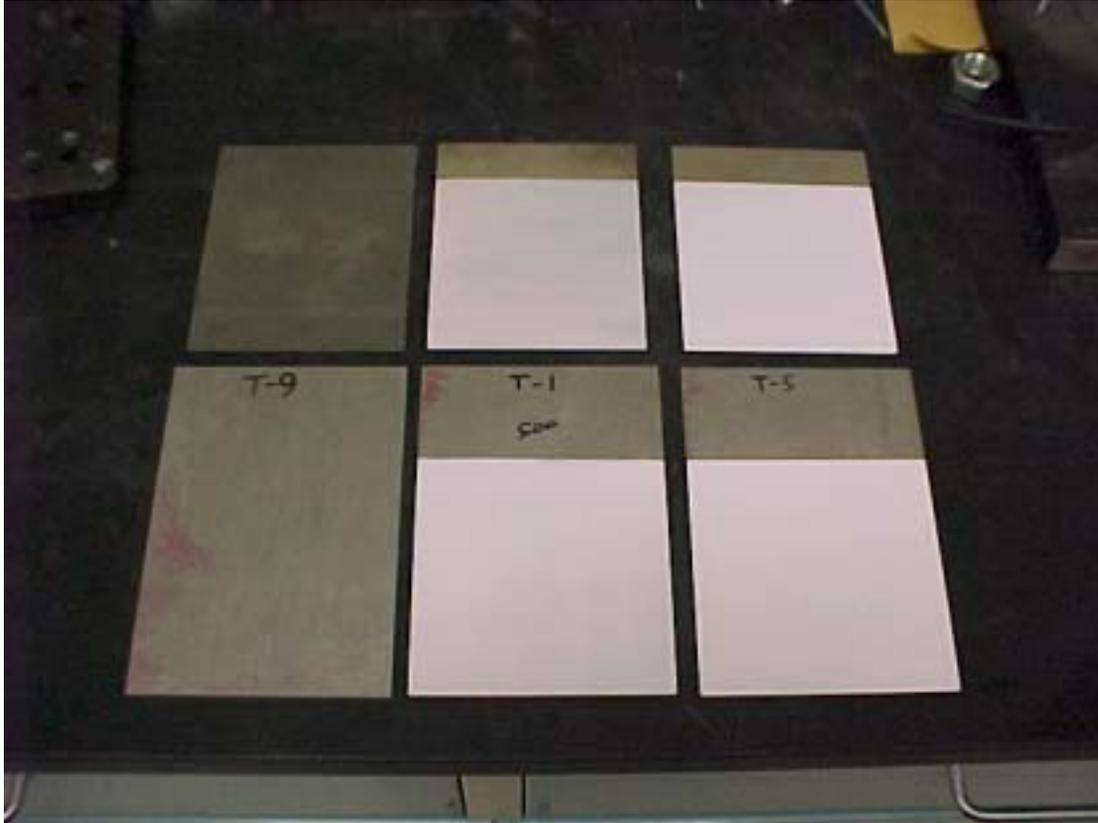
Figure 5. Titanium Plate Test Specimens. Top row: 4-1/4" x 5-1/4" x .050" thin plates; bottom row: 4-1/2" x 6-1/2" x .125" thick plates. Both rows, left to right: uncoated, thin coated, and thick coated specimens, respectively.

Table 1. Plate Usage, Thin Plates

Plate #	Coating Thickness (in., ea.side)	Dynamic Ping	Sine Sweep, B&K	Holography	Vibrometry	SPATE	Fatigue
B72	0.000	X	X	X		X	
B76	0.000		X	X			
116A1	0.000		X				
116A2	0.000						
116A3	0.000				X		X
116A4	0.000						X
116A5	0.005		X				
116A6	0.005				X		
116A7	0.005						
116A8	0.005						
116A9	0.010						
116A10	0.010						
116A11	0.010						
116A12	0.010		X		X		

Table 2. Plate Usage, Thick Plates

Plate #	Coating Thickness (in., ea.side)	Dynamic Ping	Sine Sweep, B&K	Sine Sweep, U-D	Vibrometry	SPATE	Fatigue
T-1	0.010						
T-2	0.010		X	X			X
T-3	0.010						X
T-4	0.010						
T-5	0.005						
T-6	0.005		X		X		
T-7	0.005			X			X
T-8	0.005						
T-9	0.000	X					
T-10	0.000		X	X	X		X
T-11	0.000		X	X			X
T-12	0.000			X			X
T-13	0.000						
T-14	0.000						
T-15	0.000						

Natural Frequency vs. Resonance Frequency

The frequencies determined mathematically and by the finite element method are the undamped natural frequencies, but the frequencies to which they are being compared as measured in the laboratory are damped resonance frequencies. Resonance occurs when a system is forced to vibrate at or near its natural frequency (Rades, 2001). For viscoelastic damping, natural and damped frequencies are related by the damping ratio:

$$\omega_d = \omega_n \sqrt{(1 - 2\zeta^2)} \qquad (6)$$

(Meirovitch, 1986).

This equation does not hold for the damping provided by hard coatings. However, a titanium plate in a cantilevered condition is very lightly damped, providing the boundary condition is good; damping will not cause a significant shift in the natural frequency. Thus, assuming $\omega_r = \omega_n$ does not introduce any significant error into this investigation.

Dynamic Ping Testing

Dynamic Ping is a quick method of obtaining resonance frequencies. In this procedure, a hammer is used to tap the test specimen. This tap generates a random excitation. An accelerometer sends a response signal through an amplifier to a signal processor, which performs a fast Fourier transform (FFT) on the time-dependent data to produce a frequency response curve as output. Peak amplitudes on the curve indicate resonance frequencies. The main advantage in using dynamic ping testing is its portability; all equipment can be stored in two bags the size of laptop computer cases and taken to the test specimen, rather than having to bring the specimen into the laboratory. See Fig. 6.

The test plate had double-sided tape applied to the area to be clamped, to help prevent slippage in the clamp and to prevent fretting. The plate was then placed between two metal mounting blocks, each 2" x 3" x 7". The blocks were secured by two bolts. Three set screws were inserted through one of the blocks to apply pressure to the test plate. One inch of the thin plate (two inches of the thick plate) was held within the mounting blocks, allowing a 4-1/4" x 4-1/4" area subject to vibration. The mounting blocks were secured in a vise.

An accelerometer was attached to the lower left corner of the plate, then connected to an amplifier. A hammer was also connected to the amplifier. The amplifier fed into the Spectral Dynamics Bobcat signal processor, which was attached to a laptop computer for data analysis. The laptop ran Bobcat Data Acquisition software, version 4.00.

The hammer was calibrated to ensure a consistent force was being applied. The test specimen was tapped eight times with the hammer. The software performed ensemble averaging; each successive tap resulted in refinement of the data. Output was an amplitude-versus-frequency curve, with resonance frequencies at peaks of the curve. The procedure was conducted three times, and values were averaged. The procedure was then repeated for the thick plate.
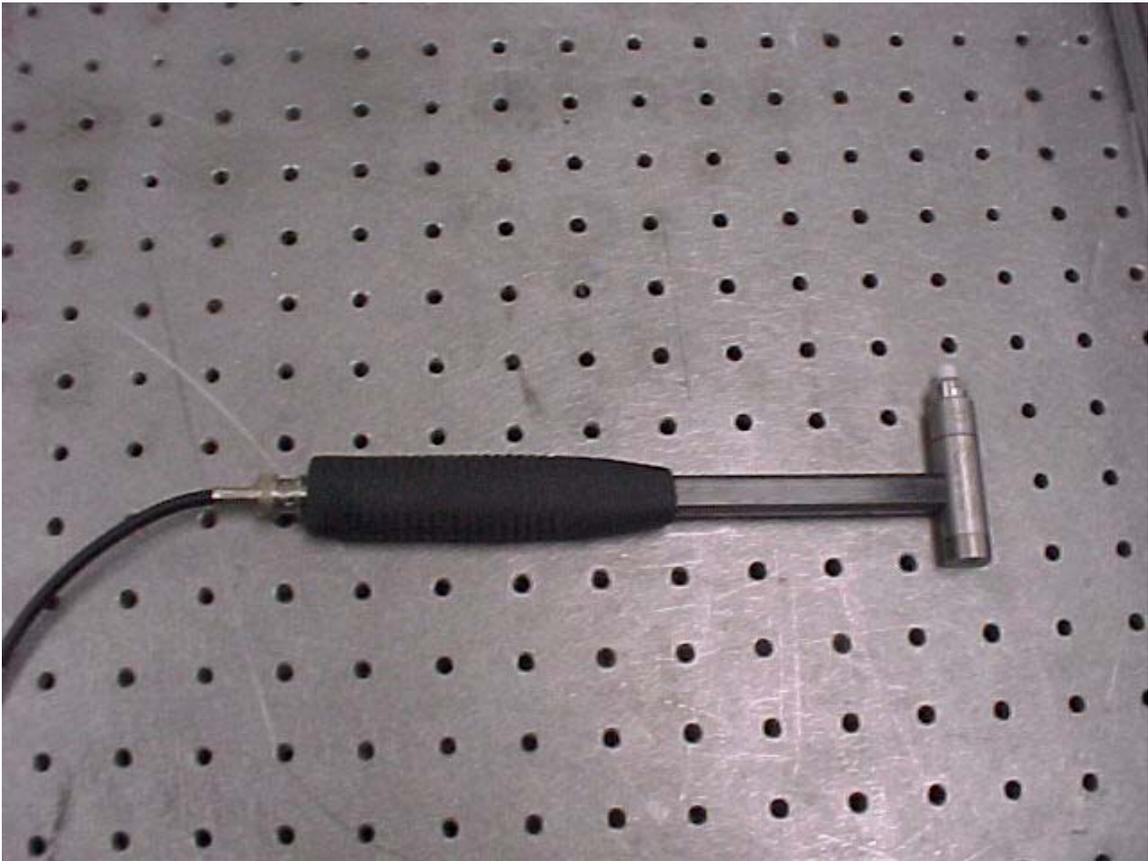
Figure 6. PCB Piezotronics Modally Tuned Hammer, the excitation source for the Dynamic Ping test. The wire at the base transmits the applied force through an amplifier to the control software for comparison to the response.

Sine Sweeps

Sine sweeps were conducted using the Bruel & Kjaer (B & K) system, running the PULSE LabShop software, version 5.1. Sine sweeps are used to determine resonance frequencies and structural damping of the test specimens. See Fig. 7.

The test specimen was loaded into mounting blocks, as in the Dynamic Ping test. For the thin plate, a magnet was used as the excitation source. As titanium's magnetic properties are low, a small cobalt disc was glued to the plate, and the magnet pulsed the plate through the cobalt disc. The mass of the disc was extremely small; the resultant mass loading was minimal. The magnet was controlled by a Hewlett-Packard Model 3325B function generator, which was attached to the B & K. An accelerometer was attached to the plate with wax, and fed into a Kistler Type 5010 amplifier, which was attached to the B & K.
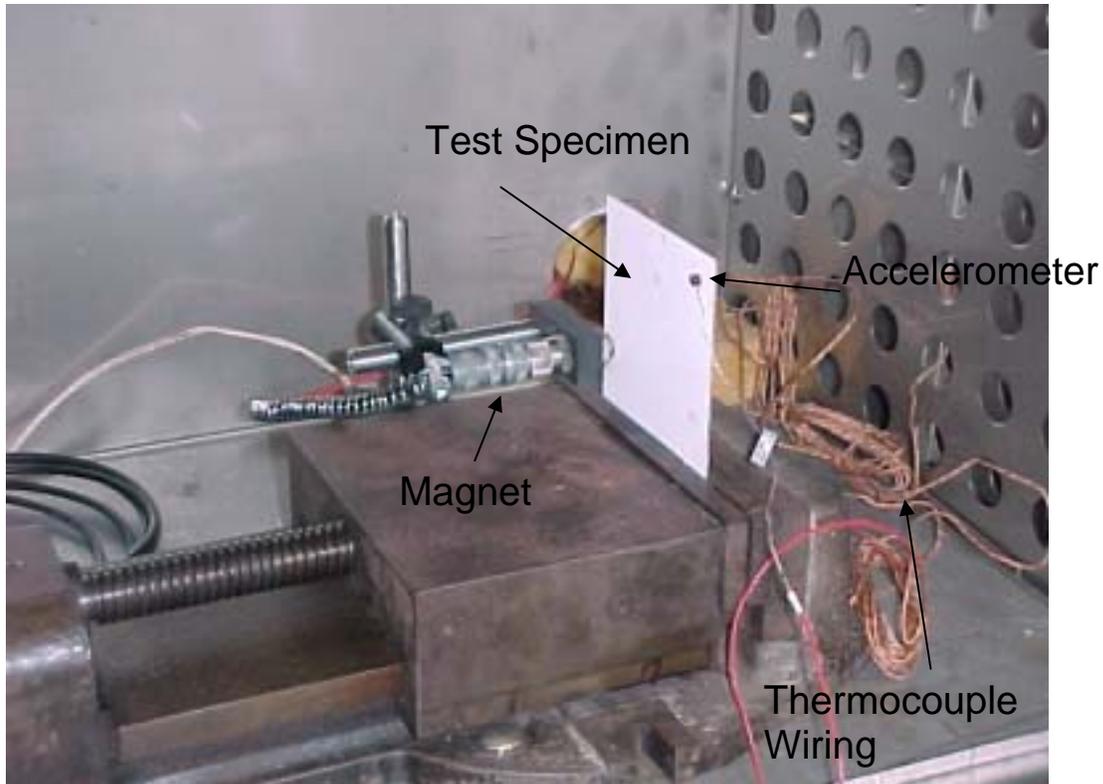
Figure 7. Test plate in oven, set up for sine sweep at elevated temperature. Mounting blocks are not used in this configuration.

The function generator was set for a sine sweep, the frequency range to be swept (50-3,200 Hz), time (200 seconds), and voltage (5V peak-to-peak).

The software takes as input the signal being used to excite the test specimen as a function of time, and the response of the plate as measured by the accelerometer as a function of time. It compares the reference signal to the response signal, and converts this time-dependent data into the frequency domain by conducting a fast Fourier transform. The output is an amplitude (in decibels) versus frequency (in Hertz) graph; see Fig. 8. Resonance frequencies are at the peaks on the graph. Damping is a function of the shape of the curves, and is determined by the half-power method. The half-power is calculated by dropping down three decibels from the peak and measuring the

bandwidth (the width of the frequency curve) at that point (Meirovitch, 1986). The

damping ratio, in percent, is found from

$$\zeta = \frac{\Delta\omega}{2\omega_n} \qquad (7)$$

As an example, if the resonance frequency is 692 Hz, and the width of the curve 3 dB

below the peak is 23.9 Hz, then the damping ratio is

$$\zeta = \frac{23.9}{2(692)} = 0.0173 \text{ or } 1.73\% \qquad (8)$$

The LabShop software determines the -3 dB point, the width of the curve at this point,

and calculates the damping ratio.

While the damping parameter output by the LabShop software is the damping

ratio, the parameter most commonly used in damping investigations is the quality factor,

Q. The damping ratio is the mathematical quantity represented by ζ in the equation of

motion for the common mass-spring-damper model:

$$\ddot{x} + 2\zeta\omega_n\dot{x} + \omega_n^2 x = F(t) \qquad (9)$$

The quality factor was developed by electrical engineers as a measure of the clarity of a

signal. The quality factor is inversely proportional to the damping ratio. They are related

by:

$$Q = \frac{1}{2\zeta} \qquad (10)$$

(Meirovitch, 1986). For the example in Eq. (10),

$$Q = \frac{1}{2(0.0173)} = 28.9 \tag{11}$$

As damping increases, ζ increases, and Q decreases. Electrical engineers looking to improve signal quality desire a high Q value, while mechanical engineers trying to dissipate energy from a system desire a low Q value.
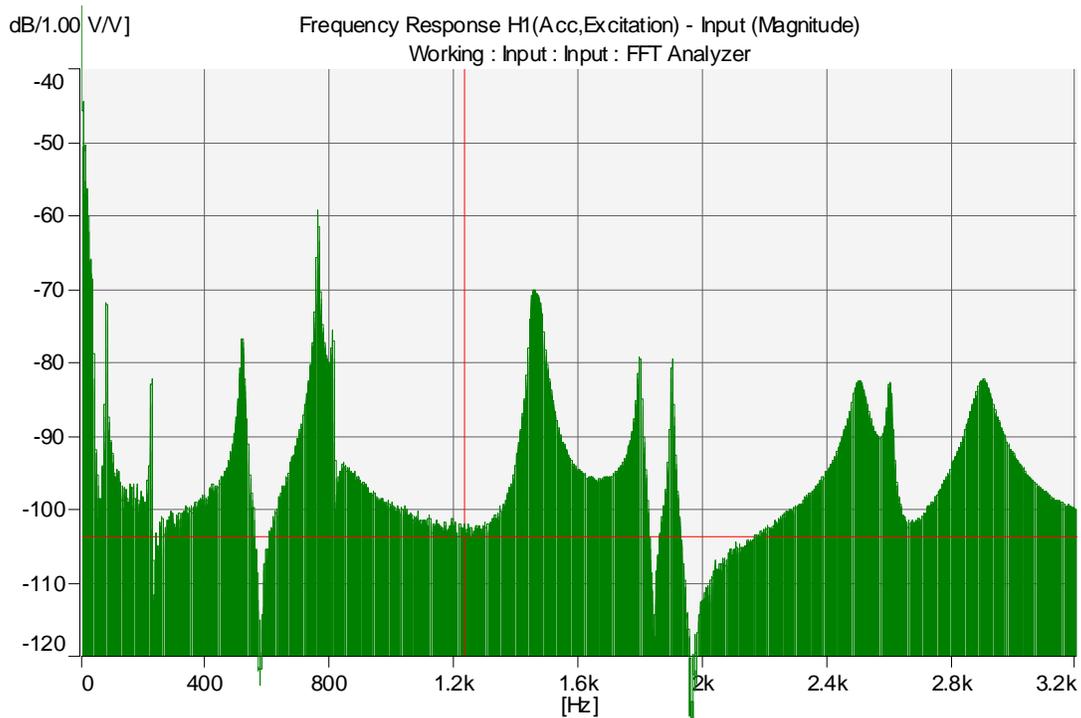
Figure 8. Broadband sine sweep of an uncoated thin Ti-6Al-4V plate. Peaks are resonance frequencies; steepness of peaks determines damping.

There are eleven peaks in Fig. 8, each indicating a different resonance mode (the high amplitude at 0 Hz is not a resonance frequency; the sweep was started at 50 Hz). The y-scale has been converted to decibels by the software (by multiplying 20 times the natural logarithm of the measured value), so the half-power method can be used to determine the damping. The resonance frequencies and damping values are obtained by

26

placing the cursor at each peak (the intersection of the two red lines in the figure). The responses for the two modes below 400 Hz are very weak; the magnet does not do a good job of excitation at low frequencies (this can be seen by examining the coherence graph, which has not been presented here. Several examples are in Chapter IV for the thick plate). At just below 800 Hz, there are two peaks very close together. Visually, it cannot be discerned if they are separate modes, or part of the same mode. By examining the mathematical and finite element models, as well as the mode shapes obtained through vibrometry, we see that there are indeed two modes in this range. If other methods were not available to which these modes could be compared, conducting a slow sweep over a narrower band in this region would provide better resolution for these modes. Sharp valleys appear at three frequencies on this graph; around 600 Hz, 1800 Hz, and 1950 Hz. These are anti-resonance points. Anti-resonance is a localized condition where the system most strongly resists vibration (Rades, 2001).

For the thin plate, the sine sweep procedure was conducted twice for each plate (uncoated, thin coated, and thick coated), and the frequency and damping values obtained were averaged.

For the thick plate, an air horn was used as the excitation source. Plates were loaded into 2" deep mounting blocks, which were held in a vise. Double-sided tape was not used. The accelerometer used was a charge-type. It was placed 1.3" up from the clamped end, 0.3" in from the edge. The air horn was placed at about the same position on the opposite edge of the plate, as close to the plate as possible without touching. PULSE version 6.1 software was used to control the procedure and analyze the data. A function generator internal to the B&K system controlled the signal. Specimens used in

this procedure were T-11 (uncoated), T-2 (thin coated), and T-6 (thick coated). In the characterization of the thin plate, a single sweep of about 3,000 Hz was conducted on each specimen. To observe the first ten modes of the thick plate, 6,000 Hz needed to be swept. To ensure reasonable resolution, the sweep was divided into 400 or 800 Hz segments. For the uncoated plate, sweeps were run at the following bandwidths: 0-400; 400-800; 750-1,150; 1,000-1,400; 1,400-2,200; 2,200-3,000; 3,000-3,800; 3,800-4,600; 4,600-5,400; 5,400-6,200. The first, second, and fourth runs were conducted at a sweep rate of 25 Hz/sec (parameter in control software); all others were conducted at 100 Hz/sec. The slower sweep rate provides better clarity, but takes longer than the fast rate. The faster rate was used where the better clarity was not needed. All runs were conducted at a voltage of 3.0 volts, root-mean-square. Data was averaged five times by the software.

Based on results from the uncoated specimen and resonance frequency data obtained from laser vibrometry, the bandwidths of the sweeps on the thin coated and thick coated plates were adjusted, so that the same data that took 10 runs to collect for the uncoated plate was collected in 6 for the coated plates. The following bandwidths were swept: 0-400; 400-800; 1,100-1,900; 3,000-3,800; 3,700-4,500; 5,000-5,800. The first two bandwidths were swept at 25 Hz/sec; all others were swept at 100 Hz/sec. All other setup parameters were the same as for the uncoated plate.

For the thick plate, the Unholtz-Dickie 6,000-lb. shaker system was used to conduct sine sweeps at higher amplitudes of applied force. The controlling software, VWIN, version 4.74, was similar to the PULSE LabShop used by the B&K system, except that it calculated damping in terms of Q, rather than ζ. The system could only

28

scan a limited frequency range, so only the first five modes were obtained by this method. The setup is described in the "Resonant Dwell" section of this chapter.

For elevated temperature testing, a thin uncoated plate and mounting blocks were placed in a Blue M oven. This oven had an analog temperature control, and no window to observe the test apparatus inside. An accelerometer was glued to the plate (the wax used at room temperature has a melting point below the elevated temperature test point, and thus is not an effective medium for attaching the accelerometer for this test). The air temperature in the oven was measured using an Omega Monogram digital thermometer. (Attaching a thermocouple directly to the test specimen would have added mass and damping to the specimen, resulting in skewed values for resonance frequencies. While this is also true of the accelerometer, there is no non-contact method of measuring response in this setup.) See Fig. 7. Once 275 F was reached, the system was allowed to soak for a period of one hour, to ensure the test specimen was at the same temperature as the air to reduce thermal gradients and transients.

A second procedure was developed for temperature testing of the thick plates, utilizing a free-free-free-free boundary condition. Both ends of a thin wire were welded to one of the short sides of a thick uncoated plate. This wire was used to suspend the plate from a test stand in an Espec oven. (As no clamp was used, the test section was 6 ½" x 4 ½", rather than the 4 ½" x 4 ½" in the cantilevered condition. Since the intent is to measure relative damping between three specimens of the same size in this condition, this is okay.) An electromagnet was used to excite the specimen. The specimen's velocity was measured with a laser vibrometer; the oven had a small opening in one side through which the beam could be sent. To measure material temperature, a thermocouple

was attached a second plate, which was identically configured and likewise placed in the oven. Unlike the Blue M oven, this oven is digitally controllable, and is capable in reducing the temperature from ambient. The software was configured to drop the temperature to 35 F, wait for the temperature of the material to stabilize, measure damping at this temperature, raise the temperature 25 F and hold until stable, measure the damping, and continue until 250 F was reached and measured. The data was analyzed using MATLAB. The procedure was then performed on a thick coated plate. See Figs. 9 and 10.
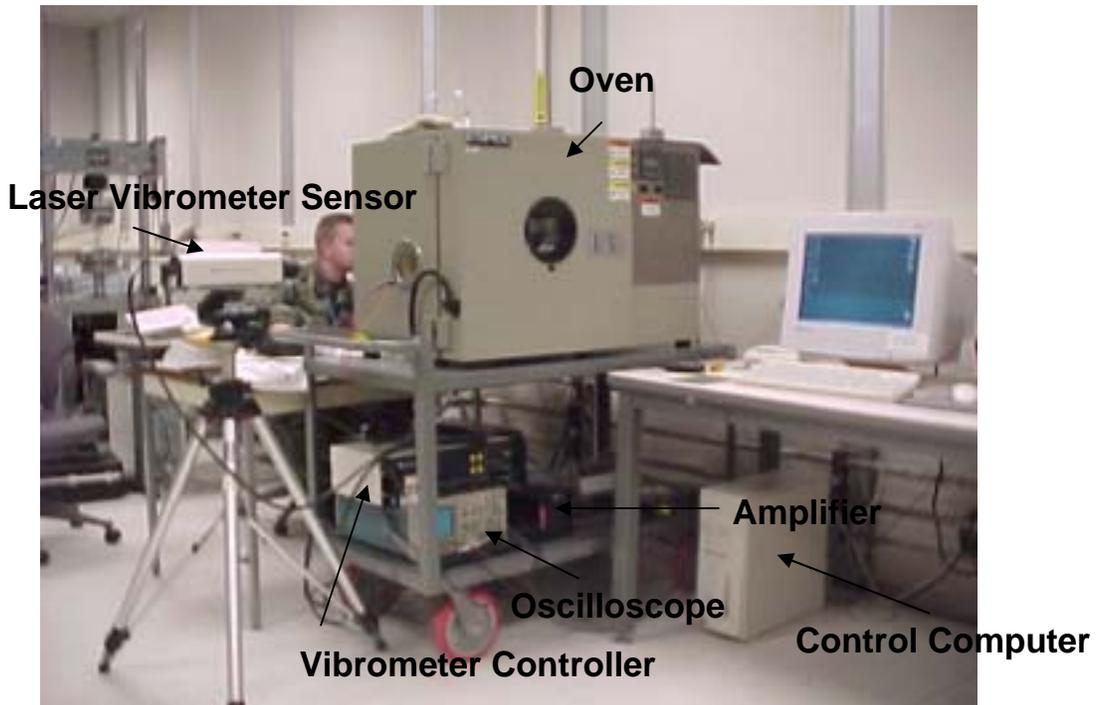
Figure 9. Test Equipment Setup, Elevated Temperature Testing, Free-Free-Free-Free Boundary Condition.
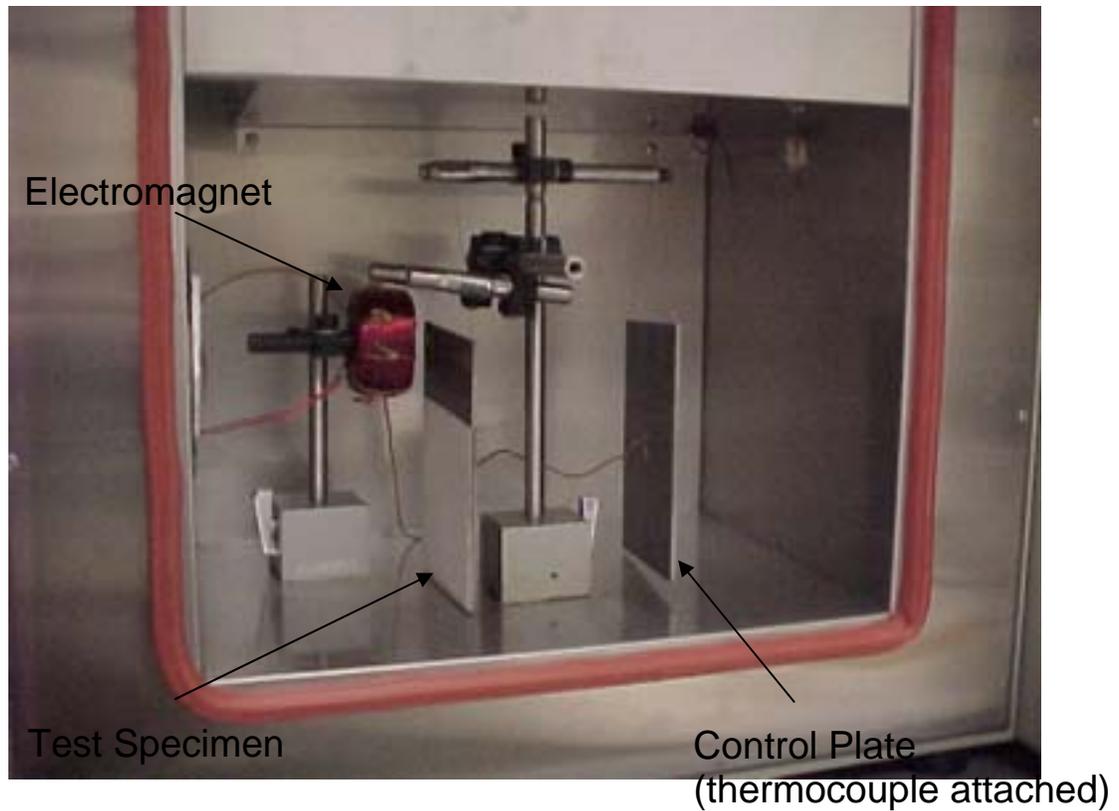
Figure 10. Test Specimen Setup (inside oven), Elevated Temperature Testing, Free-Free-Free-Free Boundary Condition.

Laser Holography and Laser Vibrometry

Laser holography and laser vibrometry were used to identify the mode shapes at each resonance frequency. Holography is an optical process. The system compares images of the motionless specimen with that of the specimen being excited. When a resonance frequency is reached, bands appear in the image, denoting relative displacements. One face of the specimen was sprayed with Magna-Flux Spot Check SKD-S2 Developer, a white powder, to provide contrast and aid in viewing. The plate was held in a similar manner as in the sine sweep procedure: in mounting blocks, which were held by a vise. The vise was bolted to the table, and the table was floated, to

prevent interference from other vibration sources. A black curtain was placed behind the setup, to contrast with the white plate. A piezo crystal was used as the vibration generator. It was attached to the vise (which means boundary imposed displacement). A test lead connected the piezo crystal to an amplifier, which was connected to a computer through a transformer box. In addition, a NEC model TI-324A CCD camera was connected to the computer. The control software was PCHOLO. See Fig. 11.
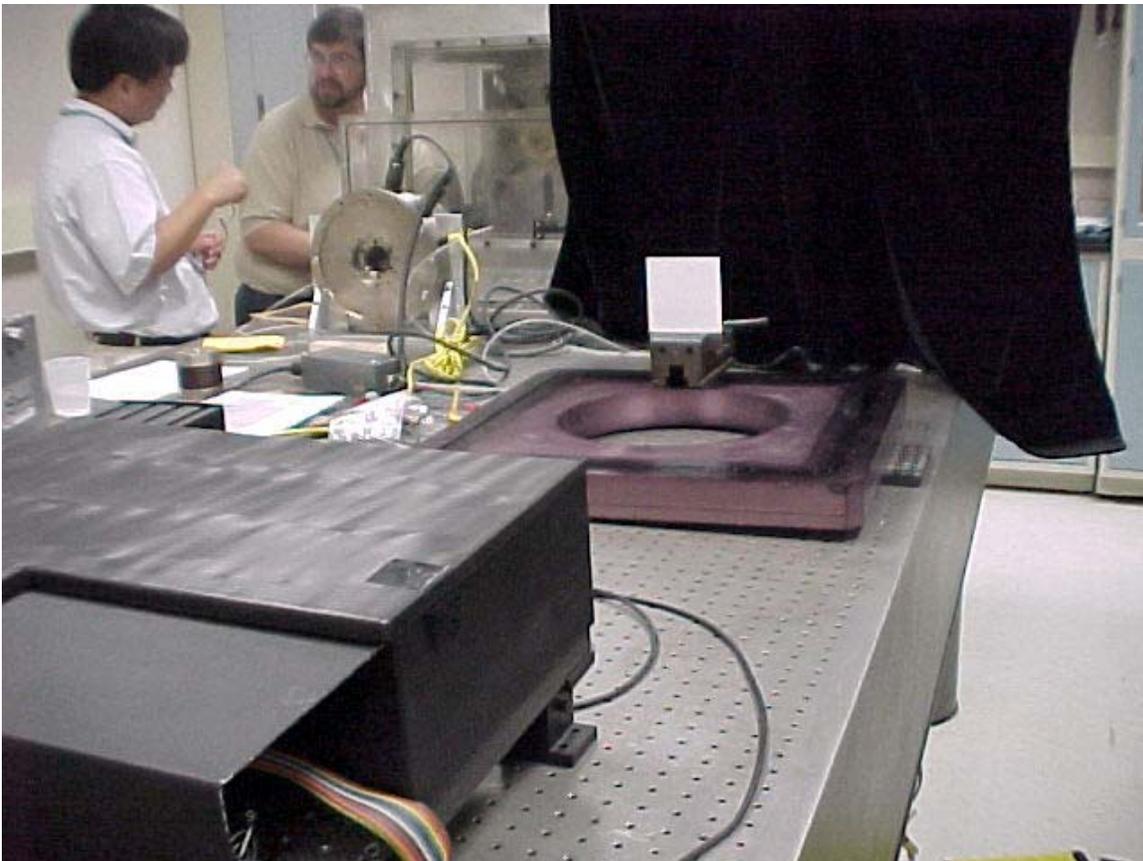
Figure 11. Laser holography setup. Camera is in foreground, test plate is in front of curtain.

Holography was only conducted on the thin plate. The mode shape information obtained from the holography procedure can also be obtained from the vibrometry

procedure, which is easier to conduct, is more precise (as it is a quantitative procedure, while holography is qualitative), provides clearer pictures, and also provides three-dimensional video of the mode shapes. Thus, vibrometry was conducted in lieu of holography for the thick plate.

Vibrometry is a non-contact procedure, where a laser is used to determine and map the velocity of a vibrating object at discrete points. The Laser Doppler Vibrometry system utilizes the concept of interferometry to measure the velocity (and displacement) of the vibrating object. Interferometry is the optical interference between two coinciding light beams. The intensity of the coincident beam is a function of the phase difference between the two individual beams (in this case, the reflected or modified beam, and the reference beam):

$$I(\Delta\phi) = \frac{I_{max}}{2}(1 + \cos(\Delta\phi)) \tag{12}$$

The phase shift is related to the path difference by:

$$\Delta\phi = 2\pi \cdot \frac{\Delta L}{\lambda} \tag{13}$$

where λ is the wavelength of the laser and the path difference, ΔL, is a function of time if one of the beams is scattered back from a moving object. The reflected beam also undergoes a Doppler shift in its frequency, which is a function of the object's velocity:

$$f_D = 2 \cdot \frac{|v|}{\lambda} \tag{14}$$

(Polytec Laser Doppler Vibrometer User Manual)

The vibrometry system determines the velocity of the vibrating object from the Doppler shift and the known wavelength of the laser. Given the right software, it can

also determine displacement by measuring the intensity of the beam and the phase difference. This software is not available in the Turbine Engine Fatigue Facility.

The Polytec Laser Doppler Vibrometer system is comprised of two parts: the controller (OFV-3001) and the sensor head (OFV-303.8). See Figure 12. Two types of sensor heads are available: single point and scanning lasers. When velocity is used as a control parameter in a test (such as the elevated temperature testing in Fig. 9, or fatigue testing), the single point laser is used. The scanning laser is used to find velocities at multiple points on the specimen, which is what is needed to determine mode shapes. Test parameters are input to the controller, which controls the sensor head. The sensor head generates the beam, which is split into the reference beam and the object beam. The object beam is reflected off of the test object and returned to the sensor head as the modified beam. It is combined with the reference signal and sent to the controller, which compares the frequencies and phases and calculates velocities and displacements. This procedure is repeated for 25 points on the test object (5x5 grid), with the result being a map of the velocity as a function of position along the object.

One specimen from each group (thick and thin plates; uncoated, thin coated, and thick coated) went through the vibrometry procedure. The air horn was used as the excitation source. A broadband sweep (to 3,000 Hz for the thin plates, to 6,000 Hz for the thick plates) was run first to locate the resonance frequencies, then a fast scan procedure (shorter time, narrower frequency band) was run at specific frequencies to generate better detail for modes of interest. For the thin uncoated plate, fast scans were run at each of the first eight modes; for the other specimens, fast scans were only run for the third (second bending) and fourth (first chordwise bending) modes.
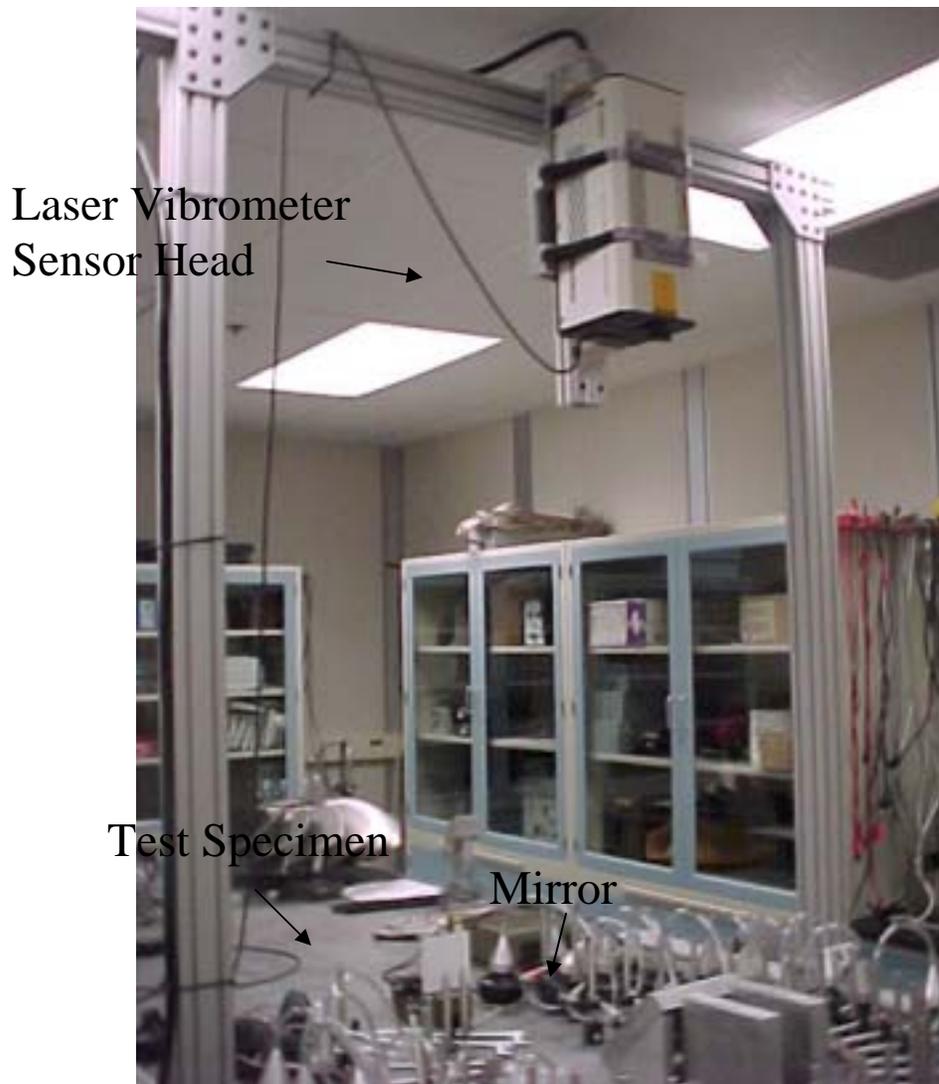
Figure 12. Laser Vibrometry setup. The sensor head is hung overhead. The beam reflects off of the mirror to the test specimen, and returns to the sensor head the same way.

SPATE

SPATE is a thermal imaging system. As a cyclic load is applied, a temperature gradient develops across the plate. The SPATE system senses the minute temperature differences, makes a comparison to a reference load signal, and determines and maps the peak-to-peak sum of the principal stresses (Gucfa, 1986).

In the Holography process, the test specimen needed to be white to provide a useable image; for SPATE, it needs to be black. The white powder coating applied for Holography was removed, and the specimen was sprayed with a flat black enamel. Double-sided tape was applied to the area of the plate to be clamped. The plate was loaded into mounting blocks attached to a MB Dynamics 100-pound shaker; which applies an acceleration to the plate through the base; see Figure 13. An accelerometer was attached to the plate with wax, ½" up from the clamp, ½" in from the edge. The accelerometer fed into an oscilloscope, through an amplifier. The resonance frequency was refined by maximizing the amplitude of the response signal on the oscilloscope. The shaker was controlled by a Hewlett-Packard model 3325B function generator, which was connected to the shaker through a power amplifier. The function generator also sends a reference signal to the SPATE controller, a desktop computer with Delta Vision version 11 software installed and running. The function generator was set to generate a sine wave. The frequency input to the function generator was selected to generate a resonance condition according to the results of the sine sweep, then was adjusted to maximize the amplitude on the oscilloscope. The Delta Vision software controlled the optical equipment, which was also made by Delta Vision. See Figure 14.

In executing the process, the camera scans the test area of the specimen, and the software produces a colored map of the stress along the plate. In order to calibrate the scale of the map to determine the principal stresses at any point, it is necessary to measure the strain by attaching strain gages (Gucfa, 1986). For the work conducted in this thesis, it was only necessary to evaluate stress patterns; strain was not measured.
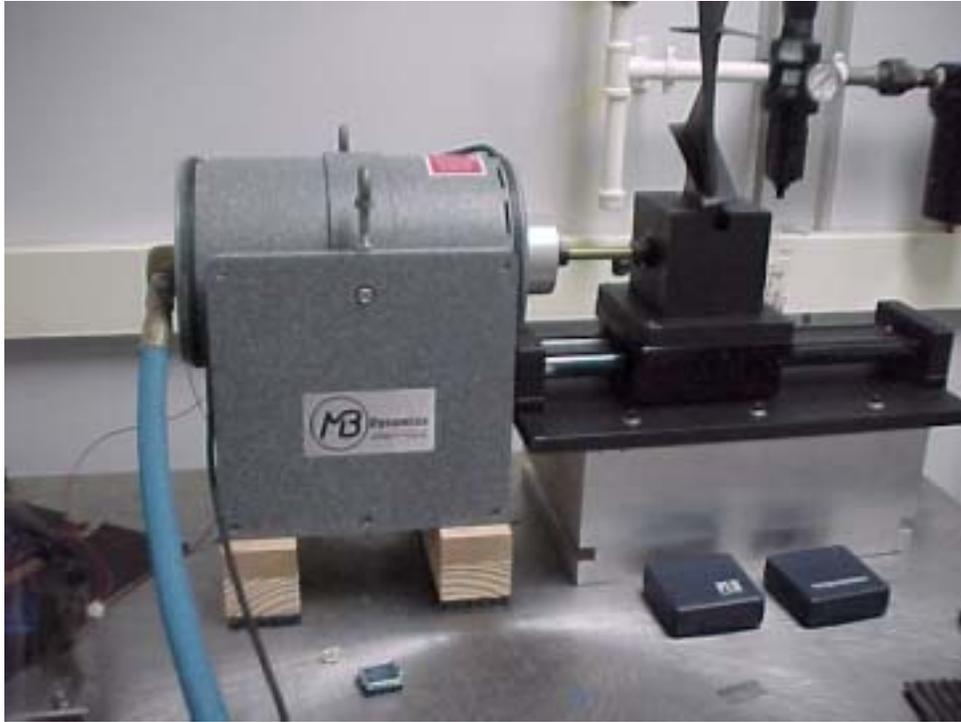
Figure 13. MB Dynamics 100-Lb. Shaker
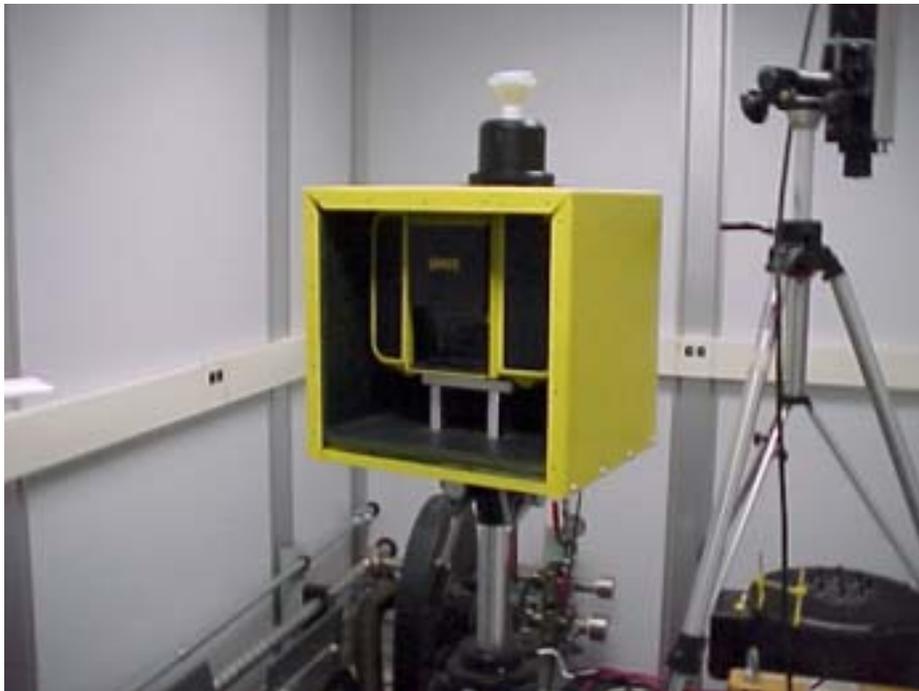
Figure 14. Delta Vision SPATE Optical System.

Resonant Dwell

      Resonant dwell was conducted on the thick plate specimens for the two-stripe

mode using a 6,000 lb. shaker. The two-stripe mode has a region of high stress at the

edge opposite the clamp, which is characteristic of high order modes. The target

endurance limit was 1,000,000 cycles. The fatigue limit stress was determined to be 77

ksi for 1,000,000 cycles from a constant life diagram (Henry, 1995). Values for Young's

modulus, Poisson's ratio, and density for Ti-6Al-4V were found in Mil-Handbook-5H.

The strain at failure was determined by Hook's Law:

$$\sigma = E\varepsilon \tag{15}$$

$$77{,}000 = (16 \times 10^6)\varepsilon \tag{16}$$

$$\varepsilon = 0.0048 \text{ in/in, or 4,800 microstrain } (\mu\varepsilon) \tag{17}$$

Estimated time to failure was calculated by dividing the target endurance limit by the

frequency at which the specimen would be excited.

$$t = \frac{1000000}{1600} = 625 \text{ sec, } = 10.4 \text{ min.} \tag{18}$$

      The test specimen was clamped between two mounting blocks, which were bolted

horizontally to the shaker. See Figure 15. A laser was used to measure the velocity of

the specimen. The laser vibrometer sensor head was hung from a frame above the

specimen, and leveled. It was aimed at a reflective target attached to the specimen near,

but not on, a node line. For the two-stripe mode, this target was placed 3.0" down from

the edge opposite the clamp, and 0.50" in from one side. An accelerometer was fixed to the base plate of the shaker. A strain gage was attached to the specimen at the anticipated point of maximum stress, as determined by SPATE. See Fig. 16. The system was controlled by Unholtz-Dickie VWIN software, version 4.74.

A sine sweep was run to determine the resonance frequency. As the response is non-linear (not symmetric about the resonance frequency), the sweep was run down, rather than up. The SmartOSC routine was run, which controls the resonant dwell process. The frequency was set at the determined resonance frequency. The initial acceleration condition at the clamp was varied, and the velocity and strain were measured at each setting, until the strain gage failed. At each acceleration, the frequency was varied to maximize the response. Displacement was determined by:

$$\delta = \frac{v}{\omega} \tag{19}$$

where

δ = displacement

v = velocity

ω = frequency, in radians/sec

From this data, a strain vs. displacement relationship was graphed; the curve was linear, and the displacement at the target failure strain of 4,800 $\mu\varepsilon$ was determined using the slope of the line. The velocity needed to generate 4,800 $\mu\varepsilon$ was determined from the displacement. Using the VWIN software, the acceleration of the shaker was increased until this velocity was reached. The resonance frequency was monitored. As the specimen began to fatigue, the resonance frequency dropped. The frequency of the

excitation force was manually altered to maintain the resonance condition. Failure occurred when the target velocity could no longer be maintained.

To compare the coated plates to the baseline uncoated, the coated plates were excited at the same velocity as the uncoated, which results in an equivalent displacement, and thus an equivalent strain. As the strain is the basis for the fatigue of the material, it is anticipated the titanium alloy will fatigue at the same stress when coated as it did when uncoated. However, as the coating increases the damping, it is anticipated more force will be required to displace and strain the plate with the coating added than was required for the uncoated specimens. As force varies linearly with acceleration, and the mass is not changing significantly, comparing the change in acceleration between the specimens is equivalent to comparing the applied force. It should be noted that the acceleration is being measured at the boundary, not on the specimen; the value of the acceleration cannot be used to evaluate the force at any point on the specimen. However, as the intent is only to compare similar specimens to each other, and the boundary conditions are the same between trials, this limitation on the acceleration is acceptable.
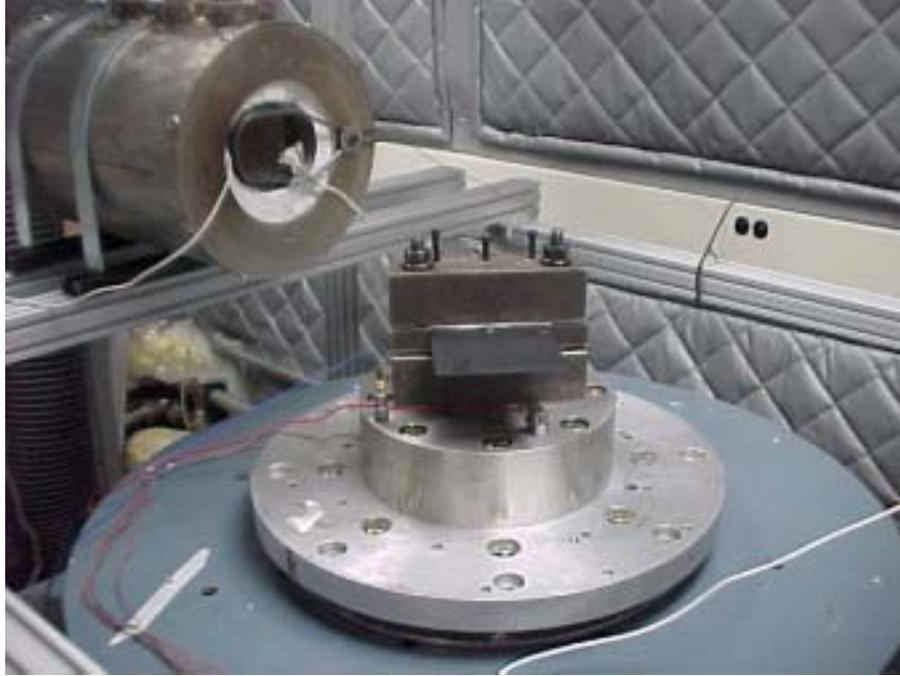
Figure 15. Thin test plate mounted on 6,000 lb. shaker.
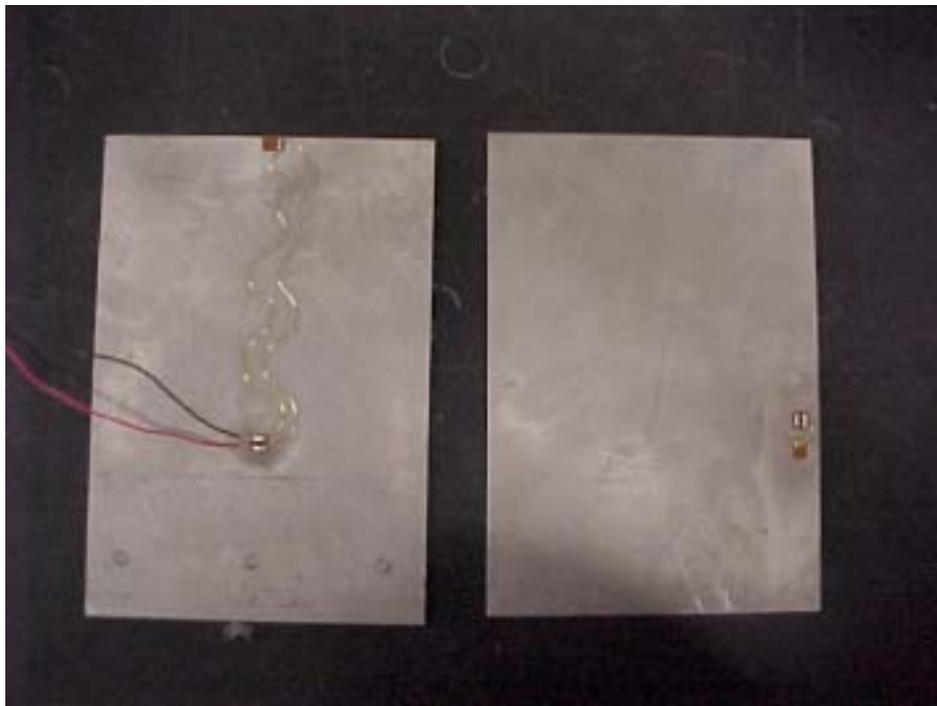
Figure 16. Strain-gaged thick plates. Left plate is gaged for testing at two-stripe mode; right is gaged for testing at second bend mode.

Initially, fatigue testing was conducted on the thin plates. However, the amount of energy needed to fatigue these plates could not be generated by the equipment available, so the thick plates were substituted.

Strain gages were not attached to the coated plates. The gages did not bond well to the coating, and in this configuration, they would not measure the strain in the plate, but rather the strain in the coating. Thus, the strain-displacement curve generated for the uncoated plates was used for the coated plates, as well.

IV. Results and Discussion

Resonance Frequencies

Resonance frequencies were determined by dynamic ping testing, sine sweeps, and laser vibrometry, and were compared in certain cases to the natural frequencies predicted by Classical Plate Theory and the finite element analysis model. (As noted in Chapter III, the difference between undamped natural and damped resonance frequencies is insignificant for lightly damped titanium.) Determining the exact value of each resonance frequency by any of these methods is not an end unto itself. What is of interest is the mode shape and damping at each mode, and the comparison of the resonance frequencies of the uncoated plates to those of the coated plates. Classical Plate Theory gives the theoretical values for the uncoated plates, but only for the first five modes. If there is good correlation between the theoretical values and the values predicted by finite element analysis, the finite element predicted values can be used as a benchmark for comparison of the experimental values.   The variation between the resonance frequencies determined from experimentation and the theoretical values is a result of experimental differences, such as varying boundary conditions.

The resonance frequency is determined from peaks on a frequency response curve for each of the three experimental methods. In dynamic ping and sine sweeps, peaks can be generated by noise and shadows of natural modes (which can occur at multiples of resonance frequencies), as well as actual modes, and there is no way to differentiate between the actual modes and the noise or shadows. The vibrometry procedure yields not only the resonance frequency, but also the mode shape. Thus, noise and shadows can

be filtered out by checking the shape at each peak on the frequency response curve. A true mode will provide a recognizable shape. By comparing the dynamic ping and sine sweep results to the vibrometry results, the vibrometry results can be used to eliminate extraneous peaks from the other two test methods.

Theory and Finite Element Analysis. The first twelve natural frequencies as determined by NASTRAN are compared to mathematical predictions from Classical Plate Theory (first five frequencies) and test data for the uncoated thin and thick plates in Tables 3 and 4, respectively. The mesh in the finite element model was fine enough to provide results within 2% of the theoretical values for both the thin and thick plates. Thus, it is probably safe to assume the other seven modes determined by the finite element model are fairly accurate representations of the modes predicted by theory.

Experimentally-Determined Resonance Frequencies. Frequency was varied from 50 to 3,200 Hz for the thin plate, and from 50 to 6,000 Hz for the thick plate. For the thin plate, twelve natural frequencies were identified in the range. The variation between the resonance frequencies found in test and those predicted by the finite element model are within 10%, with a few exceptions. Variation was found between test runs, as well. These variations can be attributed to several factors, the primary one being the boundary condition created by the clamp. The type and size of clamp used, and the torque applied in tightening the bolts on the clamp made a significant difference in the resonance frequencies obtained.

Effect of Plate Thickness on Resonance Frequency. Comparing the results obtained from laser vibrometry, adding the thin coating caused an increase in resonance frequencies of 5 to 16% from the uncoated plate; the thick coating added an additional 2

to 6% increase above the thin coated frequencies.   Results were not as consistent with the sine sweep method; in some cases, increasing the thickness caused the resonance frequency to decrease. The magnitudes of the changes between the thin coated and uncoated plate resonance frequencies were much lower in the sine sweep characterization than they were when determined by vibrometry. While in the vibrometry, the increases were 5% or more, the magnitude of the change in the sine sweep method was less than 2% for 11 of the 12 modes. The frequency changes between methods were much more comparable going from the thin coated to the thick coated plate. See Tables 5 and 6.

Table 3. Comparison of predicted to measured natural frequencies for the 4-1/4" x 4-1/4" x .050" uncoated thin plate. Frequencies are in Hz.

Mode #	Mathematical Calculation	Finite Element Method	Test Results - Dynamic Ping	Test Results - Sine Sweep	Test Results - Vibrometry
1	92.0	91.2	90	82	76
2	225.0	221.7	214	199	206
3	564.8	560.1	529	501	490
4	723.3	714.8	---	742	706
5	820.7	810.0	765	756	758
6	---	1,414.8	1,350	1,388	1,324
7	---	1,631.5	1,570	---	1,404
8	---	1,699.7	1,670	1,668	1,634
9	---	1,880.2	1,800	1,850	1,804
10	---	2,441.5	2,400	2,429	2,308
11	---	2,546.3	2,660	2,462	---
12	---	3,216.8	2,940	2,893	---

Table 4. Comparison of predicted to measured natural frequencies for the 4-1/2" x 4-1/2" x .125" uncoated thick plate. Frequencies are in Hz.

Mode #	Mathematical Calculation	Finite Element Method	Test Results - Dynamic Ping	Test Results - Sine Sweep	Test Results - Vibrometry
1	205.2	203.1	180	198	188
2	501.7	492.2	450	480	465
3	1,259.4	1,242.9	1,100	1,202	1,147
4	1,612.8	1,586.0	1,600	1,633	1,610
5	1,830.2	1,792.5	2,230	1,742	1,685
6	---	3,122.7	2,930	3,098	3,024
7	---	3,592.0	3,215	3,487	3,319
8	---	3,749.3	3,550	3,781	---
9	---	4,135.3	3,970	4,121	4,051
10	---	4,576.5	---	---	---
11	---	5,364.9	5,175	5,439	5,339
12	---	5,585.8	---	---	---

Table 5. Resonance Frequencies Obtained by Sine Sweeps, Room Temperature, Thin Plate

Mode #	ω, Uncoated Plate (Hz)	ω, Thin Coated Plate (Hz)	% Diff	ω, Thick Coated Plate (Hz)	% Diff
1	82	81	-1.8	78	-3.7
2	199	212	6.5	223	5.2
3	501	499	-0.4	507	1.5
4	742	744	0.2	763	2.6
5	756	764	1.1	803	5.1
6	1,388	1,394	0.4	---	---
7	---	1,465	---	1,470	0.4
8	1,668	1,684	0.9	1,759	4.5
9	1,850	1,852	0.1	1,917	3.5
10	2,429	2,470	1.7	---	---
11	2,462	2,497	1.4	2,568	2.8
12	2,893	2,851	-1.5	2,896	1.6
13	3,165	3,105	-1.9	---	---

Table 6. Resonance Frequencies Obtained by Laser Vibrometry, Room Temperature, Thin Plate

Mode #	ω, Uncoated Plate (Hz)	ω, Thin Coated Plate (Hz)	% Diff	ω, Thick Coated Plate (Hz)	% Diff
1	76	88	15.8	90	2.3
2	206	224	8.7	238	6.3
3	490	544	11.0	568	4.4
4	706	756	7.1	784	3.7
5	758	818	7.9	856	4.6
6	1,324	1,470	11.0	1,544	5.0
7	1,404	1,576	12.3	1,626	3.2
8	1,634	1,770	8.3	1,856	4.8
9	1,804	1,892	4.9	1,960	3.6
10	2,308	2,604	12.8	2,658	2.1

Mode Shapes

The PATRAN plots of the first five mode shapes for the thin plate are Figs.17 through 21. Node lines appear in black, and are in the areas predicted by Classical Plate Theory; see Fig. 3 in Chapter II.

Holography. Holography images for the thin uncoated plate are in Figs. 22 and 23. Six of the first 8 modes are represented; the torsional modes (modes 2 and 5) were not detected by this procedure. In the holography images, white bands are the node lines. Modes 1, 3, and 4 in Fig. 22 can be compared to the PATRAN images in Figs. 17, 19, and 20, respectively. The node lines in modes 3 and 4 in Fig. 22 are in similar places on the plate as in Figs. 19 and 20. As expected for the first bending mode, no node line appears in the first mode in Fig. 22.

Vibrometry. The vibrometry images are not true mode shapes, in that vibrometry is not measuring displacement, but velocity. In the vibrometry images, the colors represent magnitudes of velocity. Thus, there is not a direct correlation between the PATRAN plots and the two-dimensional vibrometry images.

Figs. 24 and 25 show the first eight modes of the thin uncoated plate, as viewed by vibrometry. Nodal lines are not always apparent. In several of the images, the node lines appear as thin white bands. For example, in the first torsion image in Fig. 24, the shape is twisting about the center line running vertically through the plate (which appears in white in the image). If the left half is displaced above the plane, the right half is below. This displacement is not evident from the image; the image only shows that the areas nearest the center line (in green) have the same magnitude of velocity, and the areas of the plate in the free corners (in red) have equivalent velocity magnitudes. By

comparing the images in Figs. 24 and 25 to the corresponding modes in Figs. 22 and 23, it can be observed that for even images (those whose mode shapes are symmetric about a center line), nodes appear as dark bands. Examples are first chordwise bend, third bend, and third chordwise bend. For odd images (those whose mode shapes are anti-symmetric about a center line), the node lines can be found by bisecting the low velocity region. Examples are second bend and second chordwise bend.

The best way to compare vibrometry to the finite element mode shapes is by observing the three-dimensional vibrometry images. Figs. 26 and 27 are three-dimensional images of the second bending and two-stripe modes, respectively, for the thick uncoated plate. In both images, the dark bands are node lines. In Fig. 26, the red area has a lower velocity magnitude than the green; in Fig. 27, the green area has a lower velocity magnitude than the red. These images display similar shapes to those in Figs. 19 and 20.

Fig. 28 is comprised of several vibrometry images, and compares the change in shapes of the second bending and two-stripe modes for the thin plate as coating thickness varies. Green areas in the images have a lower relative velocity magnitude compared to the red areas (except for the uncoated two-stripe image; the colors have been reversed in this image). In the second bend mode, white or lighter green bands are node lines. The thin coated plate in second bend is missing a red band across the middle of the plate that appears in the other two second bend images. This is likely the result of an uneven coating, which could cause uneven stress across the plate. For the two-stripe mode, the dark areas between the red and green are areas of zero velocity and zero displacement

(node lines) for the uncoated and thin coated plates; the node lines appear in white in the image for the thick coated plate.

There is no significant change in the mode shapes between the thin and thick plates.
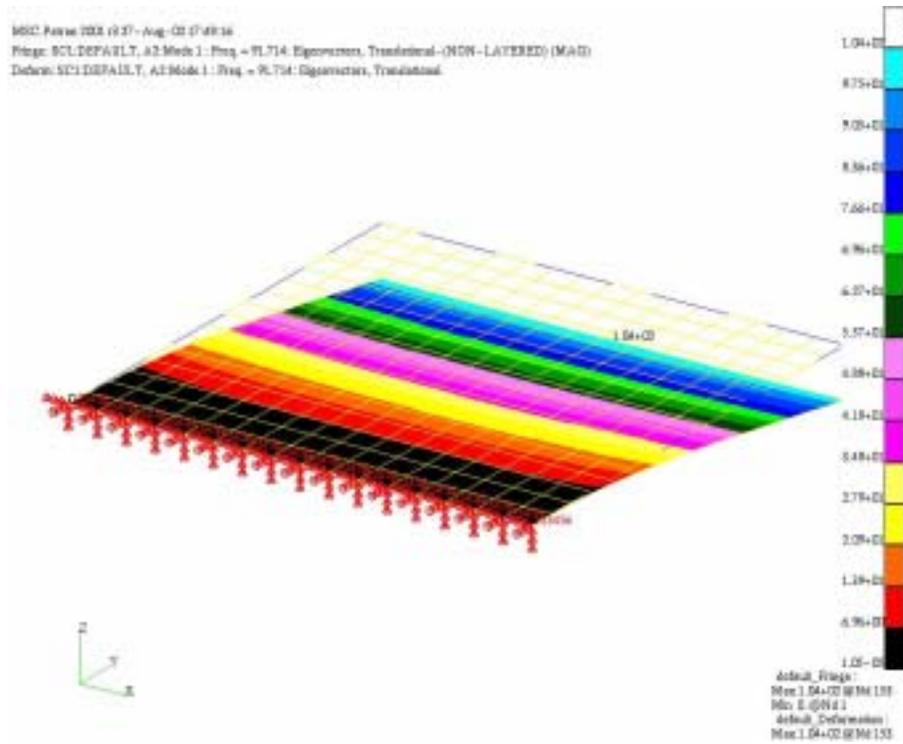
Figure 17. Thin Plate Mode 1, First Bend, ω = 91.71 Hz.
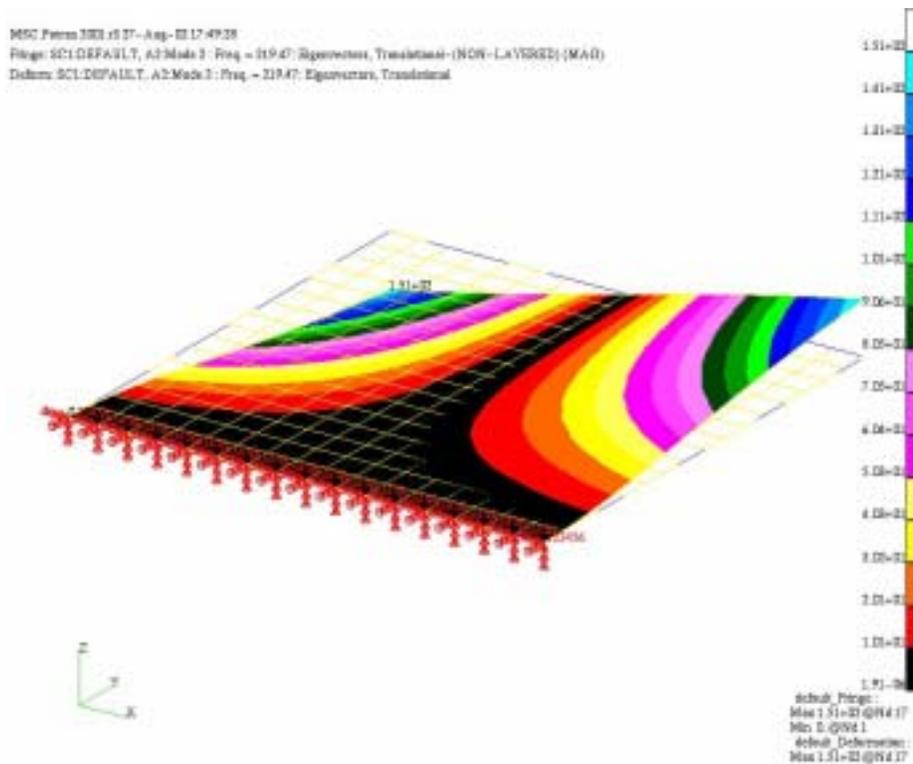
Figure 18. Thin Plate Mode 2, First Torsion, ω = 219.47 Hz.
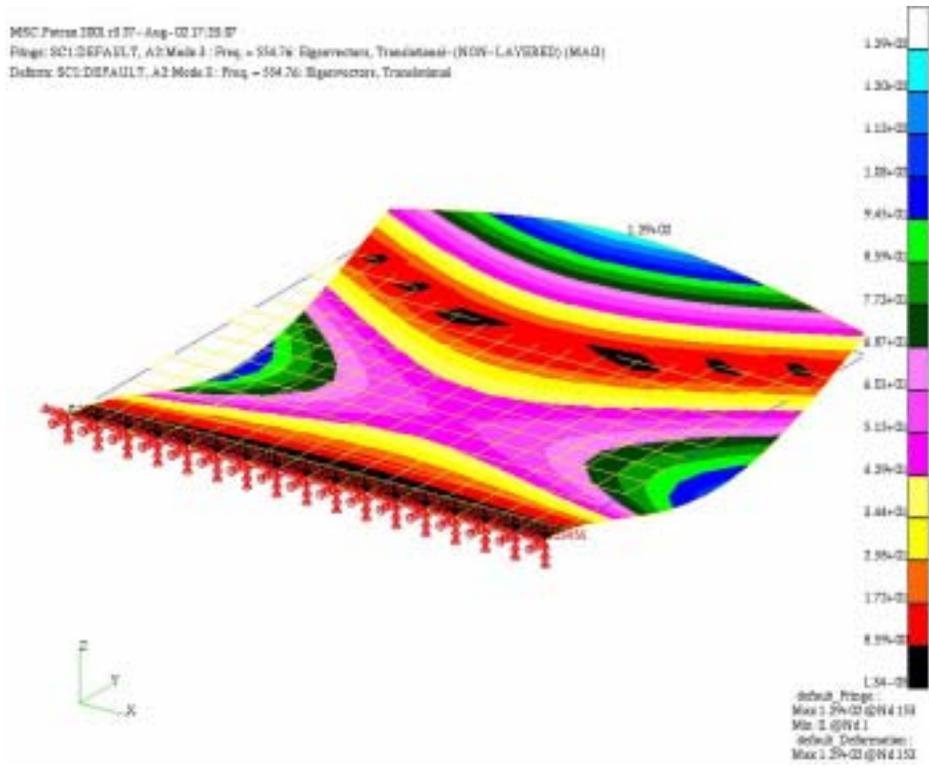
Figure 19. Thin Plate Mode 3, Second Bend, ω = 554.76 Hz.
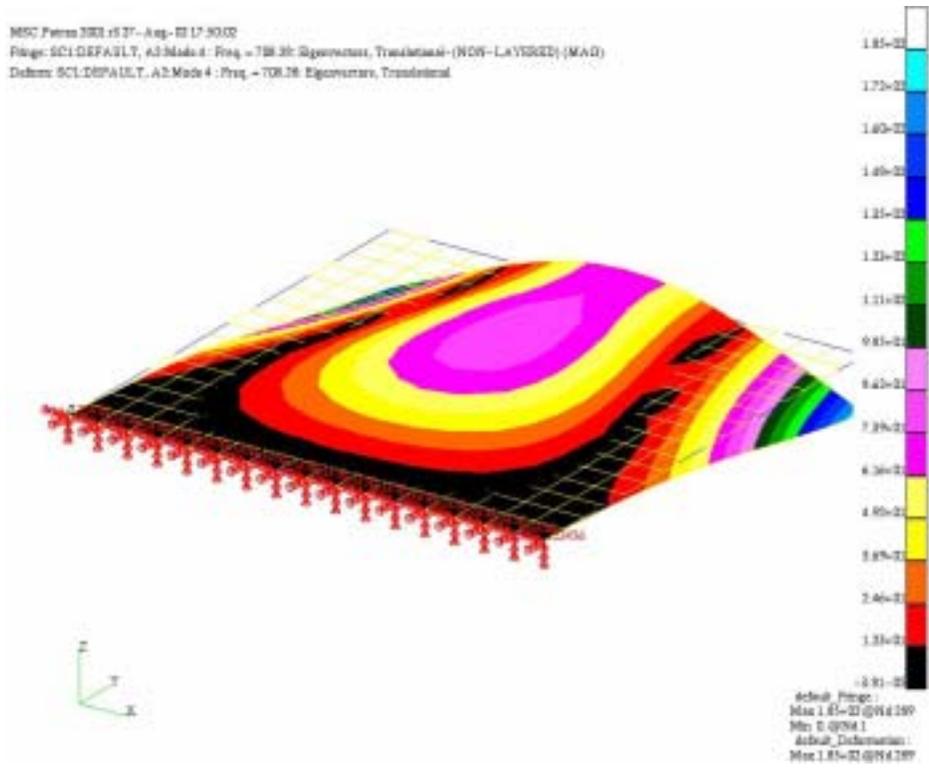
Figure 20. Thin Plate Mode 4, First Chordwise Bend, ω = 708.28 Hz.
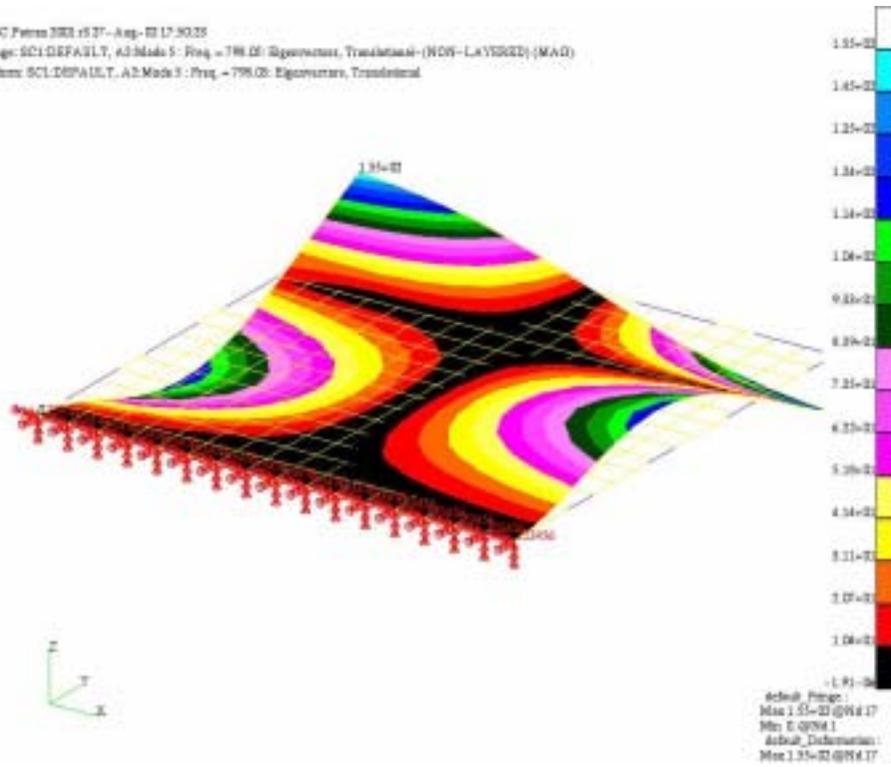
Figure 21. Thin Plate Mode 5, Second Torsion, ω = 798.05 Hz.
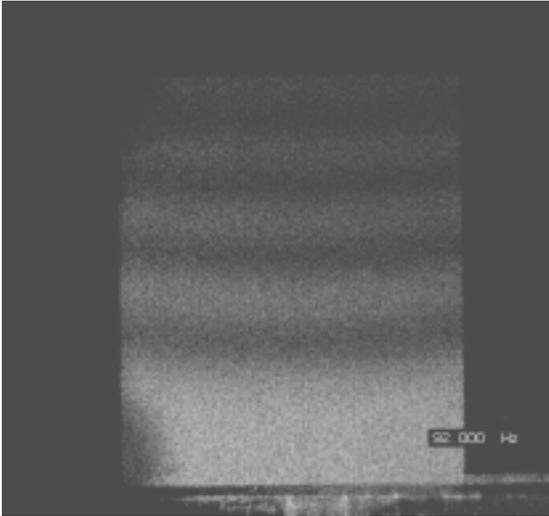
Mode 1: 1st Bend, 92 Hz
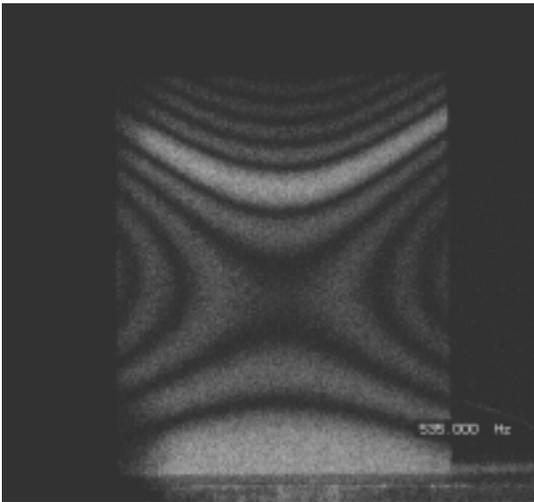
Mode 3: 2nd Bend, 535 Hz
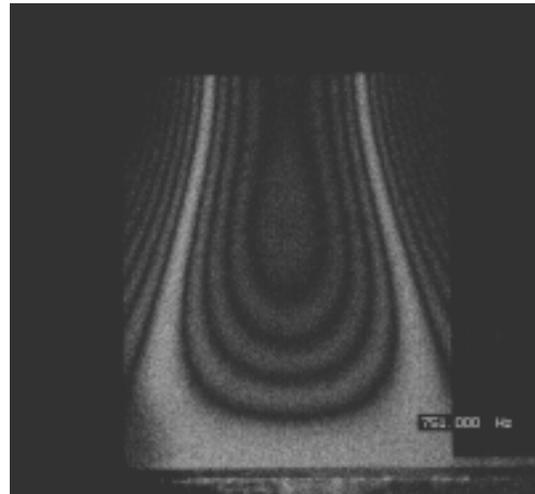
Mode 4: 1st Chordwise Bend, 751 Hz

Figure 22. Three of the first four modes, thin uncoated plate, viewed by holography. The clamped edge is at the bottom.
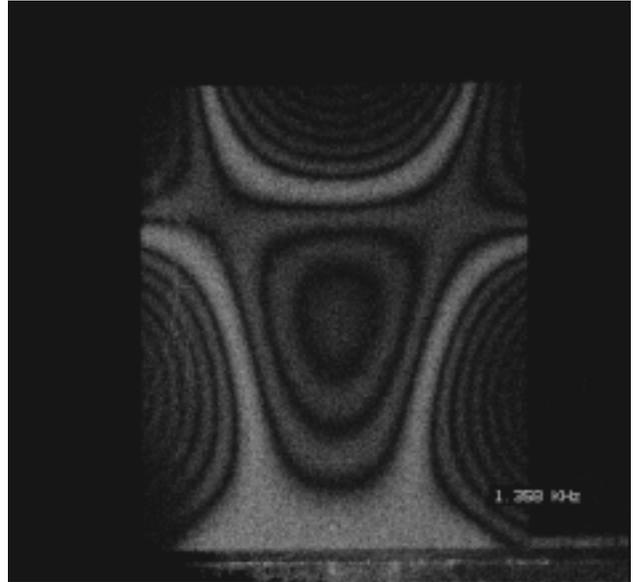
2nd Chordwise Bend, 1358 Hz
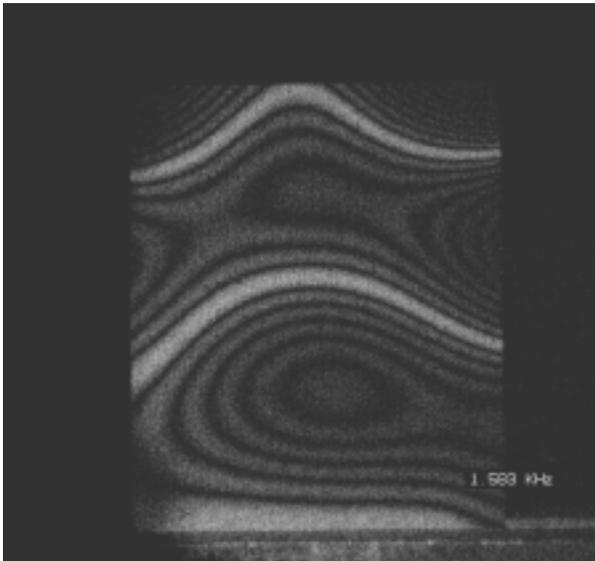
3rd Bend, 1583 Hz
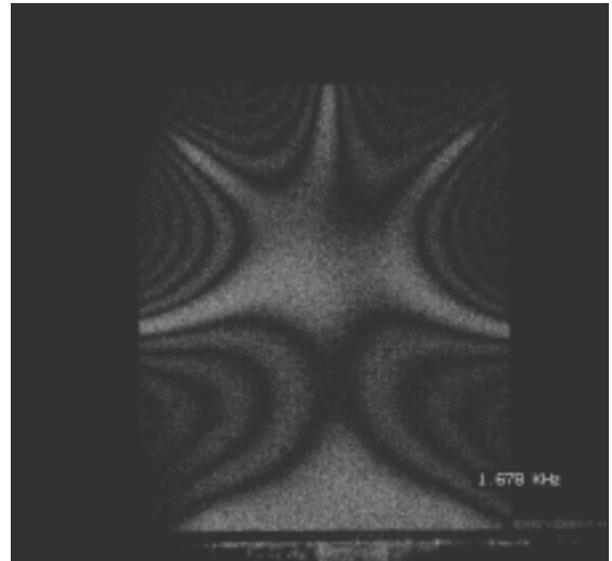
3rd Chordwise Bend, 1678 Hz

Figure 23. Modes 6 through 8, thin uncoated plate, viewed by holography. The clamped edge is at the bottom.

1st Bend, 76 Hz
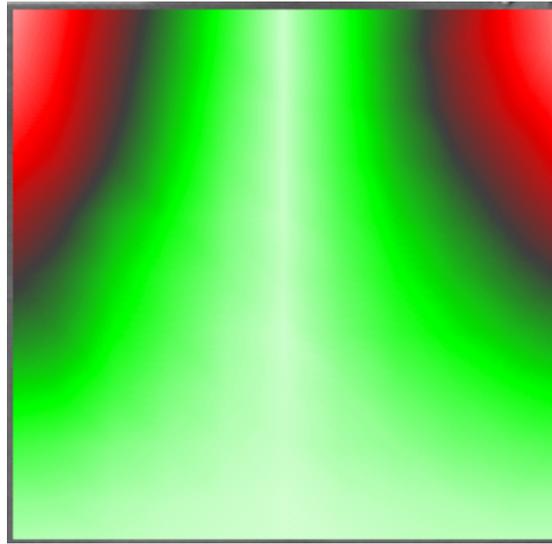
1st Torsion, 206 Hz
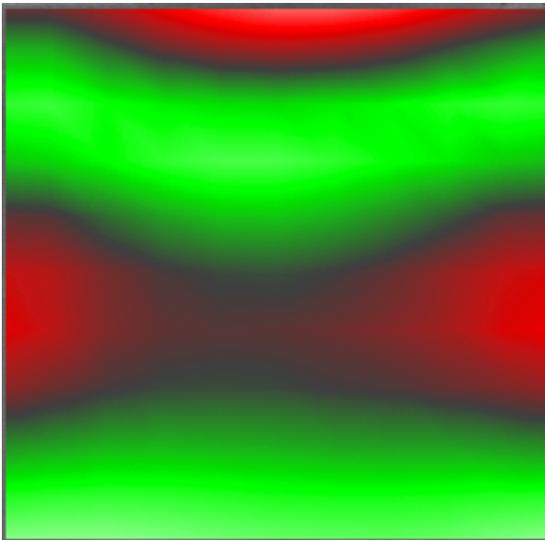
2nd Bend, 490 Hz
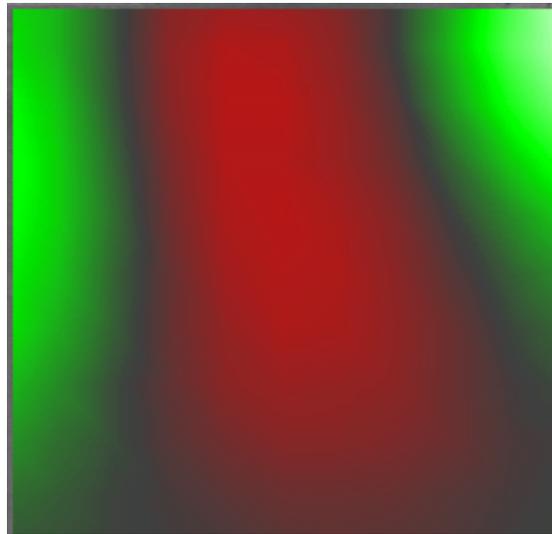
1st Chordwise Bend, 706 Hz

Figure 24. First four modes, thin uncoated plate (Plate 116A3), viewed by vibrometry
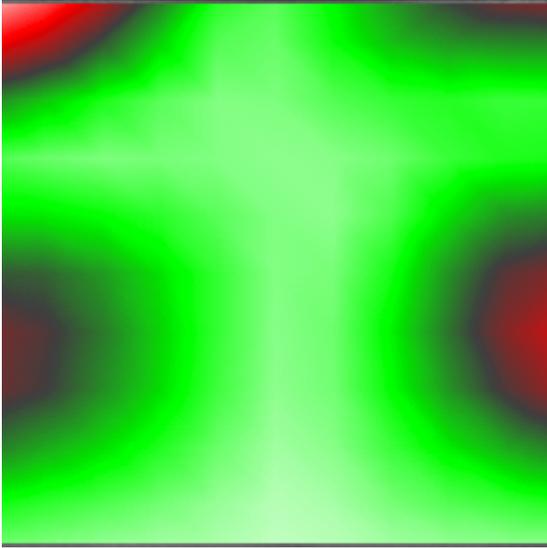
2nd Torsion, 754 Hz
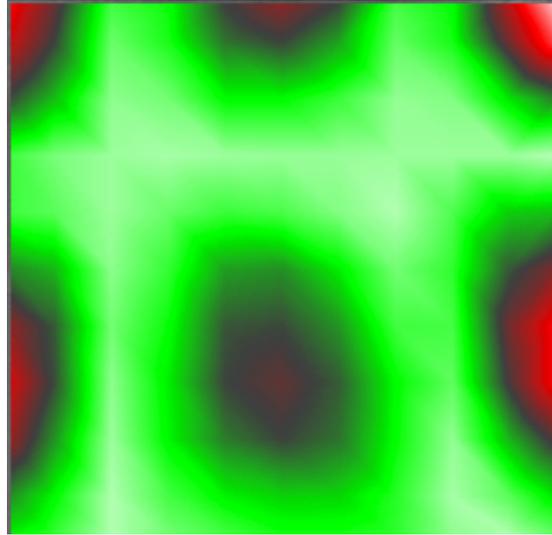
2nd chordwise bend, 1324 Hz
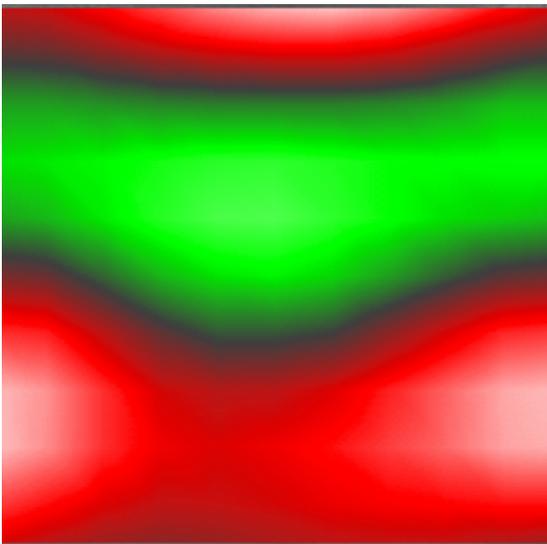
3rd Bend, 1404 Hz
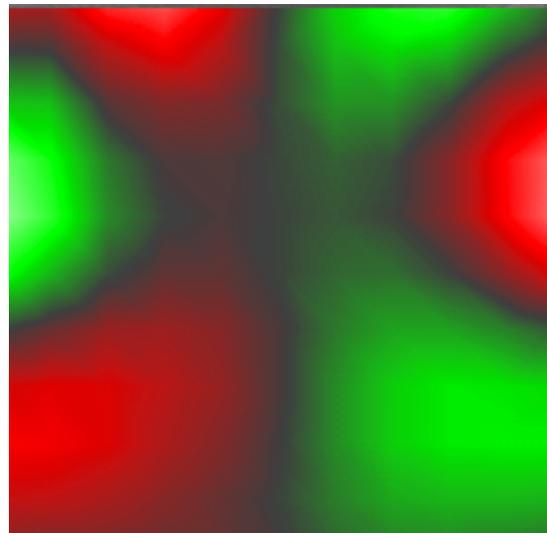
3rd Chordwise Bend, 1634 Hz

Figure 25. Modes 5 through 8, thin uncoated plate (Plate 116A3), viewed by vibrometry
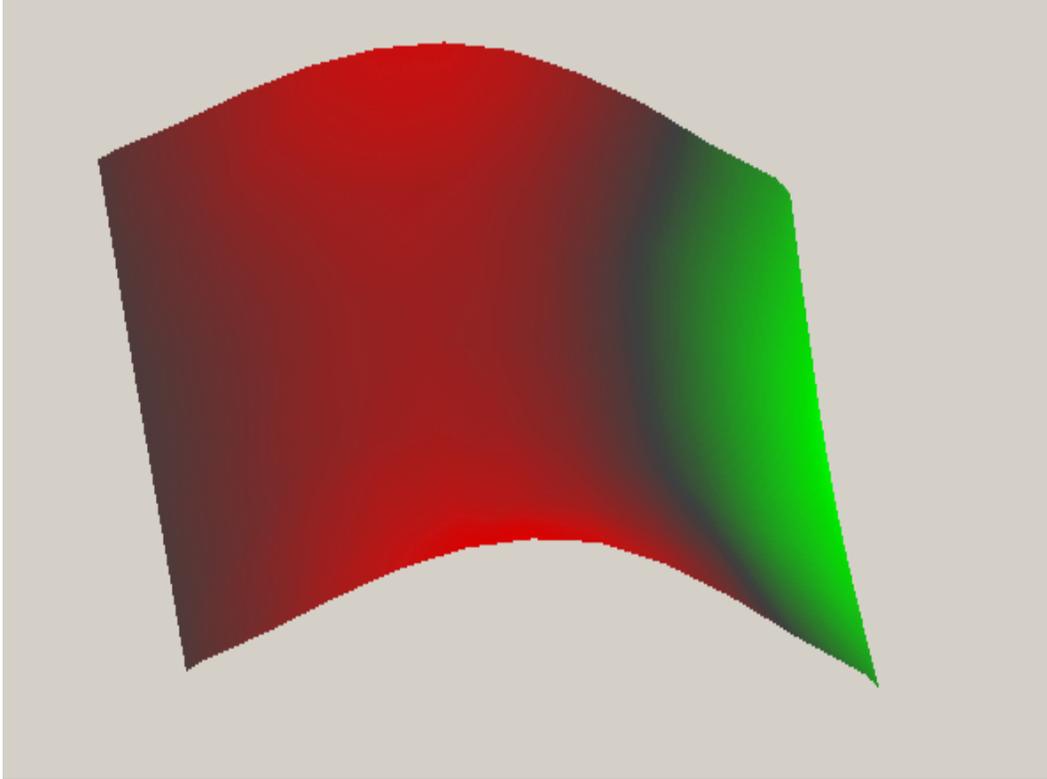
Figure 26. Second Bending Mode, Thick Uncoated Plate
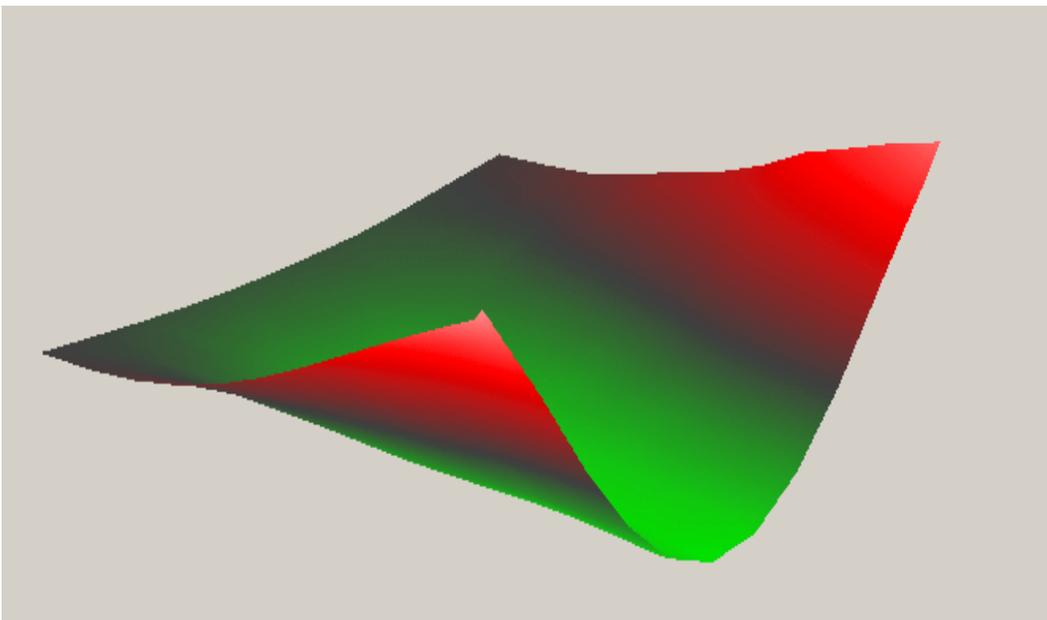
Figure 27. First Chordwise Bending Mode, Thick Uncoated Plate
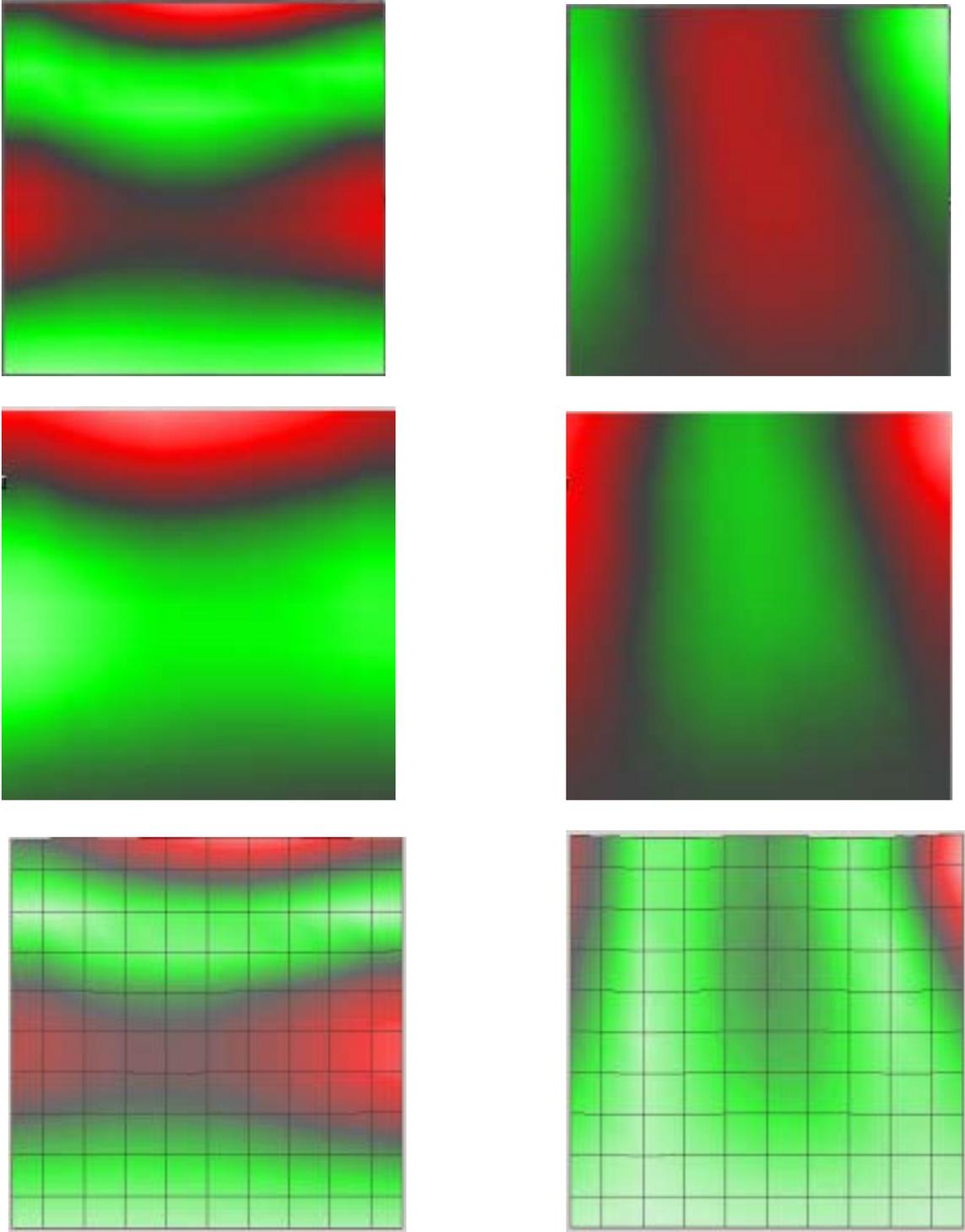
Figure 28. Second Bend and First Chordwise Bend for the Thin Plate; Uncoated (top), Thin Coated (middle), and Thick Coated (Bottom)

Stress Analysis

Stress analysis was conducted on the second bending and first chordwise bending modes of the thin plate using SPATE.   Results are in Figs. 29 and 30, respectively. The color scale is in volts, but can be converted to strain or stress. In Fig. 29, the blue areas are the areas of highest stress; in Fig. 30, the scale is reversed, and the white/yellow areas are the high stress areas. Based on these images, strain gages were placed near the clamped edge for the second bend fatigue test, and at the center of the edge opposite the clamp for the two-stripe fatigue test. It was eventually decided that second bending was not to be studied.
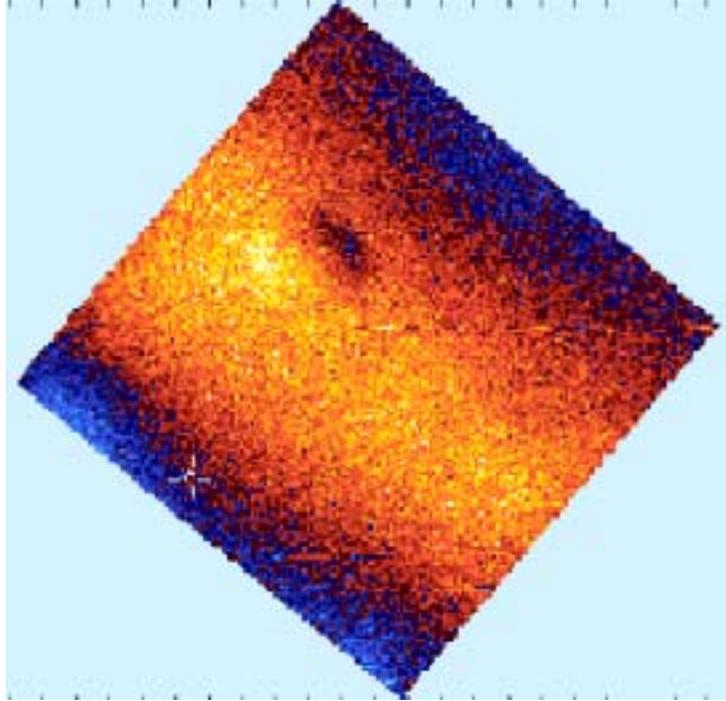
Figure 29. SPATE Scan, 2nd Bending Mode. Figure is rotated 45 degrees clockwise, so the clamped end goes from the bottom of the picture to the left side.
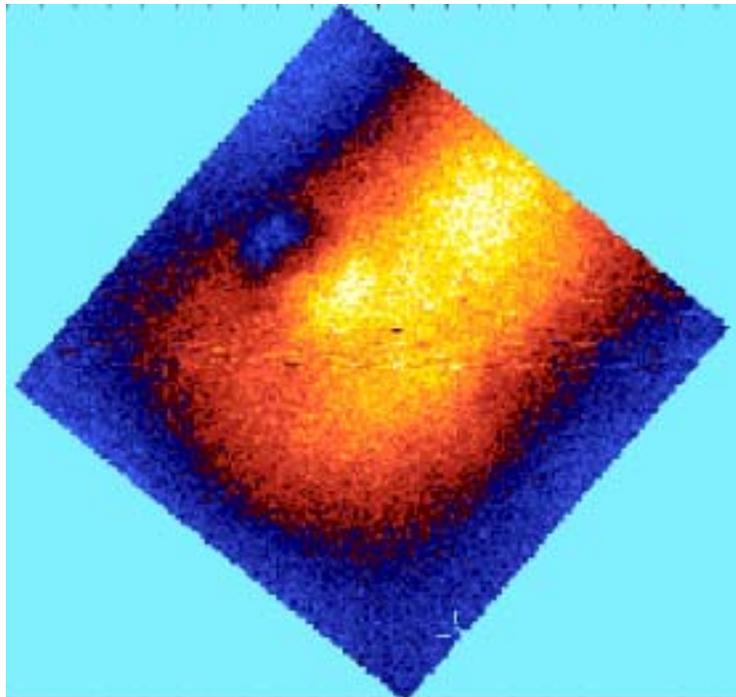
Figure 30. SPATE Scan, 1st Chordwise Bending (Two-Stripe) Mode

Damping

Damping was determined by conducting sine sweeps on uncoated, thin coated, and thick coated test specimens using the Bruel & Kjaer system. The PULSE Labshop software compared the response signal to the reference signal, performed a fast Fourier transform, and graphically displayed the results in the frequency domain. The amplitude of the graph was presented in decibels. At resonance, the amplitude peaked; the steepness of the peak was an indication of the damping for that mode. The damping was determined by the software using the half-power method.

Thin Plate. For the thin plates, a magnet was used as the excitation source. Results are in Tables 7 through 10, and are depicted graphically in Fig. 31. The damping ratio, ζ, as determined by the LabShop software, has been converted to the quality factor, Q, the preferred method of measurement in the damping community. As expected, the mag spinel coating caused an increase in the damping ratio, and the thicker coating had more of an effect than the thinner one. Damping increased between the uncoated and thin coated plates for 10 of the 12 modes measured; 6 of the 10 increases were better than 25%. When going from the thin to the thick coating, damping increased for every one of the 10 modes; 8 of these were better than 20%, and 6 were better than 40%. Q values cannot be compared between modes, as Q is dependent on strain, and the strain is different between modes for the same applied force.

Table 7. Damping values obtained from sine sweep procedure, thin uncoated plate.

Mode	Trial 1 ω_n (Hz)	Trial 1 ζ (%)	Trial 2 ω_n (Hz)	Trial 2 ζ (%)	ζ (avg.)	Q
1	82	1.32	82	1.310	1.315	38
2	199	0.575	200	0.592	0.584	86
3	501	0.301	502	0.309	0.305	164
4	742	0.165	742	0.167	0.166	301
5	756	0.175	756	0.183	0.179	279
6	1388	0.135	1389	0.124	0.130	386
7	---	---	---	---	---	---
8	1668	0.115	1668	0.117	0.116	431
9	1850	0.076	1851	0.076	0.076	658
10	2429	0.177	2431	0.178	0.178	282
11	2462	0.083	2463	0.082	0.083	606
12	2893	0.202	2895	0.191	0.197	254
13	3165	0.199	3166	0.181	0.190	263

Table 8. Damping values obtained from sine sweep procedure, thin plate, thin coating.

Mode	Trial 1 ω_n (Hz)	Trial 1 ζ (%)	Trial 2 ω_n (Hz)	Trial 2 ζ (%)	ζ (avg.)	Q
1	80	1.36	81	1.35	1.355	37
2	212	0.585	212	0.561	0.573	87
3	498	0.32	500	0.32	0.320	156
4	743	0.191	744	0.176	0.184	272
5	763	0.244	765	0.234	0.239	209
6	1393	0.218	1395	0.2	0.209	239
7	1463	0.283	1466	0.291	0.287	174
8	1682	0.25	1685	0.244	0.247	202
9	1852	0.082	1852	0.086	0.084	595
10	2469	0.162	2471	0.158	0.160	313
11	2496	0.153	2497	0.152	0.153	328
12	2848	0.21	2854	0.345	0.278	180
13	3104	0.305	3106	0.31	0.308	163

Table 9. Damping values obtained from sine sweep procedure, thin plate, thick coating.

Mode	Trial 1 ω_n (Hz)	Trial 1 ζ (%)	Trial 2 ω_n (Hz)	Trial 2 ζ (%)	ζ (avg.)	Q
1	77	1.67	78	1.61	1.640	30
2	223	0.613	223	0.612	0.613	82
3	505	0.771	508	0.703	0.737	68
4	762	0.341	764	0.318	0.330	152
5	802	0.403	804	0.396	0.400	125
6	---	---	---	---	---	---
7	1470	0.368	1470	0.363	0.366	137
8	1758	0.612	1760	0.573	0.593	84
9	1917	0.114	1917	0.114	0.114	439
10	---	---	---	---	---	---
11	2567	0.283	2568	0.272	0.278	180
12	2889	1.34	2903	1.31	1.325	38
13	---	---	---	---	---	---

Table 10. Comparison of damping results from sine sweep procedure, thin plate. A decrease in Q value is an increase in damping.

Mode	uncoated Q	thin coated Q	thin coated % Decrease	thick coated Q	thick coated %Decrease
1	38	37	3.0%	30	17.4%
2	86	87	-1.8%	82	6.4%
3	164	156	4.7%	68	56.6%
4	301	272	9.5%	152	44.3%
5	279	209	25.1%	125	40.2%
6	386	239	38.0%	---	---
7	---	174	---	137	21.5%
8	431	202	53.0%	84	58.3%
9	658	595	9.5%	439	26.3%
10	282	313	-10.9%	---	---
11	606	328	45.9%	180	45.0%
12	254	180	29.2%	38	79.1%
13	263	163	38.2%	---	---
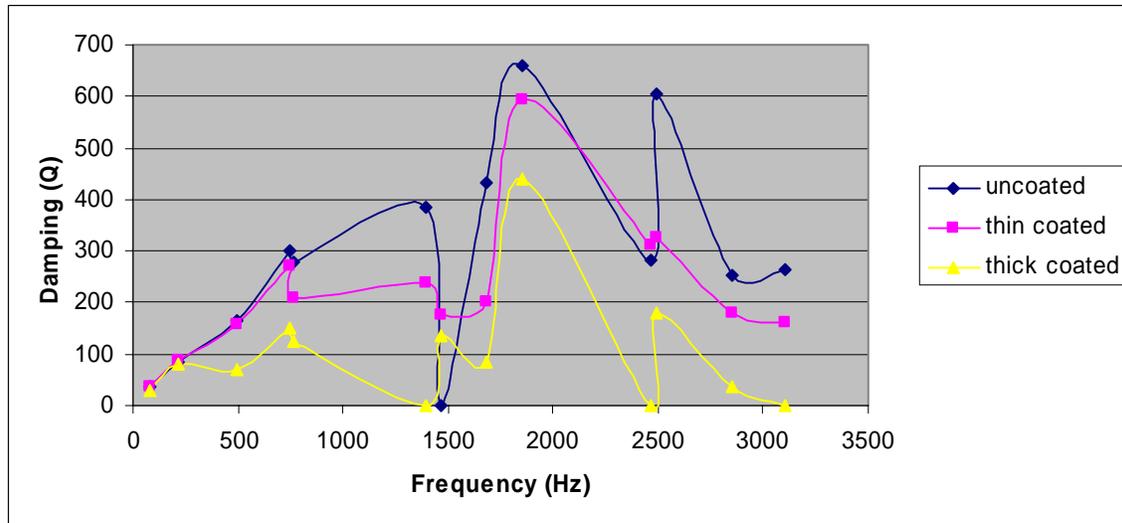
Figure 31. Damping vs. frequency, room temperature, thin plate

Thick Plate. For the thick plates, an air horn was used as the excitation source. Figs. 32 though 35, 36 through 38, and 39 through 41 present the power spectral densities containing the first five modes of the uncoated, thin coated, and thick coated test specimens, respectively. As in Fig. 8 in Chapter III, the peaks in these graphs occur at resonance frequencies, and the width of the curve 3 dB down from the peak determines the damping. Figs. 32, 36, and 39 also depict coherence. Coherence is a measure of the response signal to the input signal at each frequency. At frequencies above 400 Hz the coherence is unity (indicating the input signal is being returned) for each of the uncoated, thin coated, and thick coated plates. Below 400 Hz, the signals are noisy, except around the resonance condition. The uncoated plate has better coherence than the thin coated plate, and the thick coated plate has the poorest coherence. In general, the coherence of a signal generated by the air horn is poor below 400 Hz, because the signal is weak at these frequencies. However, the coating degraded the coherence, indicating either the coating

65

is interfering with the reference signal (which must pass through the coating to excite the titanium), or it is preventing the accelerometer from picking up the response.

Figs. 32, 36, and 39 depict the first mode (1st bend). Amplitudes are not very high for this mode. Figs. 36 and 39 also have several single point spikes. These are not resonance modes, but a result of the noise in the signal. Figs. 33, 37, and 40 depict the second mode (1st torsion). Fig. 37 also has a very distinct anti-resonance at around 635 Hz. A less distinct anti-resonance condition can be seen at the same frequency in Fig. 40. Figs. 34 and 35, 38, and 41 contain modes 3 through 5 (2nd bend, 1st chordwise bend, and 2nd torsion). The 3rd and 5th modes are very strong; the 4th mode has less amplitude, and is very close in frequency to the 5th mode. When conducting a broader sweep, it was not clear whether this was a distinct mode, or part of mode 5. This was a major part of the motivation for conducting several narrower sweeps, rather than a single broad sweep.

Resonance frequencies and damping ratios were determined from these graphs (and others containing modes 6 through 10, which are not presented here), and are recorded in Tables 11 through 13, along with calculated Q values. Table 14 compares the Q values contained in Tables 11 through 13 by mode. Figure 42 shows the data in Table 14 graphically.

It was anticipated that the results of this experiment would show that the application of mag spinel would increase the damping over the uncoated plate, and the thicker layer would dissipate more energy than the thinner layer, as was seen in the thin plate. Based on the data in Table 14 and Fig. 42, the results of this experiment must be characterized as inconclusive. While modes 1, 2, and 7 behaved as expected, modes 3 and 9 showed exactly the opposite of the premise (decreased damping from uncoated to

thin coated, and again from thin coated to thick coated), and all of the other modes were mixed.

Previous work done by Torvik et al. (2002) has shown the relationship between damping and the amplitude of the strain to be non-linear. It may be that the force applied in this experiment did not generate enough strain in these lightly damped plates for the coatings to dissipate any additional energy. Another possibility is the sweep rates were too fast (25 Hz/sec, 100 Hz/sec) to accurately characterize the damping.

A second approach used the Unholtz-Dickie (U-D) 6,000 lb. shaker as the excitation source for determining damping values for the thick plate. The shaker has the capability to apply more force to the test specimens than the air horn could. Sweep rates were drastically reduced (2 to 12.5 Hz/min, compared to 25 or 100 Hz/sec). Figs. 43 through 47 display the power spectral densities which were used to determine the damping values for the uncoated plates. Data collected during these tests is summarized in Tables 15 through 17 for the uncoated, thin coated, and thick coated specimens, respectively. Comparisons are made in Table 18 and displayed graphically in Fig. 48, and show a marked increase in damping from uncoated to the thin coated specimen (40% to 74% decrease in Q values), but not a significant difference between the thin and thick coated specimens (3 increases in Q, 2 decreases, all within 12 %). In comparing Q values between the B&K and U-D systems, (Tables 14 and 18; Figs. 42 and 48), it is observed that for 13 of the 15 data points (three specimens, 5 modes each), the damping was better (lower Q values) for the U-D system. This indicates that damping may be a function of the excitation force. To test this theory, a second set of sweeps were accomplished using the U-D system, with an increase in shaker head acceleration over the first set. Initial

testing was conducted at a shaker head acceleration of 1.0 g's for all modes except mode 4 (1st chordwise bend). The vibrometer reading was taken too close to a node line for this mode to get a strong enough return at 1 g, so its initial test was conducted at 10 g's. The second trial was conducted at 10 g's, except for mode 4, which was conducted at 20 g's, and the uncoated plate modes 1 and 3, which were conducted at 5 g's. Of the 12 points tested (five modes uncoated plate, 4 modes thin coated plate, 3 modes thick coated plate), 10 displayed increased damping (decrease in Q) over the lower acceleration trials; see Table 19. This indicates that damping is indeed a function of the excitation force.

In this work, the applied force was held constant as coating thickness was increased from 0 to .010" to .020". Thus, if the Q value decreases between thickness trials, it is fair to say the strain decreased for that mode and applied force. As Q varies with strain, and strain is different between modes for the same applied force, comparisons cannot be made between modes without knowing the strain. Likewise, in order to predict the damping behavior within a mode going from a known excitation force to a higher unknown force, the strain must be known at the higher force.

To make comparisons of damping between modes, the strain under which the damping was measured must be known. All responses were measured at the same location for each group of trials (i.e., thin plate, thick plate B&K, thick plate U-D), but the strain at this location will be different for each mode. Also for each group of trials, the applied force was held constant (except for the fourth mode of the thick plate on the U-D, as mentioned earlier). For the fourth mode, the strain can be determined for any measured velocity from the strain-displacement curve developed for fatigue testing; see

Fig. 53. This curve is mode-specific, and cannot be used to relate strain and displacement for any other mode.

Strain can be determined either by measuring it (using a strain gage) or by calculating its value from a known response signal (velocity for vibrometer, acceleration for accelerometer). To calculate strain, the relationship between strain and the measured quantity must be known. This can be accomplished either by developing the relationship in the laboratory, as was done to obtain the strain-displacement curve in Fig. 53, or analytically, such as with a finite element model.

For the tests run on the B&K system, the response signal from the accelerometer was not recorded. For the damping runs on the U-D system, the excitation force at the base was recorded as an acceleration of the shaker table, and the velocity at resonance was measured by the vibrometer at a point 1.5" from the clamp and 0.5" in from the side, which corresponds to CQUAD4 element 123 in the finite element model. The finite element model determined displacements and stresses relative to a maximum displacement of 1.0 in the z-direction for each mode. Using the velocity measured at element 123, the velocity at the maximum stress point can be found for each mode. As stress and strain are related linearly by Young's modulus, maximum strain occurs at points of maximum stress. Knowing the velocity at a specified point, the relationship between points on the test specimen for each mode, and the excitation force, the damping values obtained from the testing can be related to each other.

For the fourth mode (first chordwise bend), the strain-displacement curve in Fig. 54 can be used to determine the strain from the velocities at each of the points where damping was measured. Damping values were determined at 5, 10, and 20 g's. Fatigue

tests on the uncoated plate were run at accelerations of 19 and 25 g's. Velocities at these shaker table accelerations were about 230 mm/s and 285 mm/s, respectively. Interpolating yields a velocity of about 240 mm/s at 20 g's. As velocity and acceleration are related linearly, the velocity at 10 g's would be 120 mm/s. The microstrain at 120 mm/s is 1330. The microstrain at 240 mm/s is 2660. The microstrain at 5 g's is 665. Plotting these strains versus the measured Q values yields a straight line; see Fig. 49. In Fig. 49, the slope is extended to observe the coated plate points. At 10 g's, the thin plate had a Q of 207. On this curve, a Q of 207 occurs at a microstrain of about 3300, which translates to an acceleration of around 25 g's. Thus, the thin coated plate dissipates the same amount of energy at an acceleration of 10 g's that the uncoated plate would dissipate at 25 g's, assuming a linear relationship. While the curve is linear between 665 and 2660 $\mu\varepsilon$, it will not be at low or high strain levels. More data points are needed to characterize these areas of the curve.

Torvik, et al. (2002) found damping to be independent of frequency. In reviewing the data in Figs. 42 and 48, damping is not constant, nor does it change as a function frequency. By examining the shapes of the curves, it is observed that the shapes are similar regardless of the coating case; peaks and valleys occur in the same places. In looking more closely at the specific modes, it is observed that the lowest amplitudes (highest damping) occur at the 1st, 3rd, and 7th modes: the bending modes. The highest amplitudes (lowest damping) are at the 2nd and 5th modes: the torsion modes. Damping is not related to the frequency, but can be related to the mode shape.
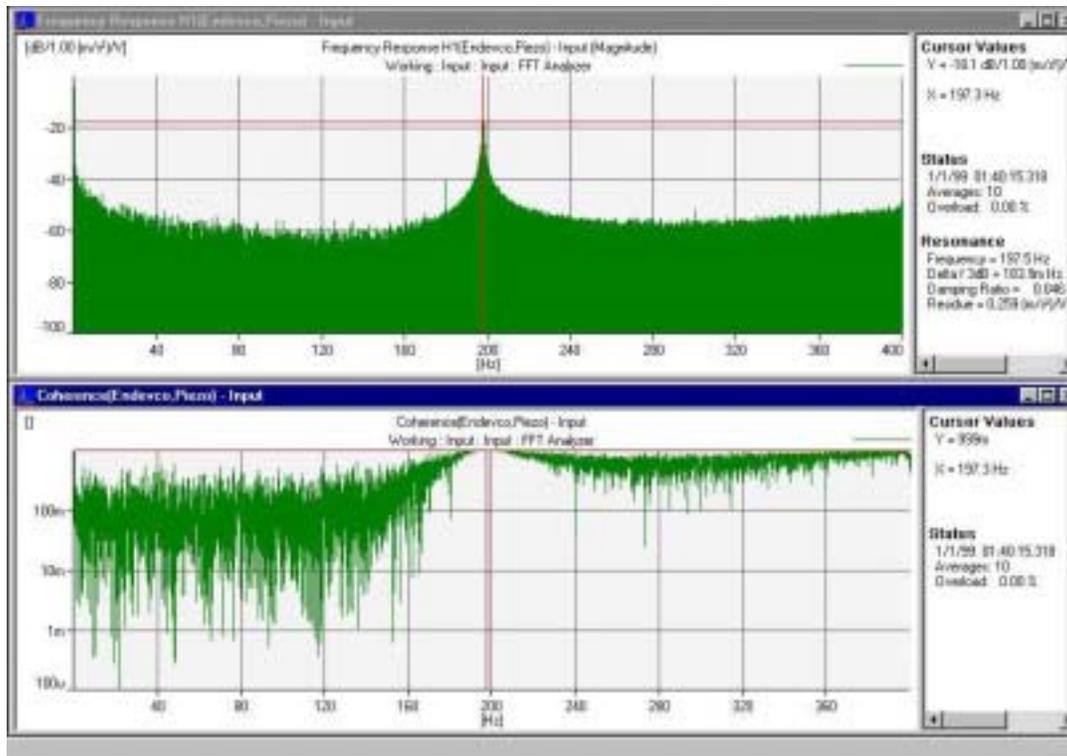
Figure 32. Power Spectral Density and Coherence curves, uncoated thick plate, room temperature, 0 to 400 Hz.
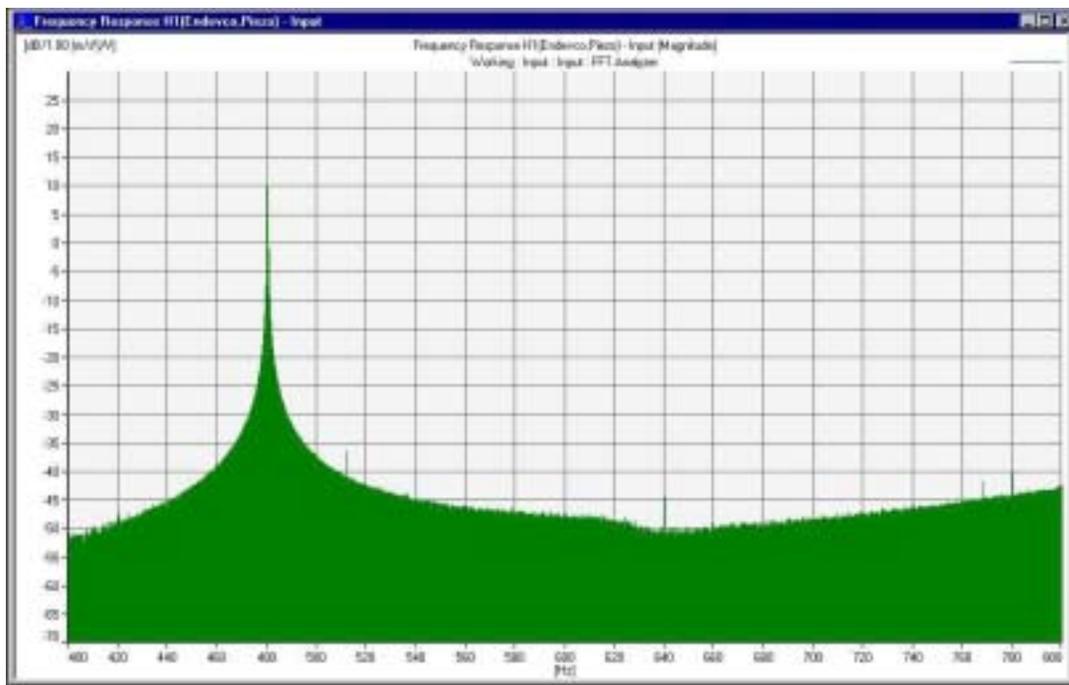
Figure 33. Power Spectral Density, uncoated thick plate, room temperature, 400 to 800 Hz.

71
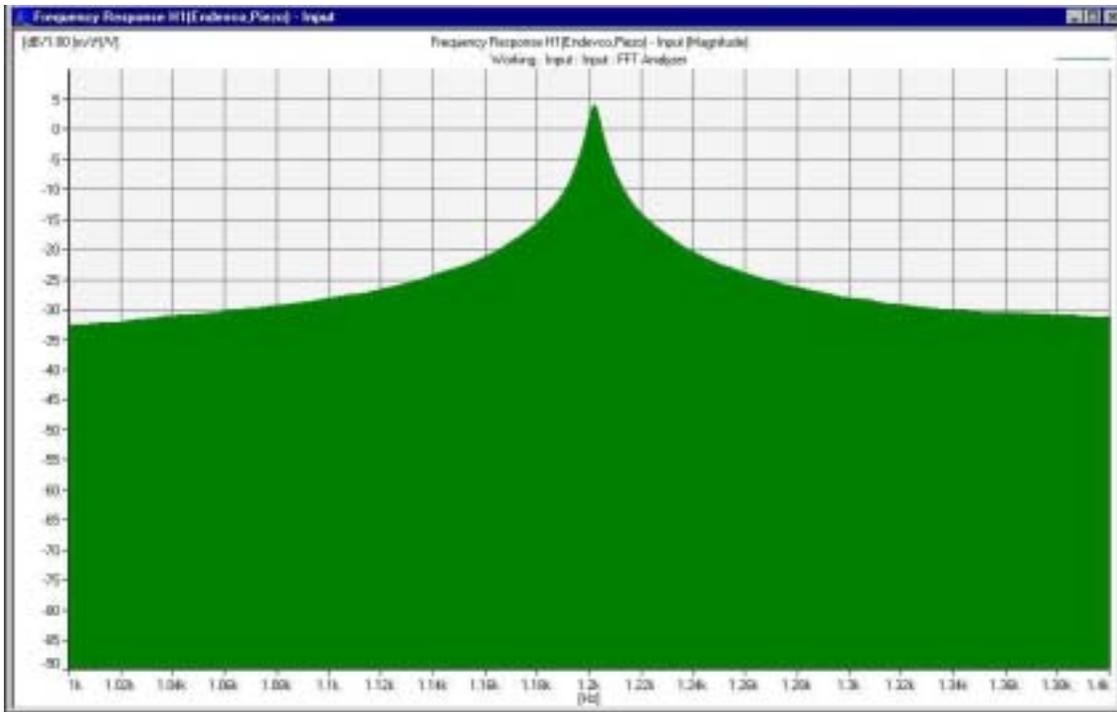
Figure 34. Power Spectral Density, uncoated thick plate, room temperature, 1000 to 1400 Hz.
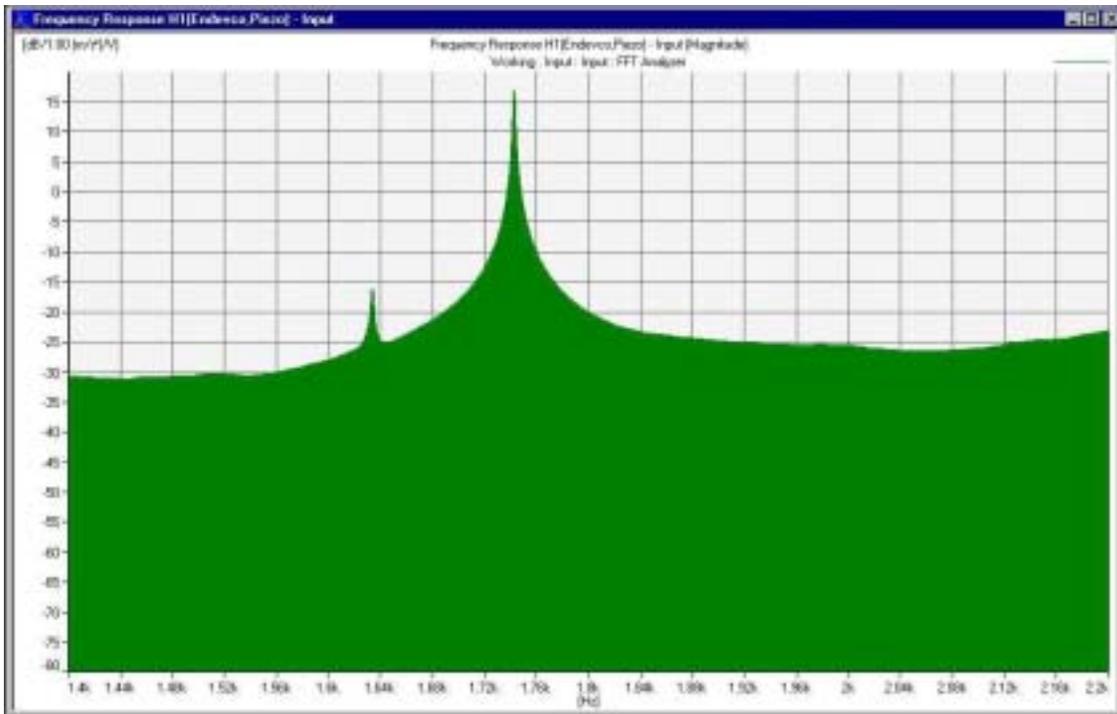
Figure 35. Power Spectral Density, uncoated thick plate, room temperature, 1400 to 2200 Hz.
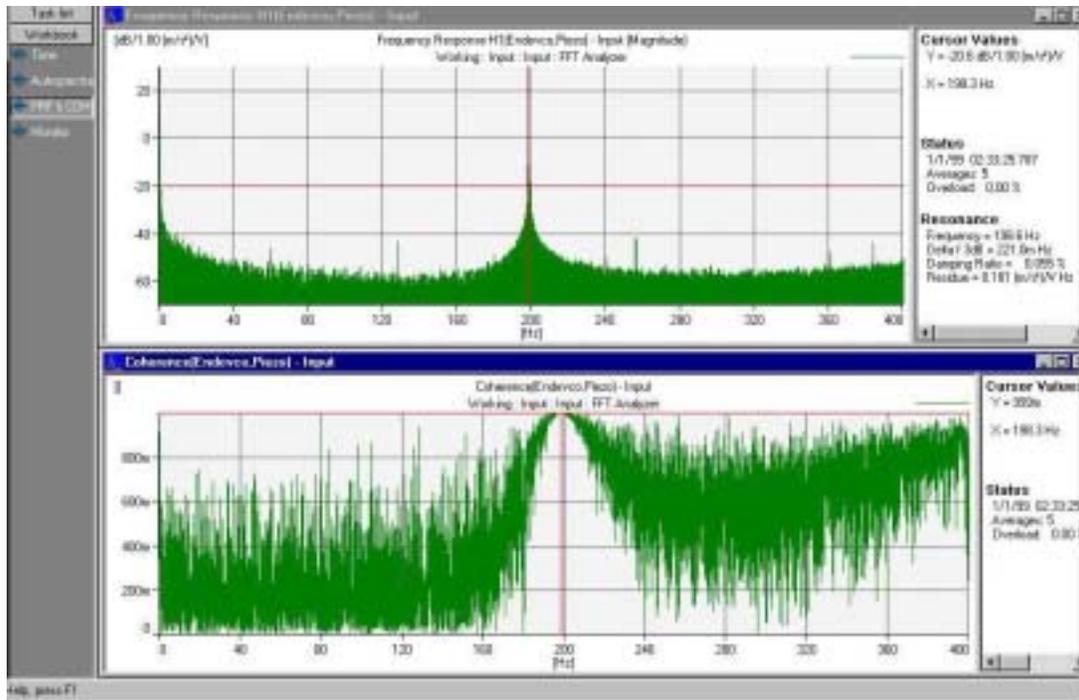
Figure 36. Power Spectral Density and Coherence curves, thin coated thick plate, room temperature, 0 to 400 Hz.
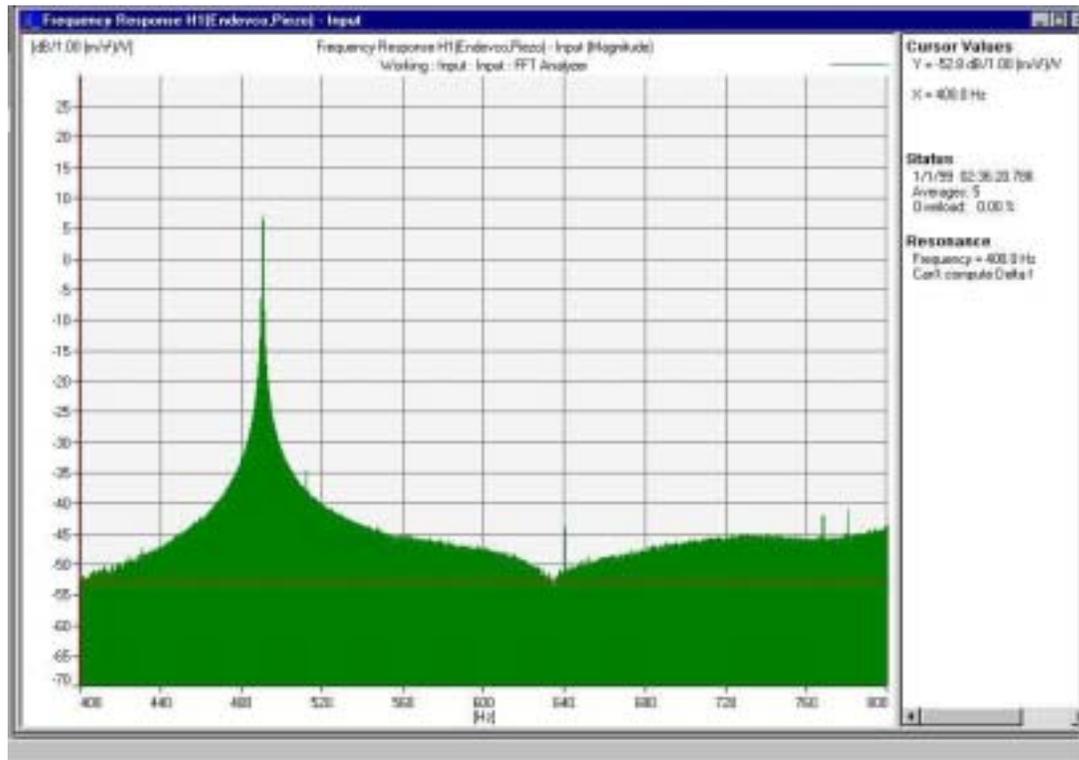
Figure 37. Power Spectral Density, thin coated thick plate, room temperature, 400 to 800 Hz.
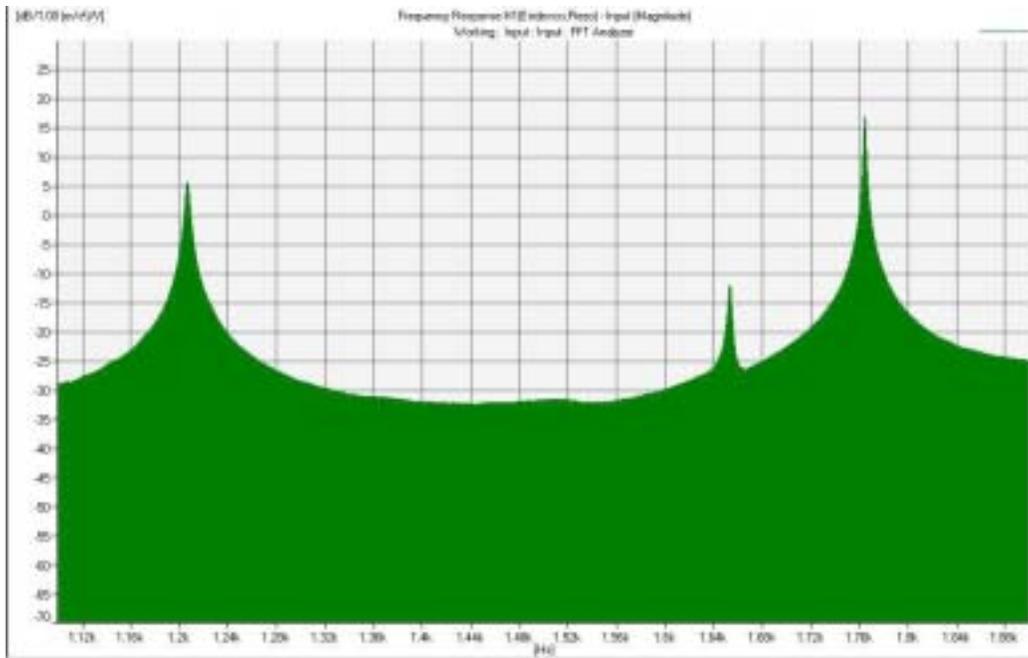
Figure 38. Power Spectral Density, thin coated thick plate, room temperature, 1100 to 1900 Hz.
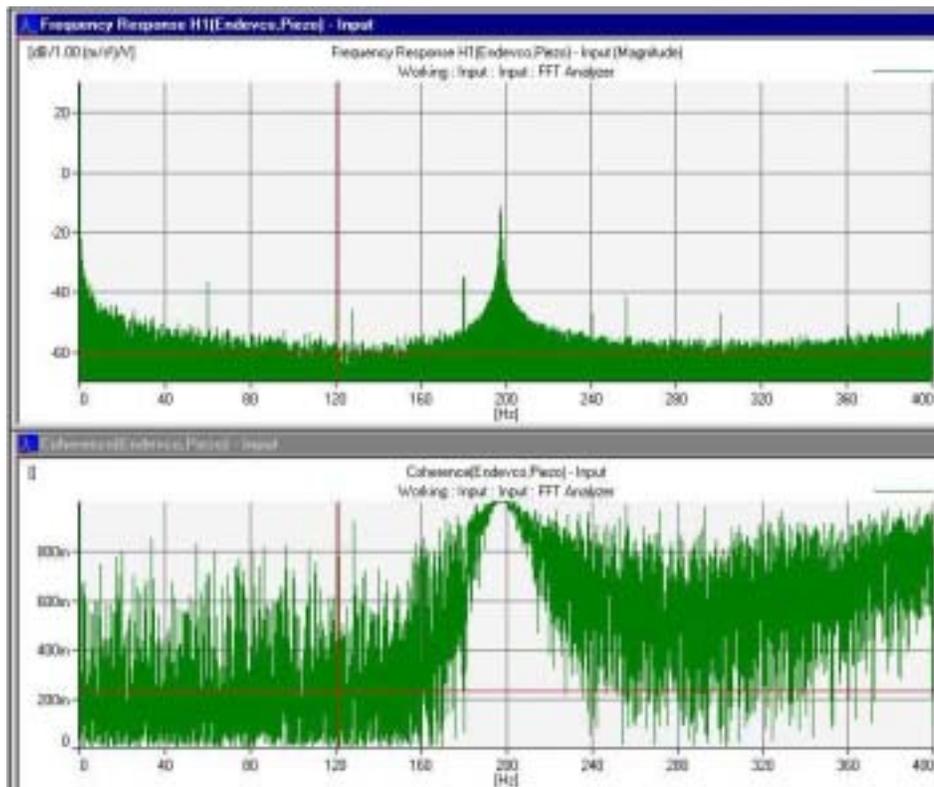
Figure 39. Power Spectral Density and Coherence curves, thick coated thick plate, room temperature, 0 to 400 Hz.
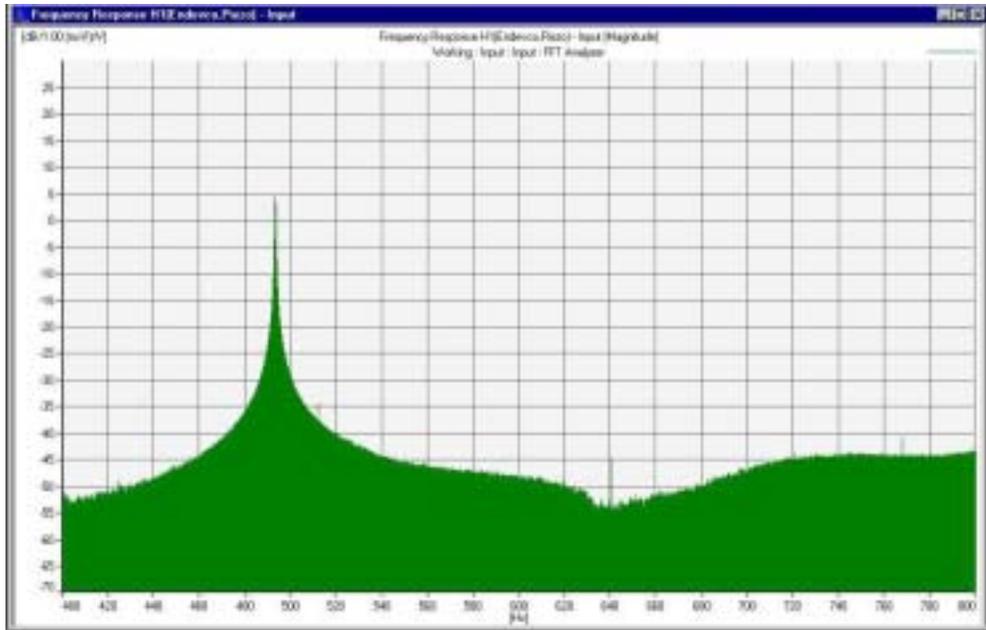
Figure 40. Power Spectral Density, thick coated thick plate, room temperature, 400 to 800 Hz.
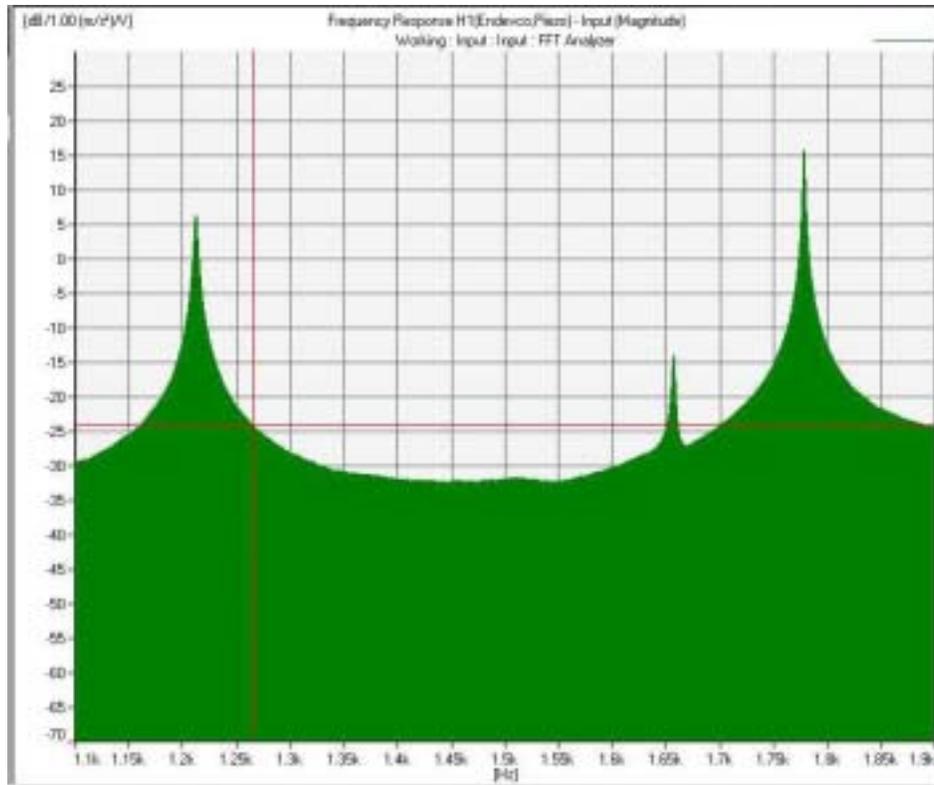
Figure 41. Power Spectral Density, thick coated thick plate, room temperature, 1100 to 1900 Hz.

Table 11. Damping values obtained from sine sweep procedure, uncoated thick plate.

Mode	ω_n (Hz)	ζ	Q
1	197.5	0.046	1,087
2	480.3	0.016	3,125
3	1202	0.188	266
4	1633	0.081	617
5	1742	0.043	1,163
6	3098	0.054	926
7	3487	0.198	253
8	3781	0.078	641
9	4121	0.196	255
10	5439	0.091	549

Table 12. Damping values obtained from sine sweep procedure, thick plate, thin coating.

Mode	ω_n (Hz)	ζ	Q
1	198.6	0.055	909
2	490.3	0.021	2,381
3	1206	0.135	370
4	1653	0.074	676
5	1764	0.039	1,282
6	3142	0.127	394
7	3458	0.306	163
8	3823	0.189	265
9	4134	0.183	273
10	5510	0.099	505

Table 13. Damping values obtained from sine sweep procedure, thick plate, thick coating.

Mode	ω_n (Hz)	ζ	Q
1	197.3	0.076	658
2	493.1	0.027	1,852
3	1212	0.124	403
4	1656	0.079	633
5	1778	0.046	1,087
6	3168	0.088	568
7	3474	0.339	147
8	3853	0.124	403
9	4137	0.137	365
10	5534	0.087	575

Table 14. Comparison of damping results from sine sweep procedure, thick plate. A decrease in Q value is an increase in damping.

	uncoated	thin coated		thick coated	
Mode	Q	Q	% Decrease	Q	%Decrease
1	1,087	909	16.4%	658	27.6%
2	3,125	2,381	23.8%	1,852	22.2%
3	266	370	-39.3%	403	-8.9%
4	617	676	-9.5%	633	6.3%
5	1,163	1,282	-10.3%	1,087	15.2%
6	926	394	57.5%	568	-44.3%
7	253	163	35.3%	147	9.7%
8	641	265	58.7%	403	-52.4%
9	255	273	-7.1%	365	-33.6%
10	549	505	8.1%	575	-13.8%
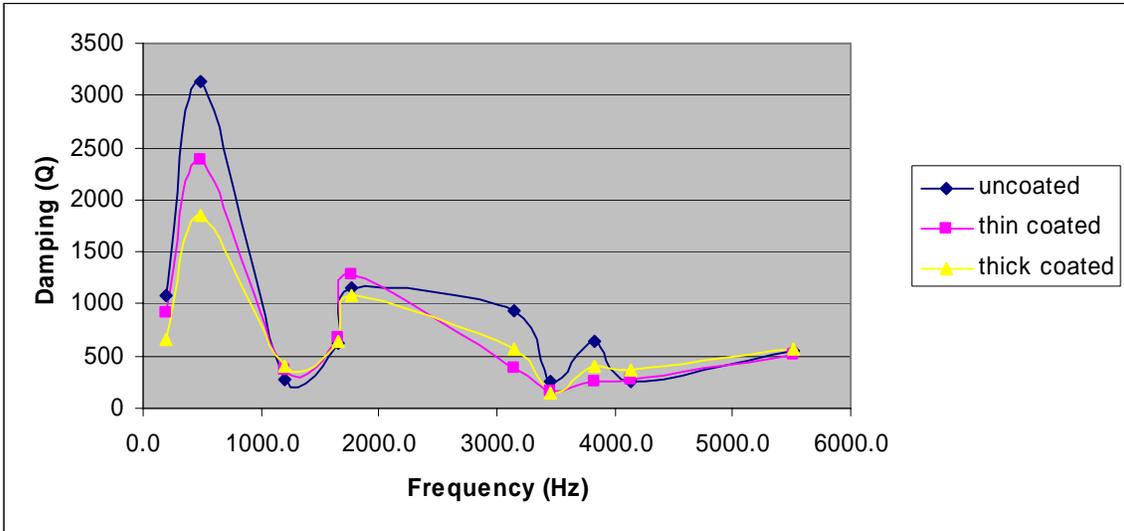
Figure 42. Damping vs. Frequency, Room Temperature, Thick Plate, B&K system
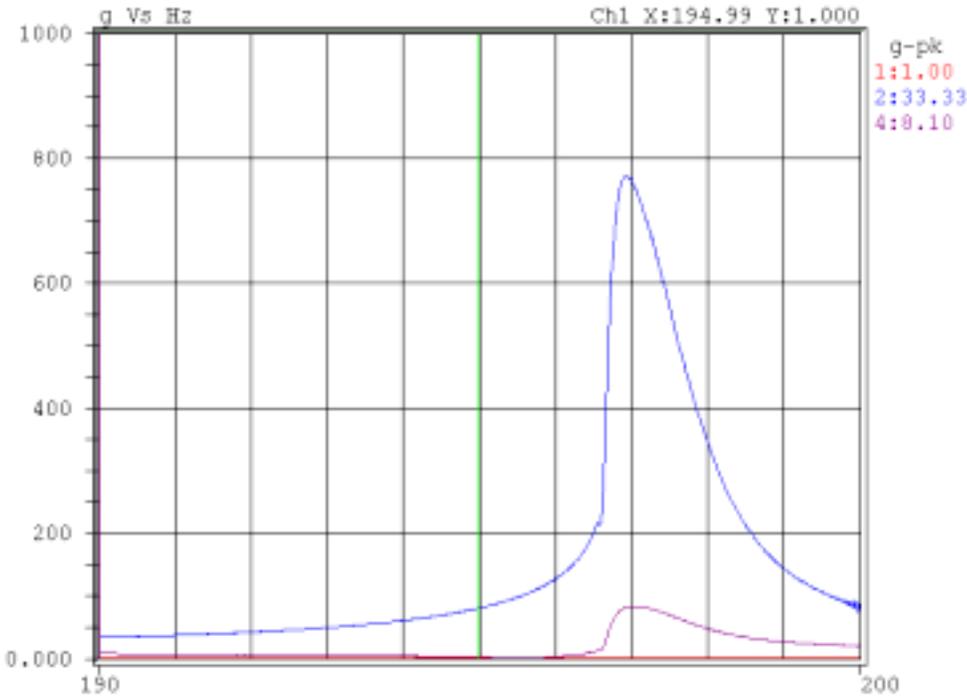
Figure 43. Power Spectral Density, U-D system, uncoated thick plate, mode 1. Channel 2 (blue line) is velocity.
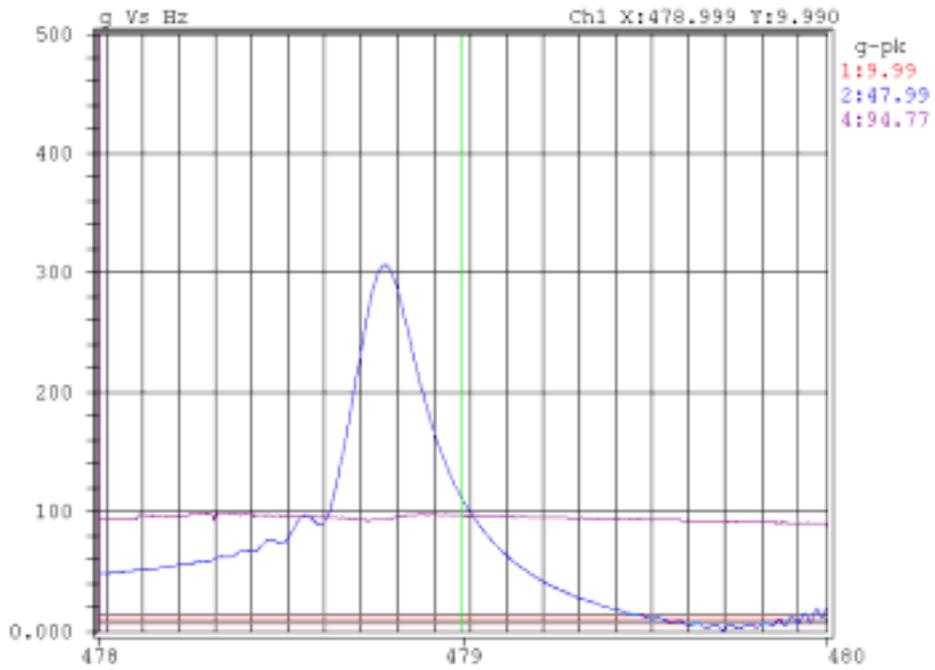
Figure 44. Power Spectral Density, U-D system, uncoated thick plate, mode 2. Channel 2 (blue line) is velocity.
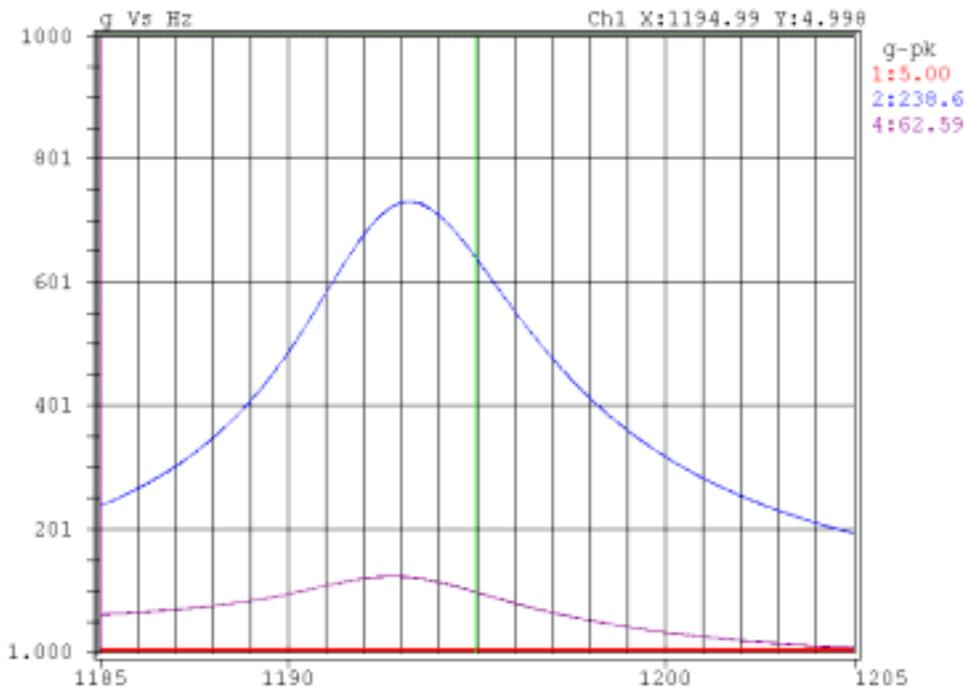
Figure 45. Power Spectral Density, U-D system, uncoated thick plate, mode 3. Channel 2 (blue line) is velocity.
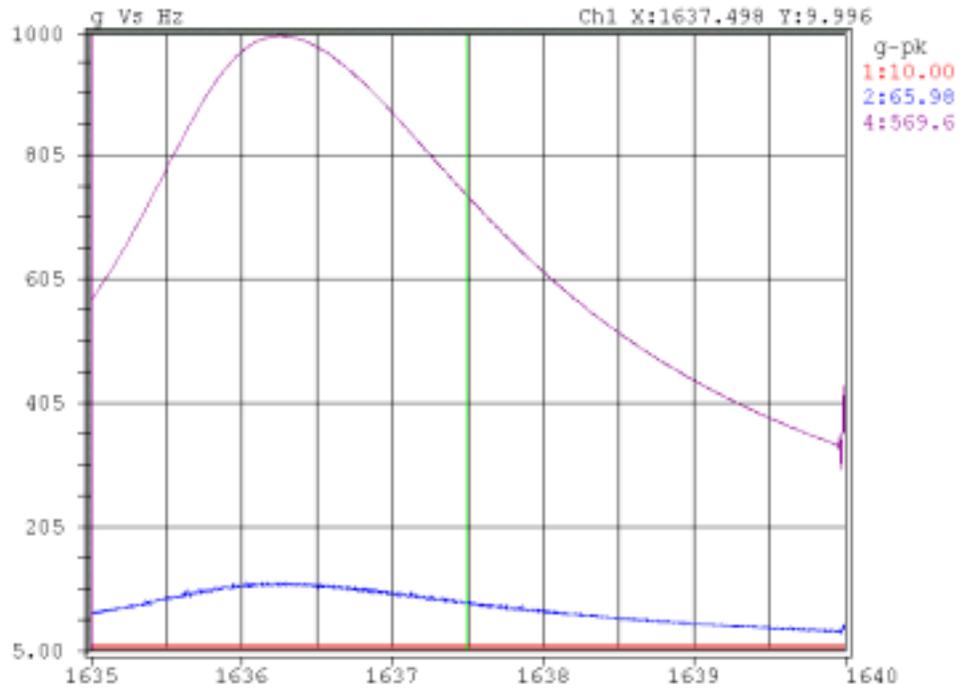
Figure 46. Power Spectral Density, U-D system, uncoated thick plate, mode 4. Channel 2 (blue line) is velocity.
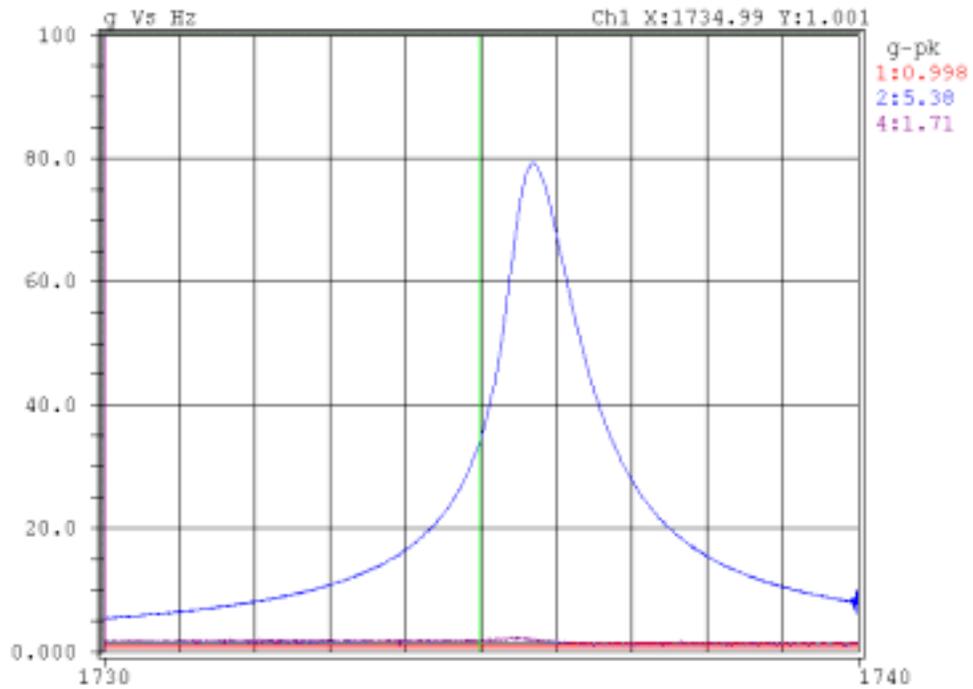
Figure 47. Power Spectral Density, U-D system, uncoated thick plate, mode 5. Channel 2 (blue line) is velocity.

Table 15. Damping Values, Uncoated Thick Plate, Sine Sweep, Unholtz-Dickie System

Mode	Shaker Table Acceleration (g's)	Sweep Rate (Hz/min)	ω_r	velocity, mm/s	Q
1	1	5	196.9	771	239
1	5	5	196.1	1225	87
2	1	2	478.8	45.2	2,610
2	10	2	478.8	307	2,870
3	1	6.67	1,194	144	194
3	5	6.67	1,193	732	194
4	10	5	1,636	114.5	796
4	20	10	1,637	87.5	381
5	1	5	1,736	79.2	1,983
5	10	5	1,735	620.7	1,486

Table 16. Damping Values, Thin Coated Thick Plate, Sine Sweep, Unholtz-Dickie System

Mode	Shaker Table Acceleration (g's)	Sweep Rate (Hz/min)	ω_r	velocity, mm/s	Q
1	1	5	194	345	103
2	1	2.5	487	11.6	1,102
2	10	2.5	485	56.9	542
3	1	8.33	1,189	95	116
3	10	8.33	1,170	781	100
4	10	7.5	1,633	44.6	207
4	20	10	1,625	78.3	185
5	1	4	1,753	31.5	641
5	10	6.5	1,745	135.1	244

Table 17. Damping Values, Thick Coated Thick Plate, Sine Sweep, Unholtz-Dickie System

Mode	Shaker Table Acceleration (g's)	Sweep Rate (Hz/min)	ω_r	velocity, mm/s	Q
1	1	5	192	269	101
2	1	3	496	11.4	1,153
2	10	3	494	58.7	592
3	1	12.5	1,200	107	128
4	10	10	1,651	33.2	183
4	20	10	1,639	51.2	139
5	1	5	1,786	29.9	678
5	10	5	1,778	151	316

Table 18. Comparison of damping results from sine sweep procedure, thick plate, Unholtz-Dickie System. A decrease in Q value is an increase in damping.

Mode	Uncoated Q	Thin coated Q	% Decrease	Thick coated Q	% Decrease
1	239	103	56.8%	101	1.6%
2	2,610	1,102	57.8%	1,153	-4.6%
3	194	116	39.9%	128	-10.2%
4	796	207	74.0%	183	11.6%
5	1,983	641	67.7%	678	-5.7%
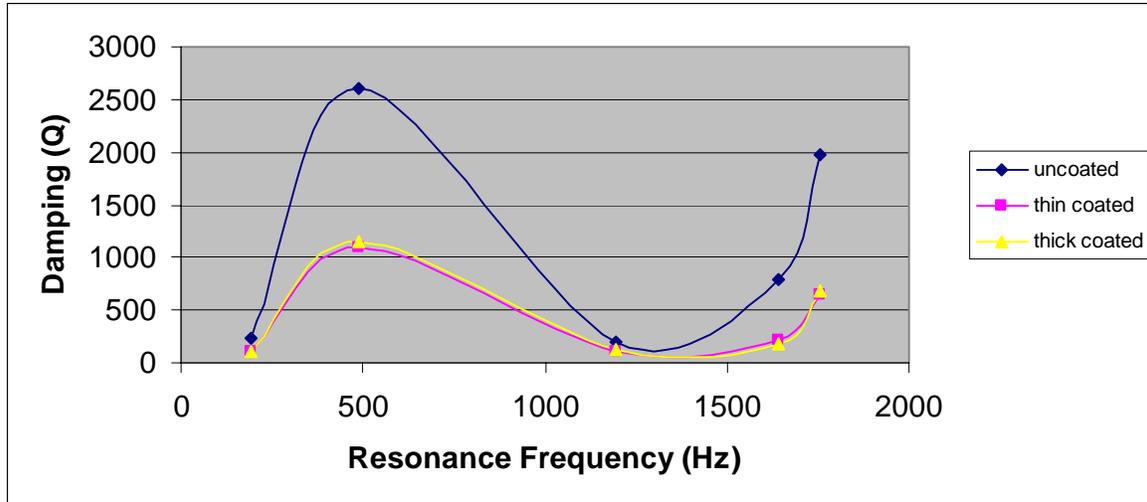
Figure 48. Damping vs. Frequency, Room Temperature, Thick Plate, Unholtz-Dickie System

Table 19. Effect of increased excitation force on damping. Damping values are in Q; a decrease indicates increased damping.

mode	uncoated plate			thin coated plate			thick coated plate		
	first run	second run	increase (+) or decrease (-)	first run	second run	increase (+) or decrease (-)	first run	second run	increase (+) or decrease (-)
1	239	87	-	103	---	NA	101	---	NA
2	2,610	2,870	+	1,102	542	-	1,153	592	-
3	194	194	No Change	116	100	-	128	---	NA
4	796	381	-	207	185	-	183	139	-
5	1,983	1,486	-	641	244	-	678	316	-
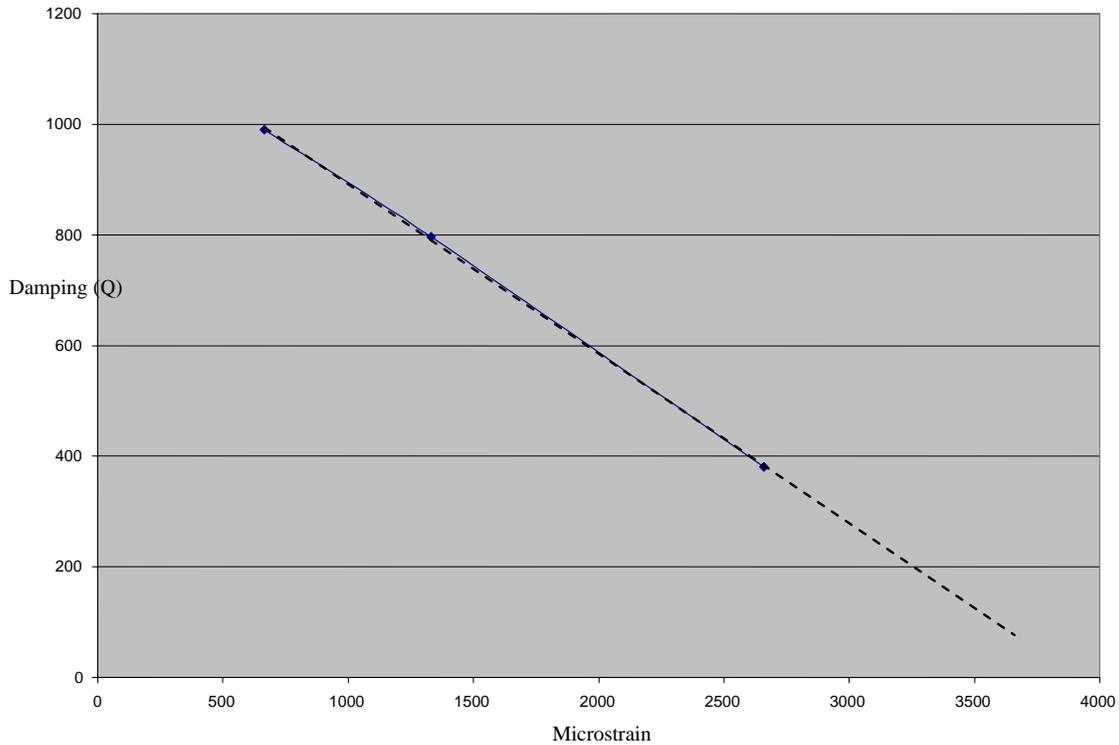
Figure 49. Damping vs. strain curve, 1st chordwise bend mode, thick plate.

Effect of Temperature on Damping. Prior to testing coated plates at temperature, a

baseline test was run on uncoated plates to verify the process. A thin uncoated plate was

set up for the sine sweep procedure in the oven. Two trials were run at room

temperature, then the oven temperature was raised to 275 F and three more trials were run

at this temperature. Results are in Tables 20 and 21, and are graphed in Fig. 50. The

graph shows that the results were repeatable between runs, but does not show a consistent

trend in damping. For some modes, the damping increases with the increase in

temperature, while it decreases for other modes. The inconsistency cannot be attributed

to changes in boundary conditions between runs, as the test specimen remained mounted

throughout this phase of testing. Looking more closely at the damping values obtained, six of the 10 modes had Q values below 200 at room temperature. These values are lower than had been seen in the previous test (see Table 7), where only three of the first 10 modes were below 200, indicating the clamp is dissipating more energy in this run than it had previously. As these results were inconclusive, the test was not run for the coated plates.

A second approach was taken for determining the effect of temperature on damping. To avoid the problems experienced trying to get uniform and repeatable boundary conditions in the mounting blocks, a trial was run utilizing a free-free-free-free boundary condition. In the first test procedure, the cantilevered edge of the plate was constrained in all six degrees of freedom. In this second method, the plate was free to move in all six degrees of freedom along each edge. Thus, not only was the effect of the variability of the boundary condition between runs eliminated, the effect of the boundary condition on damping was eliminated also. The Q values obtained from the free-free-free-free method are primarily the inherent damping properties of the material (although losses due to the plate's interaction with the air in the chamber are still present), rather than the material and clamping system.

The program was run with a temperature profile of 30 – 250 F, with data taken at about 20 degree intervals. After the temperature stabilized at each test point, a sine sweep was run to 2000 Hz. A fast Fourier transform was conducted, and a power spectral density was output. Although this sweep captured five resonance modes, only the fourth mode was analyzed. The MATLAB program determined the peak, the -3 dB point, the

frequency width at -3 dB, and calculated Q. The test was conducted on uncoated and thick coated plates. Results are in Fig. 51.

General trends for both cases are the same. Damping is at a minimum at around 90-110 F, and increases as temperature increases or decreases from there. Between 100 and 200 F, the damping increases dramatically. Above 200 F, the temperature effect dissipates, and even seems to cause damping to somewhat decrease. There are only a few data points below 90 F, and they do not present a consistent pattern.

In comparing the two curves, it appears the coating causes a slight decrease in damping at most temperatures. This includes room temperature, where it has been previously demonstrated that the coating increases damping. In reviewing the specific curves from which the Q values were determined, it is observed that the return signal from the coated plate was very noisy, making calculations imprecise. This is not the case with the uncoated plate. See Figs. 52 and 53. The "halfpower" MATLAB analysis program was not able to correctly identify the endpoints of the bandwidth due to the noise in the signal in Fig. 53. All other thick coated data points were similar. The curve for the coated plate in Fig. 51 was not developed from the "halfpower" calculated Q values, but by manually moving the -3 dB points out to the edges of the band. This made the estimate better, but with Q values in the thousands, small differences in the change in frequency can lead to large differences in Q. This source of error, coupled with the small difference between the curves, makes a comparison tenuous. The procedure needs to be further refined.

Table 20. Damping Data, Thin Uncoated Plate, Room Temperature

mode	Trial 1, Room Temp.			Trial 2, Room Temp.		
	Freq (Hz)	ζ (%)	Q	Freq (Hz)	ζ (%)	Q
1	79	1.450	34.48	79	1.450	34.48
2	197	0.513	97.47	189	1.230	40.65
3	505	0.373	134.05	502	0.297	168.35
4						
5	761	0.134	373.13	760	0.130	384.62
6	1399	0.769	65.02	1398	1.050	47.62
7	1461	0.067	746.27	1465	0.077	649.35
8	1659	0.052	961.54	1660	0.098	510.20
9	1862	0.593	84.32	1871	0.864	57.87
10	2405	0.430	116.28	2406	0.440	113.64
11	2905	1.280	39.06	2911	1.100	45.45

Table 21. Damping Data, Thin Uncoated Plate, Elevated Temperature

mode	Trial 1, 275 F			Trial 2, 275 F			Trial 3, 275 F		
	Freq (Hz)	ζ (%)	Q	Freq (Hz)	ζ (%)	Q	Freq (Hz)	ζ (%)	Q
1	83	1.06	47.17	83	0.985	50.76	82		
2	200	0.545	91.74	200	0.547	91.41	200	0.548	91.24
3	516	0.361	138.50	516	0.342	146.20	516	0.308	162.34
4	726	0.344	145.35	726	0.292	171.23	727	0.390	128.21
5	771	0.195	256.41	771	0.200	250.00	772	0.193	259.07
6	1380	0.456	109.65	1380	0.449	111.36	1379	0.459	108.93
7	1517	0.511	97.85	1517	0.539	92.76	1518	0.600	83.33
8	1692	0.102	490.20	1693	0.103	485.44	1692	0.100	500.00
9	1847	0.088	568.18	1847	0.092	543.48	1847	0.091	549.45
10	2396	0.669	74.74	2395	0.658	75.99	2396	0.619	80.78
11	2952	0.618	80.91	2952	0.572	87.41	2953	0.685	72.99
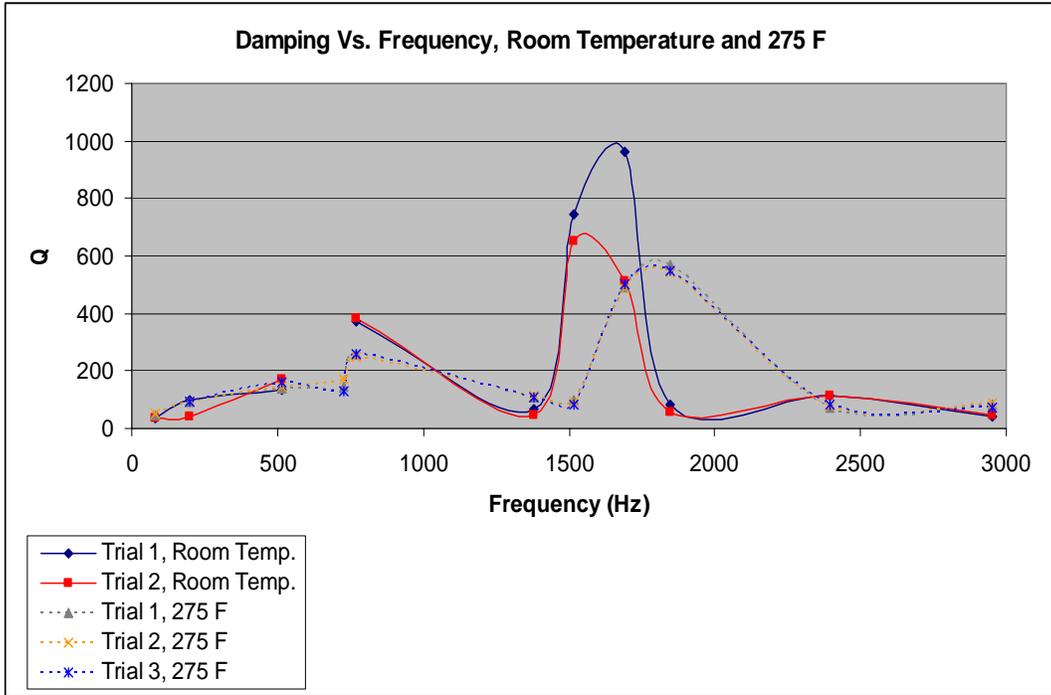
Figure 50. Damping vs. frequency, thin uncoated plate. Solid lines are room temperature values, dashed lines are elevated temperature.
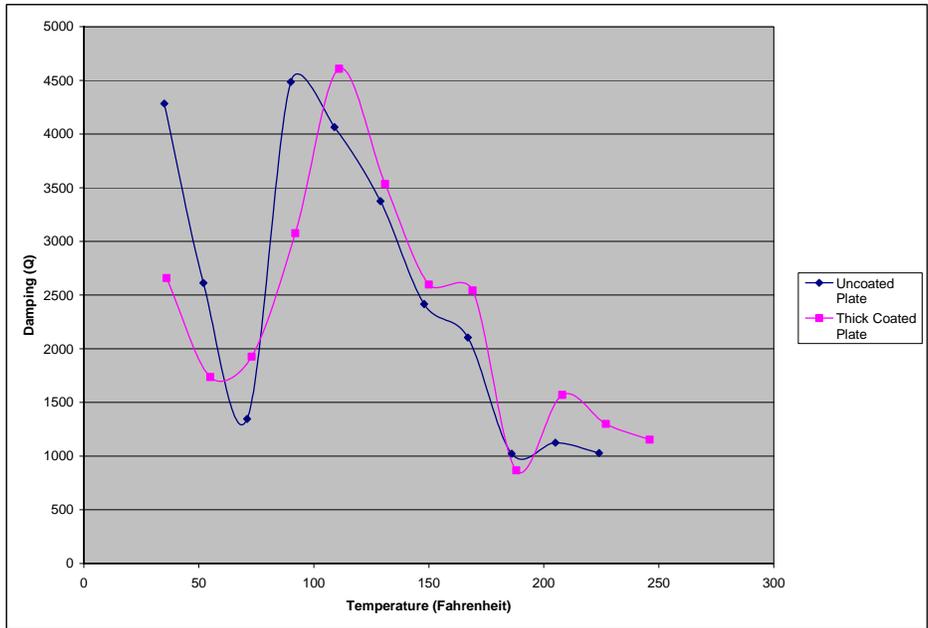
Figure 51. Damping as a function of temperature and coating thickness, thick plate, two-stripe mode.
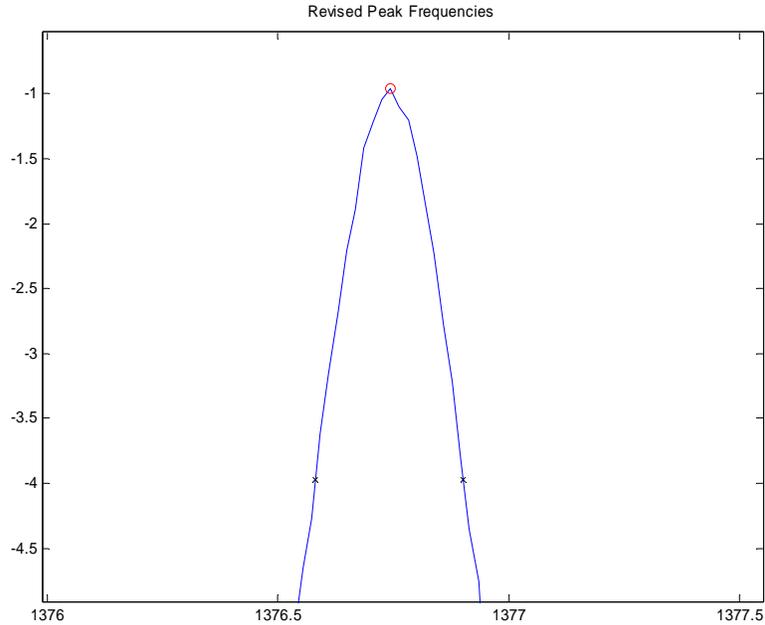
Figure 52. Power spectral density, uncoated plate at 36 F, zoomed in on fourth mode peak. Circle is maximum amplitude and X's are half-power points selected by MATLAB program. Signal is clear, so damping value is easy to calculate.
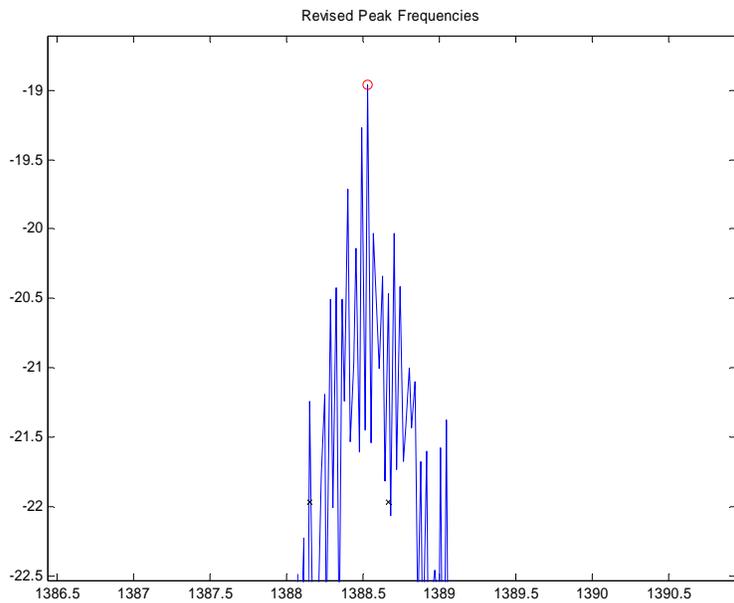
Figure 53. Power spectral density, coated plate at 35 F, zoomed in on fourth mode peak. Circle is maximum amplitude and X's are half-power points selected by MATLAB program. Signal is noisy; calculated damping value is not accurate.

Fatigue

Fatigue testing was conducted on uncoated, thin coated, and thick coated 0.125" thick plates, in the two-stripe mode.

Uncoated plate T-11 was tested first. Table 22 contains the data collected to develop the strain-displacement chart, which is plotted as run 1 in Fig. 54. Based on this curve, the velocity needed to produce a strain of 4,800 $\mu\epsilon$ (the velocity needed to fatigue titanium in 1,000,000 cycles) was determined to be 493 mm/s. The SmartOSC feature of the VWIN software was selected. The resonance frequency was set at 1630 Hz. The clock was started, and the acceleration was increased until the target velocity was reached. The acceleration at the target velocity was 66.76 g's. The frequency was varied to maximize the amplitude; resonance was found at 1628.81 Hz. It took 2 minutes to raise the acceleration and locate the resonance frequency. The velocity began falling after 3:50; the frequency of the forcing function was reduced, and the amplitude of the velocity was restored. After 5:56, the run was stopped, because the velocity could not be maintained. The specimen was removed from the test apparatus and soaked in a dye penetrant. A crack was found near the center of the free edge; see Fig. 55. The plate had fatigued. The run time was much less than the 10:20 expected. Only about 390,000 cycles were reached before the plate fatigued, rather than the 1,000,000 cycles anticipated.

Table 22. Velocity, strain, and frequency at increasing acceleration levels, two-stripe mode, Plate T-11.

Shaker Table Acceleration (g's)	Velocity (mm/s)	Displacement (mm) (calculated)	Strain (με)	Drive Volts	Freq (Hz)	Freq (rad/s)
0.52	5.7	0.00056	56	0.012	1631.32	10,249.89
1.05	10.9	0.00106	109	0.024	1630.82	10,246.74
1.48	15	0.00146	154	0.034	1630.82	10,246.74
2.08	21	0.00205	217	0.048	1630.82	10,246.74
2.94	29	0.00283	298	0.068	1630.82	10,246.74
3.7	37	0.00361	371	0.086	1630.32	10,243.60
5.24	52	0.00508	526	0.121	1630.32	10,243.60
6.6	65	0.00635	659	0.153	1630.32	10,243.60
8.35	81	0.00791	820	0.192	1630.32	10,243.60
10.56	99	0.00966	1005	0.242	1630.32	10,243.60
11.92	112	0.01094	1134	0.271	1629.82	10,240.46

The second specimen tested was uncoated plate T-10. A new strain-displacement curve was generated for this specimen. Table 23 contains the data collected to develop the strain-displacement chart, which is plotted as run 2 in Fig. 54. The strain gage did not fail as soon as the one for Plate T-11, so more data points were obtained. Compared to the curve for T-11, the shape is still fairly linear, but the slope is significantly higher; see Fig. 54. As Plate T-11 did not come close to reaching 1,000,000 cycles at 77 ksi, it was decided to obtain several data points at 1,000,000 cycles for stresses below 77 ksi before fatiguing Plate T-10. Table 24 shows the calculated strain and target velocities for four different stress data points, the largest being the anticipated fatigue point. Strains were

calculated from Hook's Law. Displacements were found from the slope of the line in Fig. 54 for each strain; velocities were determined by multiplying the displacements by the resonance frequency.

For this specimen, the resonance frequency was determined from a sine sweep to be 1622.9 Hz. This yields a test time of 10:16. The 60 ksi test point was run first. A velocity of 292 mm/s was reached at an acceleration of 31.15 g's. Resonance was found at 1622.81 Hz. Shortly after the clock was started, the velocity climbed to 298 mm/s; as this was still significantly less than the next test point, no adjustment was made. After about 6 minutes, the velocity began to fall. The frequency of the forcing function was lowered to try and maintain the amplitude. After about 40 seconds, the velocity could not be maintained. The run was stopped. A sine sweep was run, and the resonance frequency was found to have dropped to 1572 Hz. Resonant dwell was attempted at this frequency, but after applying over twice the acceleration, the velocity had only risen to 83 mm/s. The plate was removed and soaked in dye penetrant. A crack was found near the center of the free edge. See Fig. 55. The plate had fatigued after about 600,000 cycles, at a stress believed to be only about 80% of the fatigue stress.

Table 23. Velocity, strain, and frequency at increasing acceleration levels, two-stripe mode, Plate T-10.

Shaker Table Acceleration (g's)	Velocity (mm/s)	Displacement (mm) (calculated)	Strain (με)	Drive Volts	Freq (Hz)	Freq (rad)
0.115	1.1	0.000107815	15	0.003	1623.81	10202.699
0.328	3	0.00029404	42	0.008	1623.81	10202.699
0.52	5	0.000490066	67	0.012	1623.81	10202.699
0.74	6.8	0.000666696	96	0.017	1623.31	10199.558
1.05	10	0.000980435	137	0.024	1623.31	10199.558
1.47	15	0.001470652	194	0.034	1623.31	10199.558
2.07	20.8	0.002039304	273	0.048	1623.31	10199.558
2.61	26	0.00254913	340	0.061	1623.31	10199.558
3.29	32	0.003137391	422	0.076	1623.31	10199.558
4.14	40	0.003921739	519	0.096	1623.31	10199.558
5.22	49	0.00480561	645	0.121	1622.81	10196.416
6.62	62	0.006080568	823	0.153	1622.81	10196.416
7.4	70	0.006865157	928	0.171	1622.81	10196.416
8.33	79	0.00774782	1033	0.192	1622.81	10196.416
9.37	86	0.008434336	1140	0.216	1622.81	10196.416
10.53	96	0.009415073	1252	0.242	1622.81	10196.416
11.94	105	0.01030091	1400	0.271	1622.31	10193.274
13.4	120	0.011772468	1576	0.304	1622.31	10193.274
15.04	137	0.013440235	1766	0.342	1622.31	10193.274
16.91	153	0.015009897	1941	0.383	1622.31	10193.274
19.17	172	0.016879074	2180	0.43	1621.81	10190.133

Table 24. Strain and target velocity for given stress levels, Plate T-10.

Stress (ksi)	Strain (με)	Velocity (mm/s)
60	3,750	292
65	4,063	316
70	4,375	340
77	4,800	373

The first two tests resulted in failures at points far short of expectations. Either the material was not behaving as expected, or the strain being generated was higher than desired. For the third test, it was decided to begin with a low stress, and climb toward the fatigue stress.

Uncoated plate T-12 was strain gaged for two-stripe mode. A sine sweep was run to determine its resonance frequency for the two-stripe mode. The sine sweep indicated resonance was at $\omega_r = 1634.8$ Hz, $Q = 990.4$. A strain-displacement curve was generated in the same manner as for the other two uncoated plates; the data is recorded in Table 25. The curve was linear; its slope fell between the ones generated for plates T-10 and T-11; see Fig. 48. Time to reach the target 10^6 cycles was 10:12.

The target stress for the first run was 20 ksi. To achieve this stress, a velocity of 120 mm/s was needed. This was reached with an acceleration of 11.49 g's. The resonance frequency was at 1633.3 Hz. The target time of 10:12 was reached without failure. Runs of 30, 40, and 50 ksi were also run without failure. The next run was targeted at a velocity of 350 mm/s, which translates to a stress of 65 ksi. An acceleration of 35.59 g's initially reached this velocity, but as the laser was reflecting off of a vibrating plate, the reading varied considerably. What initially appeared to be a

94

fluctuation of 350-360 mm/s climbed to 380-390 mm/s after about a minute; by 3

minutes, the velocity was in the 400-410 range. Between the 5 minute mark and the end

of the run, the velocity was much steadier, holding between 420 and the 430s. For the

run, the average velocity was estimated to be around 420 mm/s, which translates to a

stress of about 74 ksi. The next run was conducted at the next voltage increment, which

resulted in an acceleration of 40.32 g's and a velocity of 440–460 mm/s. After about 4

minutes the velocity began to fall. The frequency was reduced to try and relocate the

dropping resonance condition. At 4:35, resonance was located at 1627.8 Hz, but the

magnitude of the velocity was 158 mm/s. The plate had fatigued.

The fatigue stress was determined by interpolating between the stress at failure

and the last known data point:

$$\sigma_A = \sigma_{pr} + \frac{N_f}{N_t}(\sigma_f - \sigma_{pr}) \tag{20}$$

where

σ_A = alternating stress

σ_{pr} = previous stress (the stress at the previous successful run)

N_f = cycles at failure

N_t = target number of cycles

σ_f = stress at failure.

(Maxwell, 1998)

Using this method, the fatigue stress for the uncoated plate was determined to be 76.4 ksi,

which is within a reasonable margin of error of the accepted value of 77 ksi. As this test

produced results close to the expected results, the strain-displacement curve for this plate

is probably more accurate than the other two, which produced results unexpected when considering the accepted fatigue stress value. Additionally, if the Run 3 strain-displacement curve is accurate, the velocity used to fatigue Plate T-11 in 390,000 cycles generated a stress of about 87 ksi, rather than the 77 ksi intended, which explains the premature failure of this plate. This does not explain the early failure of Plate T-10.

Table 25. Velocity, strain, and frequency at increasing acceleration levels, two-stripe mode, Plate T-12.

Shaker Table Acceleration (g's)	Velocity (mm/s)	Displacement (mm) (calculated)	Strain (με)	Drive Volts	Freq (Hz)	Freq (rad/s)
0.11	1.35	0.000131	15	0.002	1635.32	10275.02
0.157	1.9	0.000185	21	0.003	1635.32	10275.02
0.198	2.4	0.000234	27	0.004	1635.32	10275.02
0.249	3	0.000292	34	0.005	1635.32	10275.02
0.315	3.7	0.000360	42	0.007	1635.32	10275.02
0.397	4.8	0.000467	52	0.009	1635.32	10275.02
0.499	5.9	0.000574	66	0.011	1635.32	10275.02
0.628	7.7	0.000750	84	0.014	1634.82	10271.88
0.8	10	0.000974	107	0.017	1634.82	10271.88
1	12	0.001168	136	0.022	1634.82	10271.88
1.26	15	0.001460	170	0.027	1634.82	10271.88
1.41	17	0.001655	192	0.03	1634.82	10271.88
1.78	21	0.002044	239	0.038	1634.82	10271.88
1.99	24	0.002336	266	0.043	1634.82	10271.88
2.23	26	0.002531	295	0.048	1634.82	10271.88
2.51	29	0.002823	326	0.054	1634.82	10271.88
2.85	34	0.003311	373	0.061	1634.32	10268.74
3.2	38	0.003701	418	0.068	1634.32	10268.74
3.58	42	0.004090	474	0.076	1634.32	10268.74
4.02	47	0.004577	529	0.086	1634.32	10268.74
4.51	53	0.005161	591	0.096	1634.32	10268.74
5.06	59	0.005746	653	0.108	1634.32	10268.74
7.17	78	0.007596	867	0.153	1634.32	10268.74
9.07	91	0.008862	1030	0.192	1634.32	10268.74
10.25	110	0.010715	1224	0.216	1633.82	10265.59
11.51	122	0.011884	1353	0.242	1633.82	10265.59
12.94	133	0.012956	1485	0.271	1633.82	10265.59
14.57	147	0.014320	1630	0.304	1633.82	10265.59
16.55	174	0.016955	1890	0.342	1633.32	10262.45
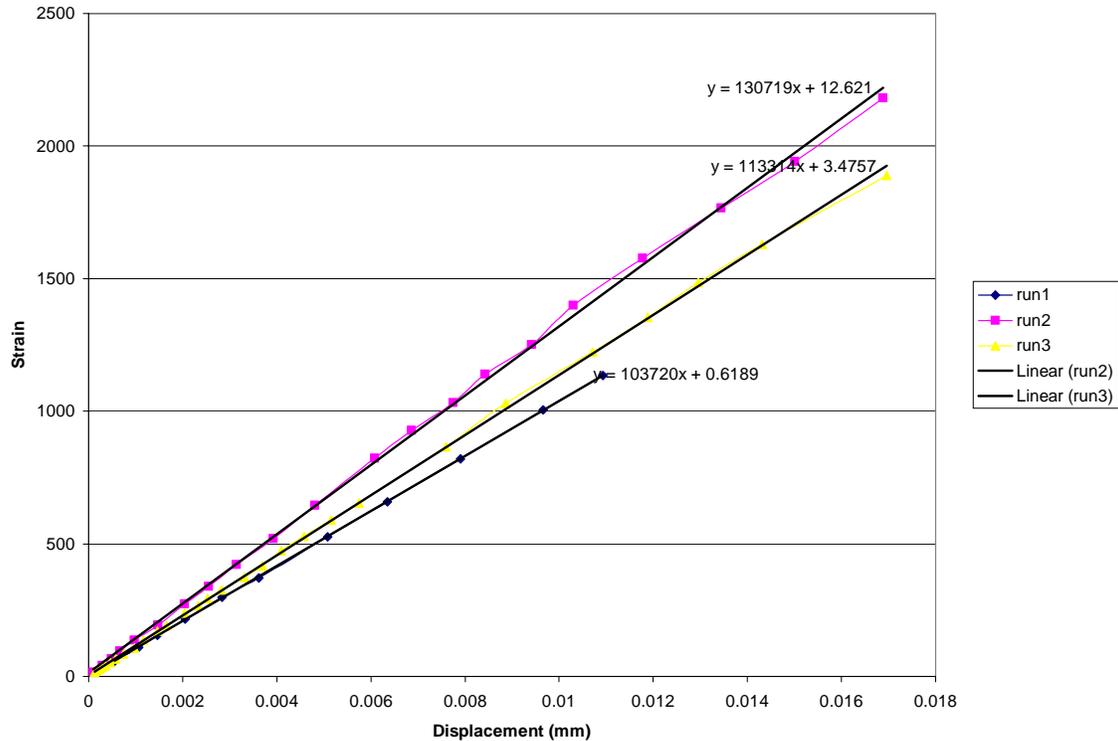
Figure 54. Strain vs. displacement, two-stripe mode, thick plate. Run 1 is Plate T-11, run 2 is Plate T-10, run 3 is Plate T-12.

Thin coated plate T-3 was tested using the same method as T-12. A sine sweep was run, and resonance was found at 1628.7 Hz at 10 g's, with Q = 233. The strain-displacement curve developed for Plate T-12 was used, with the displacement calculation altered to account for the change in frequency between T-12 and T-3. Accelerations were applied to reach the same velocities as with the uncoated plate. The first test point was at a stress of 20 ksi, velocity of around 120 mm/s. For the uncoated plate, this stress was reached at an acceleration of 11.49 g's; for Plate T-3, it took 31.07 g's. The target 1,000,000 cycles was reached without failure. Test points at 30 ksi and 60 to 65 ksi were achieved successfully. The next test point attempted was $\sigma = 75$ksi, $v = 425$ mm/s. An acceleration of 65.10 g's was needed to achieve this velocity. The 10^6 cycles were

97

completed. The plate failed 5:50 into the next run at 90 ksi, 69.23 g's. The plate was inspected, and no damage to the coating was visible. The 5:50 run time completed about 556,500 cycles. Interpolating the stress data results in a fatigue stress of 83.3 ksi, slightly higher than that calculated for the uncoated plate. Using the same interpolation formula to determine the acceleration at fatigue yields an acceleration of 38.39 g's for the uncoated plate, and 67.4 g's for the thin coated plate, for an increase of 80%.

Thick coated plate T-7 was tested in the same manner. From the sine sweep, ω_r was found to be 1610 at 10 g's, and Q was 245, slightly lower than the 284 found for the thin coated plate. The strain-displacement curve for Plate T-12 was used, with revised resonance frequencies substituted into the displacement equation. The first test point was $\sigma = 40$ ksi, target velocity of 220 mm/s. The velocity was achieved at an acceleration of 67.68 g's, but the resonance frequency had dropped to 1574.8 Hz. The next point was around 70 ksi, velocity around 100 mm/s, a = 84.24 g's. After completing the target cycles, the acceleration was increased to 87.06 g's, resulting in a velocity of 450 mm/s and a stress of 82 ksi. A visual inspection was conducted after the target cycles were completed. A section of the coating was missing, exposing an area of bare metal, 1/3" x 2/3" on the top surface in the high strain area where the strain gage had been placed on the uncoated plates; see Fig. 56. As the plate had not failed, the test continued. The target cycles were completed for test points at 108 and 130 ksi, with accelerations of 118.1 and 119.5 g's, respectively. The plate failed after 527,000 cycles at 175 ksi,. The acceleration at this point was 133.2 g's. Interpolation yields a fatigue stress of 153,700 psi, and an acceleration at this stress of 126.7 g's. Visual inspection following the test

showed that the uncoated section on the top surface had grown to 1 ¼" x ½", and a small section on the underside had also lost some coating.

While the fatigue stress is twice what is expected, the force required to reach fatigue should be sufficiently accurate for use in comparison with the other specimens. The stress value is calculated based on the velocity as measured by the laser, which is located near a node line. The velocity gradient is steep in this region, so a slight misalignment of the laser could result in sizable errors in the velocity reading. The finite element model can provide some insight. In the model, elements are 0.225" x 0.225". The laser target was in CQUAD4 element 123, which extended from 0.45" to 0.675" in from the left edge of the plate. The previous and following elements in the x-direction were elements 122 and 124. The program results included relative displacements. Translations in the z (thickness) direction for the fourth mode for elements 122, 123, and 124 are -0.0653, -0.0230, and 0.0212, respectively (no units). Thus, having the laser aligned .225" too far towards the edge results in a displacement error of 184%; having the laser aligned .225" too far in from the edge results in a displacement error of 192%. As velocity is related to displacement by the frequency at which the test is run, and the frequency is not affected by the laser misalignment, the velocity error is the same as the displacement error. For laser misalignment to have caused the 100% error observed in the thick coated plate trial, the laser only needed to be off by 1/8" in the x-direction. As each new plate is mounted, the laser must be realigned. Care is taken to place the laser target as near to the 3.0" x 0.5" point as possible, but these are hand measurements, and are not very precise. A 1/8" error is quite possible.

The accelerometer, however, has been constant throughout the series of tests. Nothing has been altered that would affect the accelerometer readings between runs. The thick plate did complete 1,000,000 cycles at an acceleration of 119.5 g's, and failed after 527,000 cycles at 133.2 g's. Thus, the acceleration at the fatigue stress is between 119.5 g's and 133.2 g's. Interpolation yields a value of 126.7 g's. This is 88% higher than the acceleration (and, equivalently, force) at the fatigue stress for the thin coated plate, and 238% higher than the uncoated plate. Thus, at 10^6 cycles, the thin coated plate can withstand a force 1.8 times as great as the uncoated plate, the thick coated plate can withstand a force 1.88 times as great as the thin coated plate, and the thick coated plate can withstand a force 3.38 times as great as the uncoated plate.

A second procedure was run, to determine the increase in the life of the coated specimen over the uncoated specimen at a given applied force. Thin coated plate T-2 was excited at the force required to fatigue the uncoated specimen at 10^6 cycles. From the test conducted on Plate T-12, the acceleration needed to apply this force was 37.48 g's. An acceleration of 38 g's or greater was applied to T-2, and the time to fail was measured, which could be converted back to cycles. A sine sweep was run at 10 g's to locate the resonance frequency. The frequency was found to be 1641.6 Hz, and Q was calculated as 256. The test specimen was accelerated to 39.33 g's, resulting in a velocity of 79-80 mm/s. After about 7:00, the velocity had fallen into the low-70s. The frequency was adjusted to maximize the magnitude. The frequency was reduced 8.5 Hz, and the maximum velocity was found to be 100-110 mm/s, much higher than previously attained. However, the acceleration at this point was 37.10. The voltage to the system was increased, bringing the acceleration up to 40.51, and the velocity to 120-130. Frequency

was adjusted several times over the next few minutes, trying to locate the resonance point. By 17:00, the velocity had peaked at about 150 mm/s. The cycles accumulated after this time were counted. At 31:00, the acceleration had dropped to around 38, so the voltage was again increased. The resulting acceleration was 42.89 g's, and the velocity was 165-180 mm/s. For the remainder of the time, the acceleration was above 41 g's, and the velocity was mostly in the 180 mm/s range. The test was stopped after 70:00 on the clock. Subtracting off the 17:00 it took to reach a steady state resonance condition, the plate was at resonance for 53:00. It accumulated over 5,000,000 cycles at a force greater than that which would fatigue an uncoated plate in 1,000,000 cycles. Thus, the thin mag spinel coating increases the life of titanium by over 5 times.

Figure 55. Plates T-10 and T-11, after fatigue test. Bright areas are the cracks. The cracks are not visible with the naked eye; the specimens have been treated with a dye penetrant, and are viewed under an ultraviolet light.
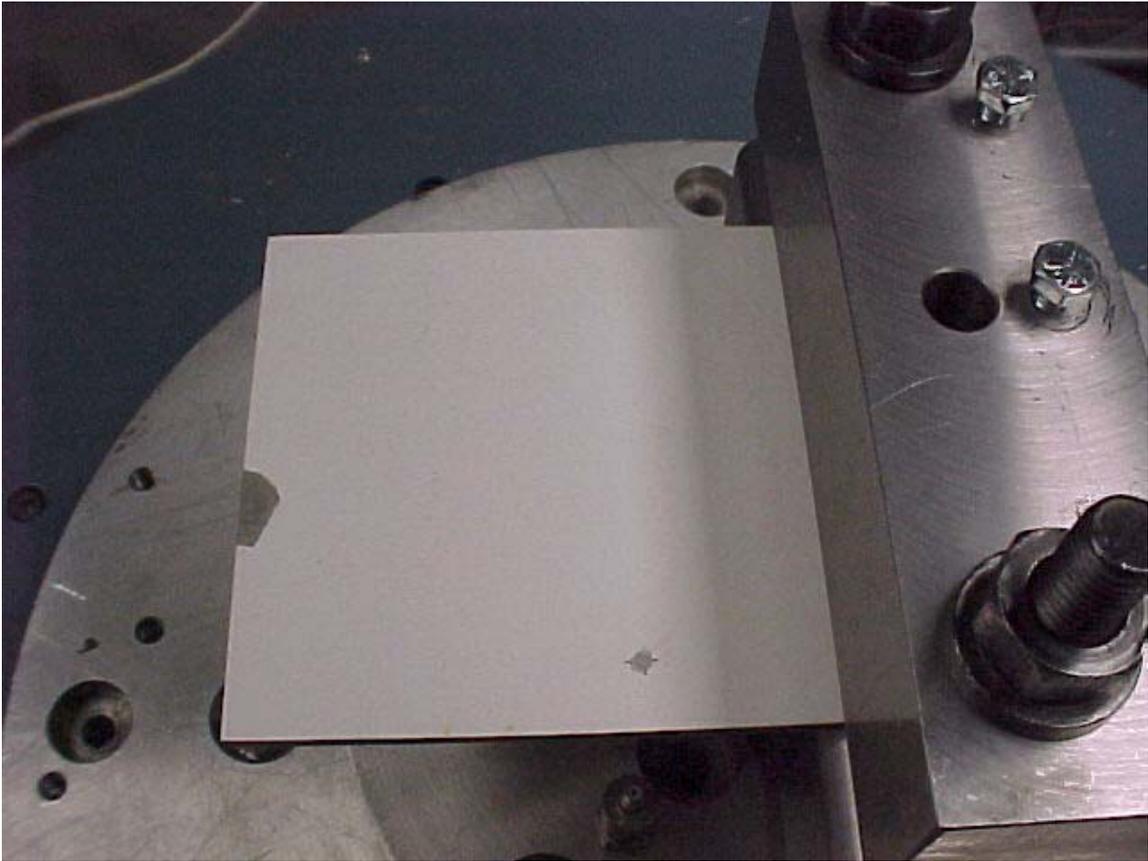
Figure 56. Thick-coated Plate T-7 in mounting blocks on 6k Unholtz-Dickie shaker, after completing 10^6 cycles at 82 ksi. A section of coating has flaked off in the high strain region along the free edge.

V. Conclusions and Recommendations

Boundary Conditions

The greatest challenge in the setup of the equipment was in getting consistent boundary conditions, both in getting a consistent plate length and a consistently rigid bond between the clamping system and the plate. Plate length variations were evidenced in changes in resonance frequencies between runs. The most obvious example of poor or inconsistent clamping was seen by increases in damping.

The difficulty in getting the plate length to be exactly 4 ½" was that the measurements were done by hand using a ruler. Measurements were taken along both sides to minimize the error. Plate lengths were estimated to be within 1/32" of the target. This variation was not viewed as a major source of error.

Several approaches were used to maximize the rigidity of the clamping of the test specimens. The application of double-sided tape to the clamped portion of the plate did not have a noticeable effect. Set screws were added to the system. Set screws go through one of the mounting blocks, and are turned against the plate to help hold the plate. This seemed to improve the clamping of the thick plate, but the thin plate did not go far enough into the mounting blocks to reach the set screws. One trial was run loading the thin plate directly into the vise, without the use of the mounting blocks. While this did provide a better hold, the fear was the sharp corner of the vise jaw against the plate would result in a stress concentration along this boundary (the mounting block edges are rounded for this reason). The best methodology for the thick plate seemed to be the mounting blocks with the set screws. The thin plates were a problem due to insufficient area for clamping (one inch deep into the blocks, versus two inches for the thick plate).

Damping

For the thin plate using the Bruel & Kjaer system, the thin coating provided increased damping over the uncoated plate for 10 of the 12 modes tested. For 8 of these 10 modes, the damping increase was 9.5% or better, and for 6 modes, it was over 25%. The thick coat provided better damping than the thin coat for all 10 modes for which they each had a common mode. Eight of the 10 modes had an improvement of better than 20%, and 6 modes had an improvement of over 40%.

The results of the thick plate damping tests were inconclusive using the B&K (air horn) system. For some modes, the coatings caused the damping to increase, for others the damping decreased with the addition of the coating. Results may have been better had slower sweep rates been used. However, results were very consistent using the Unholtz-Dickie (shaker table) system. For each of the five modes tested, damping increased by at least 40% with the addition of the thin coating over the uncoated plate. The thick coating provided increased damping over the uncoated plate, but only provided improved damping over the thin coated plate for two of the five modes tested.

The Q values obtained for the thick plate were much higher than those obtained for the thin plate. This is quite likely due in large part to the thick plate having a longer area to clamp (2", vs. 1" for the thin plate). The longer clamp area permitted a more rigid boundary, eliminating some of the damping provided by a less than ideal boundary condition.

For the thick plates, more damping was seen while using the Unholtz-Dickie system than the B&K system. It is quite likely that damping is a function of the applied

force. As the force applied by the shaker was greater than that applied by the air horn in the B&K system, the plates experienced more damping in the U-D system.

For any given plate, damping is not a constant at all frequencies, nor is it a function of frequency. Damping appears to be related to mode shape. The bending modes have the lowest Q values (greatest damping), and the torsion modes have the highest Q values. The chordwise bending modes are in the middle.

Temperature affects damping. Both the uncoated and thick coated plates had a significant increase in damping between 100 and 200 F. The damping stayed relatively level above 200 F. There was not a sufficient amount of quality data collected to reach any conclusions regarding the effect the coating has on damping as temperature varies.

Fatigue

In the first chordwise bend mode, the thin coating increases the force titanium can withstand at fatigue stress by 80%. The thick coating provides an increase of 88% over the thin coating, and 238% over the uncoated plate. At an equivalent applied force, the thin coated plate did not fail after five times the life of the uncoated plate. Thus, the thin mag spinel coating provided improved performance over the baseline bare titanium plate, and the thick coating provided better performance than the thin coating. However, the thin coating remained bonded to the plate under high stress, while high stress caused a section of the thick coating to separate.

Recommendations

All damping trials conducted in this work were related to each other. It would be worthwhile to relate damping values to the applied force. The accelerometer reading could be converted to force, but a finite element model would be needed to relate this single point reading to other locations on the test specimen.

The relationship between the amplitude of the acceleration of the shaker and the damping of the plate should be explored further.

Much work can be done regarding the effect of temperature on the damping and fatigue of mag spinel-coated titanium. The free-free-free-free procedure should be explored further. An oven has been installed which can be used in conjunction with the Unholtz-Dickie 6,000 lb. shaker, but the test specimens used in this work would not fit. Smaller test articles would need to be used.

The fatigue data collected here was only for one mode. Other modes should be investigated as well.

Only two coating thicknesses were investigated, one of which separated under high stress. More work should be done to determine the optimal coating thickness.

Appendix A: Finite Element Model Input Data, Thin Plate

```
       N A S T R A N   E X E C U T I V E   C O N T R O L   E C H O
0



     ID MECH644, IVANCIC
     SOL 103
     TIME 10
     CEND
0                                           C A S E   C O N T R O L   E
C H O
               COMMAND
               COUNT
                1       $
                2       TITLE = NATURAL MODES, TITANIUM PLATE
                3       SUBTIT = 4 1/4" X 4 1/4" X .050"
                4       $
                5       $LOAD = 20
                6       METHOD = 30
                7       SPC = 2
                8       $
                9       DISP(SORT2,PHASE) = ALL
               10       STRESS(SORT2,PHASE) = ALL
               11       LINE=9999
               12       $
               13       BEGIN BULK
0                       INPUT BULK DATA ENTRY COUNT =     562
0                                           S O R T E D   B U L K
D A T A   E C H O
               ENTRY
               COUNT           .   1  ..   2  ..   3  ..   4  ..   5  ..
6  ..   7  ..   8  ..   9  ..   10  .
                1-      CQUAD4  1       1       1       2
19      18
                2-      CQUAD4  2       1       2       3
20      19
                3-      CQUAD4  3       1       3       4
21      20
                4-      CQUAD4  4       1       4       5
22      21
                5-      CQUAD4  5       1       5       6
23      22
                6-      CQUAD4  6       1       6       7
24      23
                7-      CQUAD4  7       1       7       8
25      24
                8-      CQUAD4  8       1       8       9
26      25
                9-      CQUAD4  9       1       9       10
27      26
               10-      CQUAD4  10      1       10      11
28      27
               11-      CQUAD4  11      1       11      12
29      28
```

		12-	CQUAD4	12	1	12	13
30	29						
		13-	CQUAD4	13	1	13	14
31	30						
		14-	CQUAD4	14	1	14	15
32	31						
		15-	CQUAD4	15	1	15	16
33	32						
		16-	CQUAD4	16	1	16	17
34	33						
		17-	CQUAD4	17	1	18	19
36	35						
		18-	CQUAD4	18	1	19	20
37	36						
		19-	CQUAD4	19	1	20	21
38	37						
		20-	CQUAD4	20	1	21	22
39	38						
		21-	CQUAD4	21	1	22	23
40	39						
		22-	CQUAD4	22	1	23	24
41	40						
		23-	CQUAD4	23	1	24	25
42	41						
		24-	CQUAD4	24	1	25	26
43	42						
		25-	CQUAD4	25	1	26	27
44	43						
		26-	CQUAD4	26	1	27	28
45	44						
		27-	CQUAD4	27	1	28	29
46	45						
		28-	CQUAD4	28	1	29	30
47	46						
		29-	CQUAD4	29	1	30	31
48	47						
		30-	CQUAD4	30	1	31	32
49	48						
		31-	CQUAD4	31	1	32	33
50	49						
		32-	CQUAD4	32	1	33	34
51	50						
		33-	CQUAD4	33	1	35	36
53	52						
		34-	CQUAD4	34	1	36	37
54	53						
		35-	CQUAD4	35	1	37	38
55	54						
		36-	CQUAD4	36	1	38	39
56	55						
		37-	CQUAD4	37	1	39	40
57	56						
		38-	CQUAD4	38	1	40	41
58	57						
		39-	CQUAD4	39	1	41	42
59	58						

40-	CQUAD4	40	1	42	43
41-	CQUAD4	41	1	43	44
42-	CQUAD4	42	1	44	45
43-	CQUAD4	43	1	45	46
44-	CQUAD4	44	1	46	47
45-	CQUAD4	45	1	47	48
46-	CQUAD4	46	1	48	49
47-	CQUAD4	47	1	49	50
48-	CQUAD4	48	1	50	51
49-	CQUAD4	49	1	52	53
50-	CQUAD4	50	1	53	54
51-	CQUAD4	51	1	54	55
52-	CQUAD4	52	1	55	56
53-	CQUAD4	53	1	56	57
54-	CQUAD4	54	1	57	58
55-	CQUAD4	55	1	58	59
56-	CQUAD4	56	1	59	60
57-	CQUAD4	57	1	60	61
58-	CQUAD4	58	1	61	62
59-	CQUAD4	59	1	62	63
60-	CQUAD4	60	1	63	64
61-	CQUAD4	61	1	64	65
62-	CQUAD4	62	1	65	66
63-	CQUAD4	63	1	66	67
64-	CQUAD4	64	1	67	68
65-	CQUAD4	65	1	69	70
66-	CQUAD4	66	1	70	71
67-	CQUAD4	67	1	71	72

60	59
61	60
62	61
63	62
64	63
65	64
66	65
67	66
68	67
70	69
71	70
72	71
73	72
74	73
75	74
76	75
77	76
78	77
79	78
80	79
81	80
82	81
83	82
84	83
85	84
87	86
88	87
89	88

		68-	CQUAD4	68	1	72	73
90	89	69-	CQUAD4	69	1	73	74
91	90	70-	CQUAD4	70	1	74	75
92	91	71-	CQUAD4	71	1	75	76
93	92	72-	CQUAD4	72	1	76	77
94	93	73-	CQUAD4	73	1	77	78
95	94	74-	CQUAD4	74	1	78	79
96	95	75-	CQUAD4	75	1	79	80
97	96	76-	CQUAD4	76	1	80	81
98	97	77-	CQUAD4	77	1	81	82
99	98	78-	CQUAD4	78	1	82	83
100	99	79-	CQUAD4	79	1	83	84
101	100	80-	CQUAD4	80	1	84	85
102	101	81-	CQUAD4	81	1	86	87
104	103	82-	CQUAD4	82	1	87	88
105	104	83-	CQUAD4	83	1	88	89
106	105	84-	CQUAD4	84	1	89	90
107	106	85-	CQUAD4	85	1	90	91
108	107	86-	CQUAD4	86	1	91	92
109	108	87-	CQUAD4	87	1	92	93
110	109	88-	CQUAD4	88	1	93	94
111	110	89-	CQUAD4	89	1	94	95
112	111	90-	CQUAD4	90	1	95	96
113	112	91-	CQUAD4	91	1	96	97
114	113	92-	CQUAD4	92	1	97	98
115	114	93-	CQUAD4	93	1	98	99
116	115	94-	CQUAD4	94	1	99	100
117	116	95-	CQUAD4	95	1	100	101
118	117						

		96-	CQUAD4	96	1	101	102
119	118					
		97-	CQUAD4	97	1	103	104
121	120					
		98-	CQUAD4	98	1	104	105
122	121					
		99-	CQUAD4	99	1	105	106
123	122					
		100-	CQUAD4	100	1	106	107
124	123					
		101-	CQUAD4	101	1	107	108
125	124					
		102-	CQUAD4	102	1	108	109
126	125					
		103-	CQUAD4	103	1	109	110
127	126					
		104-	CQUAD4	104	1	110	111
128	127					
		105-	CQUAD4	105	1	111	112
129	128					
		106-	CQUAD4	106	1	112	113
130	129					
		107-	CQUAD4	107	1	113	114
131	130					
		108-	CQUAD4	108	1	114	115
132	131					
		109-	CQUAD4	109	1	115	116
133	132					
		110-	CQUAD4	110	1	116	117
134	133					
		111-	CQUAD4	111	1	117	118
135	134					
		112-	CQUAD4	112	1	118	119
136	135					
		113-	CQUAD4	113	1	120	121
138	137					
		114-	CQUAD4	114	1	121	122
139	138					
		115-	CQUAD4	115	1	122	123
140	139					
		116-	CQUAD4	116	1	123	124
141	140					
		117-	CQUAD4	117	1	124	125
142	141					
		118-	CQUAD4	118	1	125	126
143	142					
		119-	CQUAD4	119	1	126	127
144	143					
		120-	CQUAD4	120	1	127	128
145	144					
		121-	CQUAD4	121	1	128	129
146	145					
		122-	CQUAD4	122	1	129	130
147	146					
		123-	CQUAD4	123	1	130	131
148	147					

		124-	CQUAD4	124	1	131	132
149	148	125-	CQUAD4	125	1	132	133
150	149	126-	CQUAD4	126	1	133	134
151	150	127-	CQUAD4	127	1	134	135
152	151	128-	CQUAD4	128	1	135	136
153	152	129-	CQUAD4	129	1	137	138
155	154	130-	CQUAD4	130	1	138	139
156	155	131-	CQUAD4	131	1	139	140
157	156	132-	CQUAD4	132	1	140	141
158	157	133-	CQUAD4	133	1	141	142
159	158	134-	CQUAD4	134	1	142	143
160	159	135-	CQUAD4	135	1	143	144
161	160	136-	CQUAD4	136	1	144	145
162	161	137-	CQUAD4	137	1	145	146
163	162	138-	CQUAD4	138	1	146	147
164	163	139-	CQUAD4	139	1	147	148
165	164	140-	CQUAD4	140	1	148	149
166	165	141-	CQUAD4	141	1	149	150
167	166	142-	CQUAD4	142	1	150	151
168	167	143-	CQUAD4	143	1	151	152
169	168	144-	CQUAD4	144	1	152	153
170	169	145-	CQUAD4	145	1	154	155
172	171	146-	CQUAD4	146	1	155	156
173	172	147-	CQUAD4	147	1	156	157
174	173	148-	CQUAD4	148	1	157	158
175	174	149-	CQUAD4	149	1	158	159
176	175	150-	CQUAD4	150	1	159	160
177	176	151-	CQUAD4	151	1	160	161
178	177						

		Type	EID	PID	G1	G2	G3	G4
152-		CQUAD4	152	1	161	162	179	178
153-		CQUAD4	153	1	162	163	180	179
154-		CQUAD4	154	1	163	164	181	180
155-		CQUAD4	155	1	164	165	182	181
156-		CQUAD4	156	1	165	166	183	182
157-		CQUAD4	157	1	166	167	184	183
158-		CQUAD4	158	1	167	168	185	184
159-		CQUAD4	159	1	168	169	186	185
160-		CQUAD4	160	1	169	170	187	186
161-		CQUAD4	161	1	171	172	189	188
162-		CQUAD4	162	1	172	173	190	189
163-		CQUAD4	163	1	173	174	191	190
164-		CQUAD4	164	1	174	175	192	191
165-		CQUAD4	165	1	175	176	193	192
166-		CQUAD4	166	1	176	177	194	193
167-		CQUAD4	167	1	177	178	195	194
168-		CQUAD4	168	1	178	179	196	195
169-		CQUAD4	169	1	179	180	197	196
170-		CQUAD4	170	1	180	181	198	197
171-		CQUAD4	171	1	181	182	199	198
172-		CQUAD4	172	1	182	183	200	199
173-		CQUAD4	173	1	183	184	201	200
174-		CQUAD4	174	1	184	185	202	201
175-		CQUAD4	175	1	185	186	203	202
176-		CQUAD4	176	1	186	187	204	203
177-		CQUAD4	177	1	188	189	206	205
178-		CQUAD4	178	1	189	190	207	206
179-		CQUAD4	179	1	190	191	208	207

```
              180-    CQUAD4  180   1    191   192
209    208
              181-    CQUAD4  181   1    192   193
210    209
              182-    CQUAD4  182   1    193   194
211    210
              183-    CQUAD4  183   1    194   195
212    211
              184-    CQUAD4  184   1    195   196
213    212
              185-    CQUAD4  185   1    196   197
214    213
              186-    CQUAD4  186   1    197   198
215    214
              187-    CQUAD4  187   1    198   199
216    215
              188-    CQUAD4  188   1    199   200
217    216
              189-    CQUAD4  189   1    200   201
218    217
              190-    CQUAD4  190   1    201   202
219    218
              191-    CQUAD4  191   1    202   203
220    219
              192-    CQUAD4  192   1    203   204
221    220
              193-    CQUAD4  193   1    205   206
223    222
              194-    CQUAD4  194   1    206   207
224    223
              195-    CQUAD4  195   1    207   208
225    224
              196-    CQUAD4  196   1    208   209
226    225
              197-    CQUAD4  197   1    209   210
227    226
              198-    CQUAD4  198   1    210   211
228    227
              199-    CQUAD4  199   1    211   212
229    228
              200-    CQUAD4  200   1    212   213
230    229
              201-    CQUAD4  201   1    213   214
231    230
              202-    CQUAD4  202   1    214   215
232    231
              203-    CQUAD4  203   1    215   216
233    232
              204-    CQUAD4  204   1    216   217
234    233
              205-    CQUAD4  205   1    217   218
235    234
              206-    CQUAD4  206   1    218   219
236    235
              207-    CQUAD4  207   1    219   220
237    236
```

```
              208-   CQUAD4  208   1   220   221
238   237
              209-   CQUAD4  209   1   222   223
240   239
              210-   CQUAD4  210   1   223   224
241   240
              211-   CQUAD4  211   1   224   225
242   241
              212-   CQUAD4  212   1   225   226
243   242
              213-   CQUAD4  213   1   226   227
244   243
              214-   CQUAD4  214   1   227   228
245   244
              215-   CQUAD4  215   1   228   229
246   245
              216-   CQUAD4  216   1   229   230
247   246
              217-   CQUAD4  217   1   230   231
248   247
              218-   CQUAD4  218   1   231   232
249   248
              219-   CQUAD4  219   1   232   233
250   249
              220-   CQUAD4  220   1   233   234
251   250
              221-   CQUAD4  221   1   234   235
252   251
              222-   CQUAD4  222   1   235   236
253   252
              223-   CQUAD4  223   1   236   237
254   253
              224-   CQUAD4  224   1   237   238
255   254
              225-   CQUAD4  225   1   239   240
257   256
              226-   CQUAD4  226   1   240   241
258   257
              227-   CQUAD4  227   1   241   242
259   258
              228-   CQUAD4  228   1   242   243
260   259
              229-   CQUAD4  229   1   243   244
261   260
              230-   CQUAD4  230   1   244   245
262   261
              231-   CQUAD4  231   1   245   246
263   262
              232-   CQUAD4  232   1   246   247
264   263
              233-   CQUAD4  233   1   247   248
265   264
              234-   CQUAD4  234   1   248   249
266   265
              235-   CQUAD4  235   1   249   250
267   266
```

```
268    267          236-     CQUAD4  236    1        250      251
269    268          237-     CQUAD4  237    1        251      252
270    269          238-     CQUAD4  238    1        252      253
271    270          239-     CQUAD4  239    1        253      254
272    271          240-     CQUAD4  240    1        254      255
274    273          241-     CQUAD4  241    1        256      257
275    274          242-     CQUAD4  242    1        257      258
276    275          243-     CQUAD4  243    1        258      259
277    276          244-     CQUAD4  244    1        259      260
278    277          245-     CQUAD4  245    1        260      261
279    278          246-     CQUAD4  246    1        261      262
280    279          247-     CQUAD4  247    1        262      263
281    280          248-     CQUAD4  248    1        263      264
282    281          249-     CQUAD4  249    1        264      265
283    282          250-     CQUAD4  250    1        265      266
284    283          251-     CQUAD4  251    1        266      267
285    284          252-     CQUAD4  252    1        267      268
286    285          253-     CQUAD4  253    1        268      269
287    286          254-     CQUAD4  254    1        269      270
288    287          255-     CQUAD4  255    1        270      271
289    288          256-     CQUAD4  256    1        271      272
MAX                 257-     EIGRL   30                        12
0.                  258-     GRID    1               0.       0.
0.                  259-     GRID    2               0.       .265625
0.                  260-     GRID    3               0.       .53125
0.                  261-     GRID    4               0.       .796875
0.                  262-     GRID    5               0.       1.0625
0.                  263-     GRID    6               0.       1.32813
```

116

264-	GRID	7	0.	1.59375
0.				
265-	GRID	8	0.	1.85938
0.				
266-	GRID	9	0.	2.125
0.				
267-	GRID	10	0.	2.39063
0.				
268-	GRID	11	0.	2.65625
0.				
269-	GRID	12	0.	2.92188
0.				
270-	GRID	13	0.	3.1875
0.				
271-	GRID	14	0.	3.45313
0.				
272-	GRID	15	0.	3.71875
0.				
273-	GRID	16	0.	3.98438
0.				
274-	GRID	17	0.	4.25
0.				
275-	GRID	18	.265625	0.
0.				
276-	GRID	19	.265625	.265625
0.				
277-	GRID	20	.265625	.53125
0.				
278-	GRID	21	.265625	.796875
0.				
279-	GRID	22	.265625	1.0625
0.				
280-	GRID	23	.265625	1.32813
0.				
281-	GRID	24	.265625	1.59375
0.				
282-	GRID	25	.265625	1.85938
0.				
283-	GRID	26	.265625	2.125
0.				
284-	GRID	27	.265625	2.39063
0.				
285-	GRID	28	.265625	2.65625
0.				
286-	GRID	29	.265625	2.92188
0.				
287-	GRID	30	.265625	3.1875
0.				
288-	GRID	31	.265625	3.45313
0.				
289-	GRID	32	.265625	3.71875
0.				
290-	GRID	33	.265625	3.98438
0.				
291-	GRID	34	.265625	4.25
0.				

292-	GRID	35	.53125	0.
0.				
293-	GRID	36	.53125	.265625
0.				
294-	GRID	37	.53125	.53125
0.				
295-	GRID	38	.53125	.796875
0.				
296-	GRID	39	.53125	1.0625
0.				
297-	GRID	40	.53125	1.32813
0.				
298-	GRID	41	.53125	1.59375
0.				
299-	GRID	42	.53125	1.85938
0.				
300-	GRID	43	.53125	2.125
0.				
301-	GRID	44	.53125	2.39063
0.				
302-	GRID	45	.53125	2.65625
0.				
303-	GRID	46	.53125	2.92188
0.				
304-	GRID	47	.53125	3.1875
0.				
305-	GRID	48	.53125	3.45313
0.				
306-	GRID	49	.53125	3.71875
0.				
307-	GRID	50	.53125	3.98438
0.				
308-	GRID	51	.53125	4.25
0.				
309-	GRID	52	.796875	0.
0.				
310-	GRID	53	.796875	.265625
0.				
311-	GRID	54	.796875	.53125
0.				
312-	GRID	55	.796875	.796875
0.				
313-	GRID	56	.796875	1.0625
0.				
314-	GRID	57	.796875	1.32813
0.				
315-	GRID	58	.796875	1.59375
0.				
316-	GRID	59	.796875	1.85938
0.				
317-	GRID	60	.796875	2.125
0.				
318-	GRID	61	.796875	2.39063
0.				
319-	GRID	62	.796875	2.65625
0.				

118

320-	GRID	63	.796875 2.92188
0.			
321-	GRID	64	.796875 3.1875
0.			
322-	GRID	65	.796875 3.45313
0.			
323-	GRID	66	.796875 3.71875
0.			
324-	GRID	67	.796875 3.98438
0.			
325-	GRID	68	.796875 4.25
0.			
326-	GRID	69	1.0625 0.
0.			
327-	GRID	70	1.0625 .265625
0.			
328-	GRID	71	1.0625 .53125
0.			
329-	GRID	72	1.0625 .796875
0.			
330-	GRID	73	1.0625 1.0625
0.			
331-	GRID	74	1.0625 1.32813
0.			
332-	GRID	75	1.0625 1.59375
0.			
333-	GRID	76	1.0625 1.85938
0.			
334-	GRID	77	1.0625 2.125
0.			
335-	GRID	78	1.0625 2.39063
0.			
336-	GRID	79	1.0625 2.65625
0.			
337-	GRID	80	1.0625 2.92188
0.			
338-	GRID	81	1.0625 3.1875
0.			
339-	GRID	82	1.0625 3.45313
0.			
340-	GRID	83	1.0625 3.71875
0.			
341-	GRID	84	1.0625 3.98438
0.			
342-	GRID	85	1.0625 4.25
0.			
343-	GRID	86	1.32813 0.
0.			
344-	GRID	87	1.32813 .265625
0.			
345-	GRID	88	1.32813 .53125
0.			
346-	GRID	89	1.32813 .796875
0.			
347-	GRID	90	1.32813 1.0625
0.			

348-   GRID   91   1.32813 1.32813
0.
349-   GRID   92   1.32813 1.59375
0.
350-   GRID   93   1.32813 1.85938
0.
351-   GRID   94   1.32813 2.125
0.
352-   GRID   95   1.32813 2.39063
0.
353-   GRID   96   1.32813 2.65625
0.
354-   GRID   97   1.32813 2.92188
0.
355-   GRID   98   1.32813 3.1875
0.
356-   GRID   99   1.32813 3.45313
0.
357-   GRID   100   1.32813 3.71875
0.
358-   GRID   101   1.32813 3.98438
0.
359-   GRID   102   1.32813 4.25
0.
360-   GRID   103   1.59375 0.
0.
361-   GRID   104   1.59375 .265625
0.
362-   GRID   105   1.59375 .53125
0.
363-   GRID   106   1.59375 .796875
0.
364-   GRID   107   1.59375 1.0625
0.
365-   GRID   108   1.59375 1.32813
0.
366-   GRID   109   1.59375 1.59375
0.
367-   GRID   110   1.59375 1.85938
0.
368-   GRID   111   1.59375 2.125
0.
369-   GRID   112   1.59375 2.39063
0.
370-   GRID   113   1.59375 2.65625
0.
371-   GRID   114   1.59375 2.92188
0.
372-   GRID   115   1.59375 3.1875
0.
373-   GRID   116   1.59375 3.45313
0.
374-   GRID   117   1.59375 3.71875
0.
375-   GRID   118   1.59375 3.98438
0.

120

376-	GRID	119	1.59375	4.25
0.				
377-	GRID	120	1.85938	0.
0.				
378-	GRID	121	1.85938	.265625
0.				
379-	GRID	122	1.85938	.53125
0.				
380-	GRID	123	1.85938	.796875
0.				
381-	GRID	124	1.85938	1.0625
0.				
382-	GRID	125	1.85938	1.32813
0.				
383-	GRID	126	1.85938	1.59375
0.				
384-	GRID	127	1.85938	1.85938
0.				
385-	GRID	128	1.85938	2.125
0.				
386-	GRID	129	1.85938	2.39063
0.				
387-	GRID	130	1.85938	2.65625
0.				
388-	GRID	131	1.85938	2.92188
0.				
389-	GRID	132	1.85938	3.1875
0.				
390-	GRID	133	1.85938	3.45313
0.				
391-	GRID	134	1.85938	3.71875
0.				
392-	GRID	135	1.85938	3.98438
0.				
393-	GRID	136	1.85938	4.25
0.				
394-	GRID	137	2.125	0.
0.				
395-	GRID	138	2.125	.265625
0.				
396-	GRID	139	2.125	.53125
0.				
397-	GRID	140	2.125	.796875
0.				
398-	GRID	141	2.125	1.0625
0.				
399-	GRID	142	2.125	1.32813
0.				
400-	GRID	143	2.125	1.59375
0.				
401-	GRID	144	2.125	1.85938
0.				
402-	GRID	145	2.125	2.125
0.				
403-	GRID	146	2.125	2.39063
0.				

121

| 404- | GRID | 147 | 2.125 | 2.65625 |
0.
| 405- | GRID | 148 | 2.125 | 2.92188 |
0.
| 406- | GRID | 149 | 2.125 | 3.1875 |
0.
| 407- | GRID | 150 | 2.125 | 3.45313 |
0.
| 408- | GRID | 151 | 2.125 | 3.71875 |
0.
| 409- | GRID | 152 | 2.125 | 3.98438 |
0.
| 410- | GRID | 153 | 2.125 | 4.25 |
0.
| 411- | GRID | 154 | 2.39063 | 0. |
0.
| 412- | GRID | 155 | 2.39063 | .265625 |
0.
| 413- | GRID | 156 | 2.39063 | .53125 |
0.
| 414- | GRID | 157 | 2.39063 | .796875 |
0.
| 415- | GRID | 158 | 2.39063 | 1.0625 |
0.
| 416- | GRID | 159 | 2.39063 | 1.32813 |
0.
| 417- | GRID | 160 | 2.39063 | 1.59375 |
0.
| 418- | GRID | 161 | 2.39063 | 1.85938 |
0.
| 419- | GRID | 162 | 2.39063 | 2.125 |
0.
| 420- | GRID | 163 | 2.39063 | 2.39063 |
0.
| 421- | GRID | 164 | 2.39063 | 2.65625 |
0.
| 422- | GRID | 165 | 2.39063 | 2.92188 |
0.
| 423- | GRID | 166 | 2.39063 | 3.1875 |
0.
| 424- | GRID | 167 | 2.39063 | 3.45313 |
0.
| 425- | GRID | 168 | 2.39063 | 3.71875 |
0.
| 426- | GRID | 169 | 2.39063 | 3.98438 |
0.
| 427- | GRID | 170 | 2.39063 | 4.25 |
0.
| 428- | GRID | 171 | 2.65625 | 0. |
0.
| 429- | GRID | 172 | 2.65625 | .265625 |
0.
| 430- | GRID | 173 | 2.65625 | .53125 |
0.
| 431- | GRID | 174 | 2.65625 | .796875 |
0.

432-	GRID	175	2.65625 1.0625
0.			
433-	GRID	176	2.65625 1.32813
0.			
434-	GRID	177	2.65625 1.59375
0.			
435-	GRID	178	2.65625 1.85938
0.			
436-	GRID	179	2.65625 2.125
0.			
437-	GRID	180	2.65625 2.39063
0.			
438-	GRID	181	2.65625 2.65625
0.			
439-	GRID	182	2.65625 2.92188
0.			
440-	GRID	183	2.65625 3.1875
0.			
441-	GRID	184	2.65625 3.45313
0.			
442-	GRID	185	2.65625 3.71875
0.			
443-	GRID	186	2.65625 3.98438
0.			
444-	GRID	187	2.65625 4.25
0.			
445-	GRID	188	2.92188 0.
0.			
446-	GRID	189	2.92188 .265625
0.			
447-	GRID	190	2.92188 .53125
0.			
448-	GRID	191	2.92188 .796875
0.			
449-	GRID	192	2.92188 1.0625
0.			
450-	GRID	193	2.92188 1.32813
0.			
451-	GRID	194	2.92188 1.59375
0.			
452-	GRID	195	2.92188 1.85938
0.			
453-	GRID	196	2.92188 2.125
0.			
454-	GRID	197	2.92188 2.39063
0.			
455-	GRID	198	2.92188 2.65625
0.			
456-	GRID	199	2.92188 2.92188
0.			
457-	GRID	200	2.92188 3.1875
0.			
458-	GRID	201	2.92188 3.45313
0.			
459-	GRID	202	2.92188 3.71875
0.			

460-	GRID	203	2.92188 3.98438
0.
461-	GRID	204	2.92188 4.25
0.
462-	GRID	205	3.1875 0.
0.
463-	GRID	206	3.1875 .265625
0.
464-	GRID	207	3.1875 .53125
0.
465-	GRID	208	3.1875 .796875
0.
466-	GRID	209	3.1875 1.0625
0.
467-	GRID	210	3.1875 1.32813
0.
468-	GRID	211	3.1875 1.59375
0.
469-	GRID	212	3.1875 1.85938
0.
470-	GRID	213	3.1875 2.125
0.
471-	GRID	214	3.1875 2.39063
0.
472-	GRID	215	3.1875 2.65625
0.
473-	GRID	216	3.1875 2.92188
0.
474-	GRID	217	3.1875 3.1875
0.
475-	GRID	218	3.1875 3.45313
0.
476-	GRID	219	3.1875 3.71875
0.
477-	GRID	220	3.1875 3.98438
0.
478-	GRID	221	3.1875 4.25
0.
479-	GRID	222	3.45313 0.
0.
480-	GRID	223	3.45313 .265625
0.
481-	GRID	224	3.45313 .53125
0.
482-	GRID	225	3.45313 .796875
0.
483-	GRID	226	3.45313 1.0625
0.
484-	GRID	227	3.45313 1.32813
0.
485-	GRID	228	3.45313 1.59375
0.
486-	GRID	229	3.45313 1.85938
0.
487-	GRID	230	3.45313 2.125
0.

488-	GRID	231	3.45313 2.39063	
0.				
489-	GRID	232	3.45313 2.65625	
0.				
490-	GRID	233	3.45313 2.92188	
0.				
491-	GRID	234	3.45313 3.1875	
0.				
492-	GRID	235	3.45313 3.45313	
0.				
493-	GRID	236	3.45313 3.71875	
0.				
494-	GRID	237	3.45313 3.98438	
0.				
495-	GRID	238	3.45313 4.25	
0.				
496-	GRID	239	3.71875 0.	
0.				
497-	GRID	240	3.71875 .265625	
0.				
498-	GRID	241	3.71875 .53125	
0.				
499-	GRID	242	3.71875 .796875	
0.				
500-	GRID	243	3.71875 1.0625	
0.				
501-	GRID	244	3.71875 1.32813	
0.				
502-	GRID	245	3.71875 1.59375	
0.				
503-	GRID	246	3.71875 1.85938	
0.				
504-	GRID	247	3.71875 2.125	
0.				
505-	GRID	248	3.71875 2.39063	
0.				
506-	GRID	249	3.71875 2.65625	
0.				
507-	GRID	250	3.71875 2.92188	
0.				
508-	GRID	251	3.71875 3.1875	
0.				
509-	GRID	252	3.71875 3.45313	
0.				
510-	GRID	253	3.71875 3.71875	
0.				
511-	GRID	254	3.71875 3.98438	
0.				
512-	GRID	255	3.71875 4.25	
0.				
513-	GRID	256	3.98438 0.	
0.				
514-	GRID	257	3.98438 .265625	
0.				
515-	GRID	258	3.98438 .53125	
0.				

125

516-	GRID	259		3.98438	.796875
0.					
517-	GRID	260		3.98438	1.0625
0.					
518-	GRID	261		3.98438	1.32813
0.					
519-	GRID	262		3.98438	1.59375
0.					
520-	GRID	263		3.98438	1.85938
0.					
521-	GRID	264		3.98438	2.125
0.					
522-	GRID	265		3.98438	2.39063
0.					
523-	GRID	266		3.98438	2.65625
0.					
524-	GRID	267		3.98438	2.92188
0.					
525-	GRID	268		3.98438	3.1875
0.					
526-	GRID	269		3.98438	3.45313
0.					
527-	GRID	270		3.98438	3.71875
0.					
528-	GRID	271		3.98438	3.98438
0.					
529-	GRID	272		3.98438	4.25
0.					
530-	GRID	273		4.25	0.
0.					
531-	GRID	274		4.25	.265625
0.					
532-	GRID	275		4.25	.53125
0.					
533-	GRID	276		4.25	.796875
0.					
534-	GRID	277		4.25	1.0625
0.					
535-	GRID	278		4.25	1.32813
0.					
536-	GRID	279		4.25	1.59375
0.					
537-	GRID	280		4.25	1.85938
0.					
538-	GRID	281		4.25	2.125
0.					
539-	GRID	282		4.25	2.39063
0.					
540-	GRID	283		4.25	2.65625
0.					
541-	GRID	284		4.25	2.92188
0.					
542-	GRID	285		4.25	3.1875
0.					
543-	GRID	286		4.25	3.45313
0.					

126

```
              544-        GRID    287              4.25    3.71875
0.
              545-        GRID    288              4.25    3.98438
0.
              546-        GRID    289              4.25    4.25
0.
              547-        MAT1    1        1.6+7           .31
4.14-4                0.16
              548-        PARAM   COUPMASS1
              549-        PSHELL  1        1       .05     1
1
              550-        SPC1    1        123456  1       18
35      52      69      86      +000001
              551-        ++000001103      120     137     154
171     188     205     222      +000002
              552-        ++000002239      256     273
+000003
              553-        SPCADD  2        1
                          ENDDATA
0                    TOTAL COUNT=         554
```

Appendix B: MATLAB "halfpower" Code

```
function [wn,Q] = halfpower_m(filename,FRF_form,w_start,w_stop);

% [wn,Q] = halfpower_m(filename,FRF_form,w_start,w_stop);
%
% halfpower - identify damping from half power points
% manual user selection of peaks
% FRF data assumed to be in file with .frf extension
% if filename = [] (default), select file with dialog box
% else filename is path and filename of .frf file to be loaded
% if FRF_form = 0(default), assumed form [freq mag phase(rad)]
% if FRF_form = 1, assumed form [freq real imag]
% if FRF_form = 2, assumed form [w FRF(complex)]
% if tmps = 1, select .tmps file and curvefit multiple FRFs

% TAKE IN AN FRF
if nargin < 1 | isempty(filename) == 1;
    [name, path] = uigetfile('*.frf');
    eval(['cd ' path]);
    FRF = load(name);
else
    FRF = load(filename);
end

% INPUTS
if ((nargin < 2) | (FRF_form == []));
    FRF_form = 0;
end
if nargin < 3 | w_start == [] | w_stop == [];
    w_start = 0;
    w_stop = 1e10;
end

% CHECK FOR NEW FILE FORMAT
[r,c] = size(FRF);

if c == 2
    w0 = FRF(1,1);
    dw = FRF(1,2);
    FRF(1,:) = [];
    w = w0 + dw*(0:(length(FRF)-1));
    col_1 = 1;
else
    w = FRF(:,1);
    col_1 = 2;
end

% CHECK FOR FRF FORMAT
if ((FRF_form == 0) | (isempty(FRF_form) == 1))
   Rm = FRF(:,col_1);
elseif FRF_form == 1
   Rm = abs(FRF(:,col_1)+j*FRF(:,col_1+1));
elseif FRF_form == 2
   Rm = abs(FRF);
```

```matlab
else
    error('You messed up FRF_form');
end
clear FRF

% GET TRUNCATED MAGNITUDE FRF
if w_start < min(w)
    w_start = min(w);
end
if w_stop > max(w)
    w_stop = max(w);
end
[i]=find(w(:,1)<w_start | w(:,1)>w_stop);
w(i)=[];
Rm(i,:)=[];

% USER GRAPHICALLY SELECTS PEAKS WITH MOUSE
Good = 'n';
disp('Pick the Peaks.  One mouse click per peak.  Return when done.')
while Good == 'n'
    figure;plot(w,20*log10(Rm),'b-');
    [maxima y] = ginput;

% REVISED PEAK FREQUENCIES BASED ON ACTUAL (UNSMOOTHED) DATA
search = 0.05;
w_start = maxima - search*maxima;
w_stop = maxima + search*maxima;
for n = 1:length(maxima)
    [y i_start(n)] = min(abs(w - w_start(n)));
    [y i_stop] = min(abs(w - w_stop(n)));
        [y max_index(n)] = max(Rm(i_start(n):i_stop));
end
peaks_index = i_start + max_index-1;
peaks = w(peaks_index);

% HOW DID I DO?
hold on;plot(peaks,20*log10(Rm(peaks_index)),'ro');
title('Revised Peak Frequencies');

% DEFINE BANDS
Low = .5*Rm(peaks_index);
High = 1*Rm(peaks_index);
for n = 1:length(peaks)

    % FIND POINTS 50% OF PEAK ON EITHER SIDE (wll - low point, low side
of peak)
    % IN ORDER OF FREQUENCY:  [wll_i whl_i whh_i wlh_i]
    up = Rm(peaks_index(n):end) - Low(n);
    wlh_i(n) = min(find(diff(sign(up)))) + peaks_index(n);
    down = Rm(1:peaks_index(n)) - Low(n);
    wll_i(n) = max(find(diff(sign(down))));

    % REMOVE NON-MONOTONIC MEMBERS
    wl = w(wll_i(n):peaks_index(n));
    Rl = Rm(wll_i(n):peaks_index(n));
    wh = w(peaks_index(n):wlh_i(n));
    Rh = Rm(peaks_index(n):wlh_i(n));
```

```matlab
    while isempty(find(diff(Rl)<=0))==0 | isempty(find(diff(Rh)>=0))==0
       nm = find(diff(Rl)<=0);
       Rl(nm+1) = [];
       wl(nm+1) = [];
       nm = find(diff(Rh)>=0);
       Rh(nm+1) = [];
       wh(nm+1) = [];
       end

    % INTERPOLATE BETWEEN 0.5*PEAK AND 1*PEAK TO FIND .707*PEAK
    w1(n,1) = interp1(Rl,wl,0.5*sqrt(2)*Rm(peaks_index(n)));
    w2(n,1) = interp1(Rh,wh,0.5*sqrt(2)*Rm(peaks_index(n)));

    % PLOT HALF POWER POINTS
       hold on;plot([w1(n);
w2(n)],20*log10(0.5*sqrt(2)*Rm(peaks_index(n))),'kx');
end

% IDENTIFY DAMPING AND NATURAL FREQUENCY
wr = w(peaks_index)';
Q = wr./(w2 - w1);
zeta = 0.5./Q;
wn = wr./sqrt(1-2*zeta.^2);
wn = wn'
Q=Q'
zeta = zeta';

Good = input('Good?  y or n  ','s');
end
```

Bibliography

APS Materials, Inc., Magnesium Aluminate (Spinel) Datasheet, Website, www.apsmaterials.com

Baz, A. "Active Damping", *Encyclopedia of Vibration,* pp. 351-364. San Diego: Academic Press, 2001.

Braisted, William, Geoffrey Frank, Barry Benedict, Yehia El-Aini, and Frank Lieghley, "A Passive Damping Concept to Reduce HCF of Turbine Engine Fan Blades", *Proceedings, 7th National Turbine Engine High Cycle Fatigue Conference,* May 2002.

Cowles, B. A. "High Cycle Fatigue in Aircraft Gas Turbines – an Industry Perspective", *International Journal of Fracture,* 80: 147-163 (1996).

Department of Defense. *Metallic Materials and Elements for Aerospace Vehicle Structures*, Military Handbook 5H, 1 Dec 1998

England, Gordon. "Plasma Thermal Spray Process". Website, gordonengland.co.uk, 2002.

Garrison, Brian, Editor. "Foreword", *High Cycle Fatigue Science and Technology Program 2000 Annual Report*. February 2001

Grady, Joseph E. "Fundamentals of High-Cycle Fatigue", *Machine Design,* 71:86 (1999).

Green, Jeff, and Sophoclis Patsias, "A Preliminary Approach for the Modeling of a Hard Damping Coating Using Friction Elements", *Proceedings, 7th National Turbine Engine High Cycle Fatigue Conference,* May 2002.

Gucfa, Adam J., Mark S. Loehr, and Melvin L. Sherwood. "Calibration Methods for an Infrared Thermoelastic Stress Analyzer", *Society for Experimental Mechanics Conference,* June 1986.

Harris, Cyril M. *Shock and Vibration Handbook.* New York: McGraw-Hill, 1988.

Henry, Scott D., et al. *Fatigue Data Book: Light Structural Alloys.* Materials Park OH: ASM International, 1995.

Maxwell, D. C., and Nicholas, T. "A Rapid Method for Generation of a Haigh Diagram for High Cycle Fatigue", *Fatigue and Fracture Mechanics,* 29:1321, 1998.

Meirovitch, Leonard. *Elements of Vibration Analysis.* Boston: McGraw-Hill, 1986.

Nicholas, T. and J. R. Zuiker. "On the Use of the Goodman Diagram for High Cycle Fatigue Design", *International Journal of Fracture,* 80: 219-235 (1996).

Patsias, Sophoclis, Geof R. Tomlinson, and Mark A. Jones. "Initial Studies into Hard Coatings for Fan Blade Damping", *6th National Turbine Engine High Cycle Fatigue Conference,* Mar 2001.

Piezo Systems, Inc. Website, www.piezo.com/bendedu.html.

Polytec Laser Doppler Vibrometer User Manual.

Rades, M. "Resonance and Antiresonance", *Encyclopedia of Vibration*, pp.1046-1055. San Diego: Academic Press, 2001.

Ritchie, R. O., B. L. Boyce, J. P. Campbell, O. Roder, A. W. Thompson, and W. W. Mulligan. "Thresholds for High Cycle Fatigue in a Turbine Engine Ti-6Al-4V Alloy", *International Journal of Fatigue,* 21: 653-662 (1999).

Shen, M.-H. Herman. "Reliability Assessment of High Cycle Fatigue Design of Gas Turbine Blades Using the Probabilistic Goodman Diagram", *International Journal of Fatigue,* 21: 699-708 (1999).

Shen, M.-H. Herman. "Development of a Free Layer Damper Using Hard Coatings", *Proceedings, 7th National Turbine Engine High Cycle Fatigue Conference,* May 2002.

Smith, Todd. "The Effect of Plasma-Sprayed Coatings on the Fatigue of Titanium Alloy Implants", *JOM,* 46:54-56 (1994).

Torvik, Peter J., S. Patsias, and G. R. Tomlinson, "Characterising the Behaviour of Hard Coatings: Comparison of Two Methodologies", *Proceedings, 7th National Turbine Engine High Cycle Fatigue Conference,* May 2002.

Ungar, E. E. "Damping Materials", *Encyclopedia of Vibration,* pp. 327-331. San Diego: Academic Press, 2001.

Vita

Frank T. Ivancic graduated from McKeesport High School, McKeesport PA, in 1978. After attending the County College of Morris, Randolph NJ, for two years, he transferred to Penn State University, University Park PA, where he received his undergraduate degree in Aerospace Engineering in 1984.

Upon graduation, he accepted a civil service position with the Department of the Air Force to work as a reliability and maintainability engineer with the Air Force Acquisition Logistics Center at Edwards AFB CA. In 1989, he transferred to Wright-Patterson AFB to take a position as a flight test manager for the YA-7F program. He has held various positions at Wright-Patterson since then. Prior to his enrollment at AFIT, he was the environmental manager for the Propulsion Development System Office, ASC/LP, and chaired the Propulsion Environmental Working Group.

Mr. Ivancic received a Master of Science degree in Management Science from the University of Dayton in 1992, and completed Air Command and Staff College in 1999.

Mr. Ivancic began his studies at AFIT as a part-time student in Oct 2000. He was accepted as a degree candidate in May 2001. He attended full-time from Oct 2001 to Sep 2002, and finished part-time from Oct 2002 to Mar 2003. He is currently working as the project development team leader in the Pollution Prevention branch of the Acquisition Environmental Management office, ASC/ENVV, Wright-Patterson AFB OH.

REPORT DOCUMENTATION PAGE

Form Approved
OMB No. 074-0188

1. REPORT DATE (DD-MM-YYYY) 14-03-2003	2. REPORT TYPE **Master's Thesis**	3. DATES COVERED (From – To) Oct 2001 – Mar 2003

4. TITLE AND SUBTITLE

THE EFFECT OF A HARD COATING ON THE DAMPING AND FATIGUE LIFE OF TITANIUM

5a. CONTRACT NUMBER

5b. GRANT NUMBER

5c. PROGRAM ELEMENT NUMBER

6. AUTHOR(S)

Ivancic, Frank T.

5d. PROJECT NUMBER

5e. TASK NUMBER

5f. WORK UNIT NUMBER

7. PERFORMING ORGANIZATION NAMES(S) AND ADDRESS(S)
Air Force Institute of Technology
Graduate School of Engineering and Management (AFIT/EN)
2950 P Street, Building 640
WPAFB OH 45433-7765

8. PERFORMING ORGANIZATION REPORT NUMBER

AFIT/GAE/ENY/03-12

9. SPONSORING/MONITORING AGENCY NAME(S) AND ADDRESS(ES)
Dr. Charles Cross
AFRL/PRTC
1950 Fifth Street Bldg. 252
Wright-Patterson AFB OH 45433-7251

10. SPONSOR/MONITOR'S ACRONYM(S)

11. SPONSOR/MONITOR'S REPORT NUMBER(S)

12. DISTRIBUTION/AVAILABILITY STATEMENT

APPROVED FOR PUBLIC RELEASE; DISTRIBUTION UNLIMITED.

13. SUPPLEMENTARY NOTES

14. ABSTRACT

This project compares the damping and fatigue life of bare titanium plates to those coated with magnesium aluminate spinel (mag spinel). Two different coating thicknesses were tested. Test specimens were characterized by dynamic ping, laser vibrometry, sine sweeps, and SPATE. Once characterization was complete, fatigue testing was conducted on the thick plates utilizing the resonant dwell process. The strain level which would result in fatigue at 10^6 cycles, and the velocity necessary to achieve this strain were determined. The specimens were excited at this velocity, and the number of cycles to failure was noted. Results were compared for the uncoated, thin coated, and thick coated specimens. This project demonstrated that the addition of mag spinel did increase the damping of the titanium plates. The thick coating did not provide noticeably better damping results than the thin coating at the amplitudes tested. The coating allowed the titanium plate to withstand a greater stress at the same life as the uncoated plate, or to endure a much greater number of cycles at the same applied force. The thick coating had a greater impact on fatigue than the thin coating, but the thick coating was observed to flake off.

15. SUBJECT TERMS
Vibration, High Cycle Fatigue, Damping, Fatigue, Titanium, Magnesium Aluminate Spinel, Resonance, Resonance Frequency, Resonance Mode, Finite Element Analysis

16. SECURITY CLASSIFICATION OF:			17. LIMITATION OF ABSTRACT	18. NUMBER OF PAGES	19a. NAME OF RESPONSIBLE PERSON Dr. A. N. Palazotto, ENY
a. REPORT	**b. ABSTRACT**	**c. THIS PAGE**	**UU**	148	19b. TELEPHONE NUMBER (Include area code) (937) 255-3636, ext. 4599; email Anthony.Palazotto@afit.edu
U	**U**	**U**			

Standard Form 298 (Rev. 8-98)
Prescribed by ANSI Std. Z39-18